SIMULATION OF MULTIPLE-COMPONENT CHARGED AEROSOL EVOLUTION

A Dissertation

presented to

the Faculty of the Graduate School

at the University of Missouri

In Partial Fulfillment

of the Requirements for the Degree

Doctor of Philosophy

---

by

FERNANDO DE LA TORRE AGUILAR

Dr. Sudarshan K. Loyalka, Dissertation Supervisor

May 2019

The undersigned, appointed by the dean of the Graduate School,
have examined the dissertation entitled

SIMULATION OF MULTIPLE-COMPONENT CHARGED AEROSOL EVOLUTION

presented by Fernando De La Torre Aguilar,

a candidate for the degree of Doctor of Philosophy,

and hereby certify that, in their opinions, it is worthy of acceptance.

_____

Dr. Sudarshan K. Loyalka

_____

Dr. Tushar K. Ghosh

_____

Dr. Robert V. Tompson

_____

Dr. Mark A. Prelas

_____

Dr. Dabir S. Viswanath

DEDICATION

Dedicated to the memory of my relatives who saw me begin this journey but could not see me reaching the goal:

Juan José de la Torre Franco

Ma Guadalupe Andrade Bautista

Iliana Gabriela Guerrero

Dedicated to all my dear ones who believed that I could do this and encourage me with their kind words. Especially my wife, my mother, and my brother. And to my meditation teacher, venerable Yuttadhammo Bhikkhu. Without the skill to train the mind this would have not been possible.

ACKNOWLEDGMENTS

First, I would like to thank my advisor Dr. Loyalka for his patience, teachings, guidance, encouragement and support throughout the course of my Ph.D. research. Besides being an expert in his field, he is a kind and generous human being.

I would like to thank my committee members: Drs. Mark Prelas, Tushar Ghosh, Robert Tompson and Dabir Viswanath. I appreciate your contributions toward improving and reviewing this work. With especial gratitude to Dr. Prelas who also gave me the opportunity to participate in the project to write the book "Nuclear Batteries and Radioisotopes" where I learned a lot, and to Dr. Tompson who gave me directions about the generation of nanoparticles by spark discharge. It was an honor to be a student at the Nuclear Science and Engineering Institute and learn from these faculty members.

I would like to thank the staff of the NSEI, James Bennett and Latricia Vaughn, for all your help, guidance, and support during my time as Ph.D. student.

I would like to thank my fellow students who helped me during this time. Especially Matthew Simones who kindly taught me how to use aerosol instrumentation. And Kyle Walton who helped me when I worked in the laboratories.

Finally, I would like to acknowledge the support received by the Mexican *Consejo Nacional de Ciencia y Tecnología* (CONACYT) who provided me with financial support the first four years of my Ph.D. studies and by the federal grant DE-NE0008448, entitled "Am-241 Nuclear Safety and Environmental Interactions" sponsored via the Nuclear Energy University Programs of the U.S. Department of Energy.

TABLE OF CONTENTS

ACKNOWLEDGMENTS ii

LIST OF ILLUSTRATIONS v

LIST OF TABLES ix

ABSTRACT xi

Chapter Page

1. INTRODUCTION 1

1.1 Background 1

1.2 Objectives and Organization 5

2. PREVIOUS WORK 8

3. DSMC SIMULATIONS FOR MULTI-COMPONENT CHARGED AEROSOLS 17

3.1 Initial particle list 18

3.2 Electrostatic Dispersion 23

3.3 Deposition 25

3.4 Coagulation 27

3.5 Condensation 31

3.6 Final processing 32

3.7 Simulations of Carbon-Silver Aerosols 33

3.7.1 Problem 1: Particle composition of 90% graphite and 10% silver 37

3.7.2 Problem 2: Particle composition of 10% graphite and 90% Silver 60

3.8 Conclusions 85

4. POSSIBLE EXPERIMENTS 90

4.1 Two-component nanoparticles generated by spark discharge 92

4.1.1 Two spark generators 94

4.1.2 Using electrodes of different materials 95

4.1.3 Using electrodes made of alloys 96

4.2 Atomized aerosols 98

4.3 Conclusions 101

5. EXPLORATION OF WEIGHTS USING THE DSMC TECHNIQUE 103

5.1 Deposition using weights 105

5.2 Coagulation using weights 110

5.3 Other processes 112

5.4 Conclusions 113

6. DISCUSSION AND CONCLUSIONS 114

REFERENCES 117

VITA 122

LIST OF ILLUSTRATIONS

Figure Page

1. Depiction of a simulated particle representing the volumes of 3 components (V_1, V_2, and V_3) surrounded by water (stripes) and a negative charge level q. 19

2. Format for particle and component density lists used in a DSMC simulation considering aerosol particles made up of two components and water. 22

3. Particle number distributions for Problem 1 at 0, 500, 1000 and 1500 seconds..... 50

4. Mass distribution of graphite for Problem 1 at 0, 500, 1000 and 1500 seconds..... 50

5. Mass distribution of silver for Problem 1 at 0, 500, 1000 and 1500 seconds. 51

6. Mass distribution of water for Problem 1 at 500, 1000 and 1500 seconds. 51

7. Particle number distribution for Problem 1 with discrimination of charge at 0 seconds. 52

8. Particle number distribution for Problem 1 with discrimination of charge at 500 seconds. 53

9. Particle number distribution for Problem 1 with discrimination of charge at 1000 seconds. 53

10. Particle number distribution for Problem 1 with discrimination of charge at 1500 seconds. 54

11. Mass distribution of graphite for Problem 1 with discrimination of charge at 0 seconds. 55

12. Mass distribution of silver for Problem 1 with discrimination of charge at 0 seconds. 55

13. Mass distribution of graphite for Problem 1 with discrimination of charge at 500 seconds. 56

14. Mass distribution of silver for Problem 1 with discrimination of charge at 500 seconds. 56

15. Mass distribution of water for Problem 1 with discrimination of charge at 500 seconds. 57

16. Mass distribution of graphite for Problem 1 with discrimination of charge at 1000 seconds. 57

17. Mass distribution of silver for Problem 1 with discrimination of charge at 1000 seconds. 58

18. Mass distribution of water for Problem 1 with discrimination of charge at 1000 seconds. 58

19. Mass distribution of graphite for Problem 1 with discrimination of charge at 1500 seconds. 59

20. Mass distribution of silver for Problem 1 with discrimination of charge at 1500 seconds. 59

21. Mass distribution of water for Problem 1 with discrimination of charge at 1500 seconds. 60

22. Particle number distributions for Problem 2 at 0, 500, 1000 and 1500 seconds..... 74

23. Mass distribution of graphite for Problem 2 at 0, 500, 1000 and 1500 seconds..... 75

24. Mass distribution of silver for Problem 2 at 0, 500, 1000 and 1500 seconds..... 75

25. Mass distribution of water for Problem 2 at 500, 1000 and 1500 seconds. 76

26. Particle number distribution for Problem 2 with discrimination of charge at 0 seconds. 77

27. Particle number distribution for Problem 2 with discrimination of charge at 500 seconds. 77

28. Particle number distribution for Problem 2 with discrimination of charge at 1000 seconds. 78

29. Particle number distribution for Problem 2 with discrimination of charge at 1500 seconds. 78

30. Mass distribution of graphite for Problem 2 with discrimination of charge at 0 seconds. 80

31. Mass distribution of silver for Problem 2 with discrimination of charge at 0 seconds. 80

32. Mass distribution of graphite for Problem 2 with discrimination of charge at 500 seconds. 81

33. Mass distribution of silver for Problem 2 with discrimination of charge at 500 seconds. 81

34. Mass distribution of water for Problem 2 with discrimination of charge at 500 seconds. 82

35. Mass distribution of graphite for Problem 2 with discrimination of charge at 1000 seconds. 82

36. Mass distribution of silver for Problem 2 with discrimination of charge at 1000 seconds. 83

37. Mass distribution of water for Problem 2 with discrimination of charge at 1000 seconds. 83

38. Mass distribution of graphite for Problem 2 with discrimination of charge at 1500 seconds. 84

39. Mass distribution of silver for Problem 2 with discrimination of charge at 1500 seconds. 84

40. Mass distribution of water for Problem 2 with discrimination of charge at 1500 seconds. 85

41. Schematic for the experimental setup to measure coagulation obtaining several size and charge distributions from a single component aerosol. 91

42. Mechanical arrangement of the electrode unit inside a PALAS nano particle generator model DNP 3000. Electrodes are shown in solid black and grey. 93

43. Generation of aerosol from aqueous solution, using diffusion driers and heating strips to remove water from particles. 99

44. Size distribution of atomized 65-nm PSL particles using three diffusion dryers, a pressure of 15 psi in the atomizer, and heating the aerosol to 35 °C. 100

45. Size distribution of atomized 99-nm PSL particles using three diffusion dryers, a pressure of 15 psi in the atomizer, and heating the aerosol to 35 °C. 100

46. Size distribution of atomized de-ionized water (8 MΩ) with no solute, using three diffusion dryers, a pressure of 15 psi in the atomizer, and heating the aerosol to 35 °C. 101

47. Suggested experimental setup for studying coagulation in two-component aerosols using alloyed electrodes to produce nanoparticles by spark discharge, a coagulation tube to sample the aerosols at different times, an SMPS and a TDMA to obtain size and charge distributions, and a sampler to collect particles and determine their composition by ICP-MS analysis..... 102

48. Comparison of calculated number of particles in a DSMC simulation of constant deposition using regular scaling and dynamic particle weights..... 108

49. Comparison of the total volume of aerosol particles in a DSMC simulation of constant deposition using regular scaling and dynamic particle weights. 109

LIST OF TABLES

Table Page

1. Characteristics of the implementations of DSMC for homogenous aerosols. 16

2. Values for the mean, standard deviation and fraction of total particles in the lognormal distributions used to generate the initial particle list. 35

3. Simulation parameters and their values. 36

4. Number of particles and volumes for the different time steps of the simulation in Problem 1. 39

5. Mean diameter, mean mass of each component and mean density of aerosol particles for each time step in Problem 1. 40

6. Results from the interaction of particles by electrostatic dispersion (ED) in Problem 1. 41

7. Results from the interaction of particles by deposition (DEPO) in Problem 1..... 42

8. Results from the interaction of particles by coagulation and data of particles coalescing in Problem 1 43

9. Relative frequency of particles in each charge level ordered by largest from left to right, except for the last column (Problem 1). 48

10. Number of particles and volumes in the different time steps of the simulation in Problem 2.* 63

11. Mean diameter, mean mass of each component and mean density of aerosol particles for each time step in Problem 2. 64

12. Results from the interaction of particles by electrostatic dispersion (ED) in Problem 2. 65

13. Results from the interaction of particles by deposition (DEPO) in Problem 2..... 66

14. Results from the interaction of particles by coagulation, data of particles coalescing in Problem 2. 67

15. Relative frequency of particles in each charge level ordered by largest from left to right, except for the last column (Problem 2). 72

16. Mass fraction and generation rates of bimetallic particles (Byeon et al., 2008)..... 96

17. Comparison of Cu/Ni-ratios between alloyed feedstock electrodes and nanoparticles produced. 97

18. Comparison of steps followed in regular scaling versus the use of weights. 107

SIMULATION OF MULTIPLE-COMPONENT CHARGED AEROSOL EVOLUTION

Fernando De La Torre Aguilar

Sudarshan K. Loyalka, Dissertation Supervisor

ABSTRACT

The study of the nuclear source term requires the computation of aerosol dynamics. Solutions to the aerosol general dynamic equation (GDE) are difficult to obtain by analytical or numerical methods when more realistic problems are considered. The direct simulation Monte Carlo (DSMC) technique is capable of simulating aerosol evolution reducing simplifications in the implementation of the aerosol GDE. In this work we present a DSMC program for the simulation of multi-component polydisperse aerosol evolution, with the successful integration of the following processes: deposition, electrostatic dispersion, coagulation (considering charge effects) and condensation, assuming a spatially homogeneous medium and spherical particles. Two problems with different particle compositions were simulated to obtain information about the interactions through the different processes and the interacting particles as well as particle number and mass distributions with discrimination of charge levels. This information allowed us to explore the synergistic nature of these processes. It was found that the problem with denser particles had an overall stronger activity in coagulation and initially a stronger activity in deposition compared to the problem with less dense particles. Experiments to generate two-component aerosols by spark discharge in the study of aerosol coagulation with characterization of particle composition are proposed. Moreover, the use of particle weights in the DSMC method is explored.

1. INTRODUCTION

1.1 Background

Nuclear reactor plants are complex facilities which contain radioisotopes in considerable amounts. These radioisotopes could be released into the environment as radioactive aerosols in nuclear reactor accidents involving severe core damage or sabotage with explosives of either shipping casks or waste disposal sites, posing a potential risk to the public. Reactor safety studies by the U.S. Atomic Energy Commission and the U.S. Nuclear Regulatory Commission have been performed to estimate the nuclear source term considering several probable accident scenarios (DiNunno et al., 1962; U.S. Atomic Energy Commission, 1950, 1957; U.S. Nuclear Regulatory Commission, 1975). However, tracking the evolution of nuclear aerosols released during accidents is very complicated. This tracking problem is related to the nuclear source term which refers to "the amount and timing of the release of radioactive substances from a reactor plant into the environment" (Williams and Loyalka, 1991). The determination of the nuclear source term involves studying severe accident scenarios, assigning them a probability of occurrence, and analyzing what happens inside the plant with physico-chemical, neutronics, and thermal hydraulic models. For this purpose, one needs to understand the processes involved in the formation, motion, interaction, and distribution of particles, especially in the aerosol range. In accidents, aerosol formation starts in the core as a result of the vaporization of materials, which rise and find cooler temperatures condensing into aerosols (Sher and Hobbins, 2011). The computation of aerosol dynamics involves processes such as coagulation, deposition, condensation,

evaporation, and electrostatic dispersion. Besides, the complexity of these processes increases with the inclusion of particle properties such as size, composition, shape, charge, radioactivity and spatial inhomogeneity as well as environmental conditions and thermal hydraulics (Brockmann, 1987; Friedlander, 2000; U.S. Nuclear Regulatory Commission, 1981; Williams and Loyalka, 1991). Due to these factors, the models used in reactor safety studies need to implement assumptions, which result in an unsatisfactory representation of the complex aerosol mechanics in some cases. For example, condensation significantly affects the nuclear source term in nuclear reactors with wet environments (i.e., light water-based reactors) reducing the effects of shape and charge effects on aerosols, but the opposite happens in dry situations like the containment of high temperature reactors (HTRs). By not retaining fidelity to actual physics, reactor safety analysis may underestimate the releases of radioisotopes in nuclear accidents in this case (U.S. Nuclear Regulatory Commission, 2007). Another example is the error in the estimation of aerosol evolution caused by the assumption that all components have the same density in the sectional technique (Campbell and Loyalka, 2015).

The evolution of the source term (nuclear aerosols) is modelled by the aerosol general dynamic equation (GDE). The GDE is an integro-differential equation that characterizes particle volume and mass distribution in time. It may contain terms which represent coagulation, condensation, deposition, and electrostatic dispersion, as well as a source term to add particles. This equation can be solved in various ways: analytical, finite elements methods, and numerical (Friedlander, 2000; Williams and Loyalka, 1991). Unfortunately, the analytical solutions are restricted to simple cases and numerical

solutions must be used for more realistic cases. The GDE for a well-mixed, spherical, multispecies aerosol in a spatially homogeneous medium can be written as:

$$\begin{aligned}
&\frac{\partial}{\partial t} n(\boldsymbol{v},\boldsymbol{m},t) + R(\boldsymbol{v},\boldsymbol{m},t)\, n(\boldsymbol{v},\boldsymbol{m},t) + \sum_{c=1}^{N} \frac{\partial}{\partial v_c}\left[I_c(\boldsymbol{v},\boldsymbol{m},t)\, n(\boldsymbol{v},\boldsymbol{m},t) \right] = \\
&\quad \frac{1}{2}\int_0^\infty d\boldsymbol{u} \int_0^\infty d\boldsymbol{w} \int_0^\infty d\boldsymbol{q} \int_0^\infty d\boldsymbol{s}\; n(\boldsymbol{u},\boldsymbol{q},t)\, n(\boldsymbol{w},\boldsymbol{s},t)\, K(u,q \mid w,s) \\
&\quad \times \prod_{c=1}^{N} \delta(v_c - u_c - w_c)\, \delta(m_c - q_c - s_c) \\
&\quad - n(\boldsymbol{v},\boldsymbol{m},t) \int_0^\infty d\boldsymbol{u} \int_0^\infty d\boldsymbol{q}\; K(u,q \mid v,m)\, n(\boldsymbol{u},\boldsymbol{q},t) \\
&\quad + S(\boldsymbol{v},\boldsymbol{m},t)
\end{aligned} \tag{1}$$

where the number of aerosol particles of a species *c* contained in a volume v_c to $v_c + dv_c$ with masses m_c to $m_c + dm_c$ is given by:

$$n_p(\boldsymbol{v},\boldsymbol{m},t) = n_p(v_1, v_2, ..., v_N; m_1, m_2, ..., m_N, t) \tag{2}$$

and:

$$\int d\boldsymbol{v} = \int dv_1 dv_2 ... dv_N \tag{3}$$

$R(\boldsymbol{v},\boldsymbol{m},t)$ is the removal rate of particles, $I_c(\boldsymbol{v},\boldsymbol{m},t)$ is the condensation rate, $K(u,q \mid w,s)$ is the coagulation kernel for particles of total volume *u* and mass q coalescing with particles of total volume *w* and mass *s*. Delta functions allow for conservation of volume and mass in a collision, and $S_p(\boldsymbol{v},\boldsymbol{m},t)$ is a source term for aerosol production (Palaniswaamy and Loyalka, 2007b; Williams and Loyalka, 1991).

Clearly, the GDE is a complex equation and the version in equation (1) does not yet include charge effects or electrostatic dispersion. As a result of the difficulty to solve it, the codes developed to calculate the nuclear source term need to make approximations which lead to inaccurate results such as problems in the presence of strong coagulation

and condensation (Williams and Loyalka, 1991). Also, radiation, charge, and shape effects have not been adequately considered for these reactor safety studies. Notably, aerosol charge distribution has been shown to have a significant effect in the coagulation of particles, particularly for bipolar charge distributions (Ghosh et al., 2017; Palsmeier and Loyalka, 2013).

Solutions to simplified versions of the GDE have been obtained using the sectional technique in the computer programs, CONTAIN (Murata et al., 1997) and MELCOR (Gauntt et al., 2000), but they do not include the effect of the charge in aerosols as it is difficult to implement using the sectional technique (Williams and Loyalka, 1991) as well as in other methods to solve the GDE such as: the finite elements method, the analytical method, and numerical methods. However, one versatile technique that includes more physical processes without much complication is the direct simulation Monte Carlo (DSMC) technique. One example of the DSMC method's success has been found in the addition of charge effects combined with other processes (Palsmeier and Loyalka, 2013). The DSMC technique is a physically based simulation method where aerosols are modeled by many simulated particles in a computer. The number of particles used is determined by the limitations of the computer and the desired speed of simulation. This technique was first applied to model molecule collisions in gases, but it has also been shown to be applicable to aerosol dynamics. In general, an aerosol DSMC simulation involves the following: an initial particle list, a time step, physical models and random numbers. The initial particle list shows the state of the aerosol at the start of the simulation and stores particle properties such as mass, volume, and charge in the computer. These properties are dynamically modified in each time step as different

aerosol processes are applied. The time step selected is preferably smaller than the duration of the fastest process involved, and it is used both to test if particles interact and to determine the magnitude of change in their properties. The rates of the processes (condensation, coagulation, deposition, etc.) are determined using physical models, and particles are tested for interaction using random numbers. In conjunction, these two dictate changes to the particle list. This process is repeated in several time steps until the total time of the simulation is reached, updating the values in the particle list in each step.

At the Nuclear Science and Engineering Institute (NSEI) a lot of work has been dedicated to improving the application of the DSMC technique to aerosol evolution, benchmarking and comparing DSMC models using polydisperse aerosols with both single and multiple components to analytical solutions and experimental data. The latest addition to this technique for homogeneous aerosols was the inclusion of coagulation considering charge effects and electrostatic dispersion for a single-component polydisperse aerosol. Our research improves that model by combining it with the processes of condensation and deposition previously verified in DSMC simulations and by being able to handle multiple-components with different densities. We also developed experiments to take advantage of the capabilities of the DSMC program presented and explore the use of particle weights to improve the results when using the DSMC technique.

1.2 Objectives and Organization

The purpose of this work is to present a DSMC program developed for multi-component polydisperse aerosol evolution, which includes the following processes:

deposition, electrostatic dispersion, coagulation (considering charge effects) and condensation, assuming a spatially homogeneous medium and spherical particles. This dissertation is also introducing possible experiments regarding multi-component charged aerosol evolution and an investigation designed to improve simulation results by assigning different weights to simulated particles in the DSMC program.

The work is organized as follows: Chapter 2 presents a review of previous work on modeling aerosols using the DSMC technique, especially coagulation. It contains comparisons and validations (through benchmarking) between the results of this technique, exact results for simplified versions of the GDE, and other numerical methods like the sectional technique. Also, it presents a comparison between a DSMC simulation and measurements of charged single-species aerosol coagulation obtained with a tandem differential mobility analyzer (TDMA). Chapter 3 describes the DSMC program proposed in this work, explaining how the different process rates are calculated and how they are applied to a list of elements representing particles made up of different components and having an electrical charge. Two problems considering aerosols with particles containing different proportions of silver and graphite are presented and the results of the evolution of these aerosols are shown in terms of the number of interactions, characteristics of the interacting particles, particle number distributions, and component mass distributions with and without discrimination of charge. Chapter 4 explains possible experiments designed to compare the results of this model with measurements. It involves particle generation, mixing of different particle species, and measurement of the different species during the evolution of the aerosol. Several options are presented to generate two-component aerosols by spark discharge. Chapter 5 presents

an investigation on using different particle weights in the DSMC technique. A way to redistribute the weight of particles in deposition is proposed and its goal is to avoid the elimination of representative volumes in the particle list. For coagulation, we discuss the difficulties found for the implementation of particle weights. Chapter 6 presents a discussion and conclusions drawn from implementing the DSMC program and exploring particle weights. It also presents recommendations for future research in the simulation of aerosols and for experiments which can be carried out to get a more complete characterization of aerosols.

2. PREVIOUS WORK

The DSMC technique was originally developed for gas dynamics by Bird (1994) to model rarefied gas flows in a probabilistic simulation. Loyalka (2003) proposed its use in nuclear aerosols, showing that the results obtained by this technique agreed well with the results obtained by the sectional technique applied in MAEROS (Gelbard, 1982) for the coagulation of two component aerosols under the assumption that the components have the same density. MAEROS is a module used in the nuclear industry to calculate aerosol composition and mass concentration as a function of particle size and time in the containment of nuclear reactors. In this work, Loyalka developed a computer program to simulate constant coagulation in a two-component aerosol and benchmarked it to the analytical solution for this problem.

Rangaraj and Loyalka (2004) continued the study of DSMC simulations considering multiple component aerosols with different component densities. They found that the MAEROS results (using the sectional technique) do not describe well their evolution by coagulation as the difference in density affects both the particle number distribution and the component mass distribution.

Palaniswaamy and Loyalka (2006) proposed a way to apply more realistic coagulation models to the DSMC technique for aerosols, considering Brownian, gravitational and turbulent coagulation. Unlike simple cases using a constant coagulation rate, these coagulation models depend on particle size, resulting in many possible collision coefficients. The calculation of the different collision coefficients was addressed by direct sampling (DS), that is, computing a matrix of collision coefficients which is

time and memory consuming. This is because DS requires computation times the order of N^2, with N being the number of particles in the simulation. In addition, the authors successfully incorporated the Metropolis algorithm (Metropolis et al., 1953) to test particles sampled for collision. This resulted in faster computations as it does not require any collisional matrix to be maintained and updated, changing the computation time to an order of N.

Besides the Metropolis algorithm, other sampling algorithms were explored by Palaniswaamy and Loyalka (2007a): The DS algorithm, the no time counter method (NTC), and the modified DS algorithm. They verified the applicability of the Metropolis, the NTC, and the modified DS algorithms to collisional problems obtaining computation times in the order of N, thereby reducing the computation time significantly.

Continuing the effort to make the DSMC aerosol simulations more realistic, Palaniswaamy and Loyalka (2007b) incorporated the processes of deposition and source reinforcement as well as coagulation into a multicomponent aerosol dynamics problem. They first compared both DSMC and analytical techniques to calculate the total number of particles in a single-component problem considering constant coagulation and deposition rates. The results based on these two techniques were indistinguishable. Then, they tested different combinations of processes in a seven-component aerosol dynamics problem. A same component density was used for comparison with results from the sectional technique since this technique cannot handle different component densities in a multi-component problem. It was found that the results from the DSMC and the sectional technique agreed well except when the particle population decreased causing the relevant statistics to get poorer. In addition, results with different component densities were

obtained by the DSMC method alone. Palaniswaamy and Loyalka (2007b) used around 10^6 particles (based on the computer power available) and scaled the results. The results differed significantly from the same component density (mean density) results, and they concluded that "the assumption of a single mean density is not generally appropriate because the different component densities appear to have a significant effect on aerosol processes."

In a post-accident reactor environment, condensation can occur at a rapid rate in the aerosol particles increasing their mass and volume. This change affects other processes like deposition and coagulation. Thus, Palaniswaamy and Loyalka (2008) explored the feasibility of the DSMC technique when condensation occurs, either alone or combined with coagulation. Two test cases presented an analysis based solely on condensation, considering two types of condensation rates: 1) a constant condensation rate and 2) a condensation rate dependent on particle volume. In addition, three test cases zeroed in on problems including both condensation and coagulation, considering the following types of rates: 1) constant coagulation rate and volume dependent condensation rate, 2) volume dependent condensation and coagulation rates, and 3) constant condensation and coagulation rates. All these test cases have analytical solutions for single component aerosols, and these solutions were compared in terms of total number of particles, total volume, and particle number distribution with DSMC results. A very close agreement between results from the DSMC technique and the analytical solution was found. When both processes were present, they were applied in sequence at very fine time intervals to get a good approximation. Very fine time intervals are also required when very sharp changes occur in the distribution.

Aerosol particles can become charged by the way they are generated, by fission product decay, and by an ionizing atmosphere. Dry environments, like those found in high temperature gas reactors (HTGR), favor electrostatic charging. The Columbic forces due to electrical charges affect aerosol behavior, particles with like charges will be less likely to coagulate while particles with alike charges are more likely to agglomerate. Recognizing the need for programs to model the effects of charge in aerosol evolution, Palsmeier and Loyalka (2013) explored the addition of charge effects to DSMC simulations of polydisperse single-component aerosols. Accident modeling programs using the MAEROS module do not address this issue because they are designed for light water reactors in which charge effects are minimized due to high humidity. The electrical charge in aerosol particles influences the coagulation process, so Palsmeier and Loyalka (2013) modified the coagulation kernel used for neutral particles by adding a multiplier, which is a function of the charges of the coagulating particles. The NTC method was chosen as the collisional sampling algorithm for its simplicity and ease of implementation. Also, an additional term was added to the GDE, which is related to the loss of particles by electrostatic dispersion. These models were incorporated in a DSMC program to compare with several test problems from other published works. These problems are: a symmetric bipolar monodisperse aerosol in which conservation of mass is neglected in coagulation to simplify the problem (Adachi et al., 1981), and a symmetric bipolar polydisperse aerosol with conservation of mass in coagulation (Vemury et al., 1997). The difference in particles remaining for the first problem did not exceed 0.2% in any time step, and it did not exceed 0.3% for the second problem, successfully benchmarking the DSMC technique with these other numerical techniques. Palsmeier and

Loyalka also compared charged and uncharged aerosol evolution for similar systems, finding that charged particle coagulation favors the formation of large particles in bipolar charge distributions. They also noticed an alternating pattern in bipolar systems of highly charged aerosol particles coagulating to form slightly larger neutral or weakly charged particles; then, these resultant particles coagulate again with the same size group of highly charged particles. This effect fades as particle size increases and more particles become neutral.

To provide experimental data on charged aerosols and to support advances in the simulation of aerosol evolution, Simones et al. (2011) worked on the characterization of charge distribution in different materials, i.e., graphite, gold, palladium and silver. The aerosol particles were generated by spark discharge, and their particle number distributions with respect to size and charge were obtained using a tandem differential mobility analyzer (TDMA). They found asymmetry in the particle size distributions between negative and positive charges with positive charge distributions showing higher concentrations and neutral size distributions showing the highest particle concentration. This work further established the usefulness of the TDMA technique for measuring size and charge distributions of aerosols and led to a later experimental work focused on coagulation of charged aerosols (Simones and Loyalka, 2015), which we will present next.

To explore the importance of electrostatic effects in coagulation and generate experimental data about the evolution of charged polydisperse single-component aerosols, Simones and Loyalka (2015) measured the evolution of size and charge distributions over time and compared the results with the DSMC program developed by

Palsmeier and Loyalka (2013). They used a TDMA to measure size and charge distributions and created a program to automate and expedite the voltage stepping process required in the first differential mobility analyzer (DMA). Two types of single-component aerosols (graphite and silver) were generated by spark discharge to study their evolution. An open-flow coagulation tube was designed and built to facilitate the measurement of the aerosol at different residence times. More details about this work as the schematic of the experimental setup used by Simones and Loyalka (2015) are presented in Chapter 4. Results from the experimental measurements show that the silver aerosol was bipolar while the graphite aerosol showed a strong charge asymmetry with higher concentrations of positively charged particles. Comparisons between measurements of charge distributions and the DSMC program's results showed that for the spark-generated silver nanoparticles, a good agreement was found for short interaction times, but the DSMC program predicted higher concentrations for larger interaction times. For both types of aerosols, DSMC simulation results shifted toward smaller diameters for larger times suggesting the presence of additional mechanisms in coagulation, which may not be accounted for in the simulation. Simones and Loyalka (2015) concluded that possible discrepancies are the presence of background ions from the spark generation process and shape effects, especially in carbon agglomerates.

Campbell and Loyalka (2015) studied only the coagulation process in order to compare the strengths and weaknesses of both the sectional and DSMC techniques. The DSMC technique simulates multi-component aerosols with accuracy and can easily include additional processes or properties of the aerosol, but it is slower than the sectional technique, and requires several runs for statistical purposes. As its name indicates,

sectional technique results are divided into sections to calculate the particle number and mass distributions. As the section represents larger particle sizes, its width increases; thus, the assumptions made in the sectional technique affect more the accuracy of the simulation. The two main assumptions are: 1) each particle in the system has the same mass density, regardless of component type, and 2) the mass fractions for each component within a section are equal (preventing the use of different component distributions). Campbell and Loyalka (2015) investigated the approximations made in the sectional technique and explored the coupling of these two methods for improved simulations. The first method proposed for coupling was calculating the mean mass fraction for every section using a DSMC simulation; then, run the sectional technique, but changes in the latter made the computation much slower. The second method proposed was to combine both techniques in a hybrid program. The DSMC simulation would be run when the multicomponent analysis was most important; otherwise, the sectional technique would be run. The conversion from a mass distribution to a particle list required by the second approach made it computationally expensive and not feasible.

To contribute to the verification and validation of the DSMC technique for aerosols, Saldivar et al. (2018) reported additional benchmarks of this method against three analytical solutions. One was previously reported, and two were newly obtained. The three benchmark problems were:

(1) a single-component aerosol with constant coagulation, condensation, and deposition rates,

(2) a two-component aerosol with constant coagulation and condensation rates, and

(3) a two-component aerosol with constant coagulation and deposition rates. The new analytical results were obtained for problems (1) and (3). After comparing the results obtained by the DSMC technique with these exact solutions of the GDE, we found the error in the number of particles at different times of the simulation were not larger than 0.5, 0.8, and 0.67 % for problems (1), (2), and (3) respectively. The error in the estimation of component mass for problems (2), and (3) were not larger than 0.22 and 2.1%, respectively. This agreement in the results provided confidence toward making further progress in the methodology.

All the previous studies discussed thus far have assumed a homogenous distribution of aerosols particles. But Campbell et al. (2016) and Boraas and Loyalka (2018) explored spatially inhomogeneous aerosol DSMC models, trying complex geometries and various particle clustering methods. Boraas and Loyalka (2018) were able to simulate deposition, coagulation and condensation inside certain geometries considering diffusive motion.

Table 1 summarizes of the different implementations of the DSMC technique for homogeneous aerosols in chronological order. It gives an overview of the overall progress in this area by the NSEI group, which includes the processes considered and comparisons made with other solutions.

Table 1. Characteristics of the implementations of DSMC for homogenous aerosols.

Authors	Number of components	Processes included	Benchmarked/ compared to	Collisional Sampling	Comments
Loyalka (2003)	Two components aerosol with same densities	Coagulation (constant)	Sectional (MAEROS) technique and analytical solution	N/A	Started exploration of DSMC method in aerosols
Rangaraj and Loyalka (2004)	Multi-component aerosol with different densities	Brownian Coagulation	Sectional (MAEROS) technique	DS	Sectional technique had problems when component densities were different
Palaniswaamy and Loyalka (2006)	Seven components aerosol with different densities	Brownian, gravitational and turbulent coagulation	N/A	DS and Metropolis	Applied realistic coagulation kernel and reduced computation time using Metropolis algorithm
Palaniswaamy and Loyalka (2007a)	Seven components aerosol with different densities	Brownian, gravitational and turbulent coagulation	Compared the different sampling algorithms	DS, Metropolis, NTC method and modified DS.	Verified the applicability of various sampling algorithms to reduce computation time
Palaniswaamy and Loyalka (2007b)	Seven components aerosol with both the same and different densities	Brownian, gravitational and turbulent coagulation; Deposition; and Source reinforcement	Analytical solution for total number of particles and sectional technique	Metropolis	Added new aerosol processes and confirmed the problem with a single mean density assumption in the sectional technique
Palaniswaamy and Loyalka (2008)	Single component aerosol	Condensation alone and condensation combined with coagulation (linear* coagulation rate)	Analytical solutions with combinations of constant and linear* rate processes	Metropolis	Benchmarked the DSMC method with several analytical solutions and added the process of condensation
Palsmeier and Loyalka (2013)	Single-component, mono-disperse and polydisperse aerosol	Brownian coagulation with modifications for charge effects and electrostatic dispersion	Numerical solutions obtained by (Adachi et al., 1981; Oron and Seinfeld, 1989; Vemury et al., 1997)	NTC method	Incorporated charge effects to the coagulation kernel and the process of electrostatic dispersion. Compared the evolution of charged and neutral aerosols
Campbell and Loyalka (2015)	Single- and two-component aerosols	Coagulation, linear coagulation rate for single-component and constant for two-component aerosols	Analytical solutions and sectional technique	NTC method	Explored in detail the sectional technique assumptions and its coupling with DSMC model. Explained effects of particle component distribution in mass/volume determination
Saldivar et al. (2018)	Single- and two-component aerosols	Different combinations of coagulation, condensation and deposition. All with constant rates	Analytical solutions	NTC method	Presented new analytical solutions to the GDE involving more complex problems. The DSMC method was benchmarked to these solutions, resulting in a very good agreement

*Linear rates are dependent of particle volume.

3. DSMC SIMULATIONS FOR MULTI-COMPONENT CHARGED AEROSOLS

We have developed a DSMC program to simulate the evolution of multiple-species polydisperse aerosols, taking each particle as an entity having a specific percentage of several components and a specific electric charge. Each component making up a particle can have a different density. The processes simulated are: deposition, electrostatic dispersion, coagulation (considering the effect of electric charge on particles), and condensation. The equation to obtain the particle number distribution function with the above processes included for a well-mixed, multispecies polydisperse aerosol with spherical particles is the following version of GDE given as:

$$\begin{aligned}
&\frac{\partial}{\partial t} n_p(\boldsymbol{v},\boldsymbol{m},t) + R(\boldsymbol{v},\boldsymbol{m},t)\, n_p(\boldsymbol{v},\boldsymbol{m},t) + \sum_{c=1}^{N} \frac{\partial}{\partial v_c}\left[I_c(\boldsymbol{v},\boldsymbol{m},t)\, n_p(\boldsymbol{v},\boldsymbol{m},t)\right] = \\
&\quad \frac{1}{2}\sum_{q=-\infty}^{\infty} \int_0^{\infty} d\boldsymbol{u} \int_0^{\infty} d\boldsymbol{w} \int_0^{\infty} d\boldsymbol{x} \int_0^{\infty} d\boldsymbol{s}\; n_q(\boldsymbol{u},\boldsymbol{x},t)\, n_{p-q}(\boldsymbol{w},\boldsymbol{s},t)\, K_{p-q,q}(\boldsymbol{u},\boldsymbol{x}\,|\,\boldsymbol{w},\boldsymbol{s}) \\
&\quad \prod_{c=1}^{N} \delta(v_c - u_c - w_c)\, \delta(m_c - x_c - s_c) \qquad (4) \\
&\quad - n_p(\boldsymbol{v},\boldsymbol{m},t) \sum_{q=-\infty}^{\infty} \int_0^{\infty} d\boldsymbol{u} \int_0^{\infty} d\boldsymbol{x}\; K_{p,q}(\boldsymbol{u},\boldsymbol{x}\,|\,\boldsymbol{v},\boldsymbol{m})\, n_q(\boldsymbol{u},\boldsymbol{x},t) \\
&\quad - B(\boldsymbol{v},\boldsymbol{m}) \frac{e^2}{\varepsilon_0} n_p(\boldsymbol{v},\boldsymbol{m},t)\, p \sum_{q=-\infty}^{\infty} q \int_0^{\infty} d\boldsymbol{u} \int_0^{\infty} d\boldsymbol{x}\, n_q(\boldsymbol{u},\boldsymbol{x},t)
\end{aligned}$$

where $n_p(\boldsymbol{v},\boldsymbol{m},t)$ is the continuous particle size density function for particles with charge pe (e is the elementary charge and p is the number of charges), at time t, with components having volumes $\boldsymbol{v} = v_1, v_2, ..., v_c$ and masses $\boldsymbol{m} = m_1, m_2, ..., m_c$, $R(\boldsymbol{v},\boldsymbol{m},t)$ is the removal function, $I_c(\boldsymbol{v},\boldsymbol{m},t)$ is the condensation function, and $K_{p,q}(\boldsymbol{u},\boldsymbol{x}\,|\,\boldsymbol{v},\boldsymbol{m})$ is the

coagulation kernel. The delta functions help to ensure conservation of volume and mass in a collision, $B(\boldsymbol{v},\boldsymbol{m})$ is a function to calculate the mobility of the particles, ε_0 is the permittivity of free space, *q* takes the value of the different charge levels found in the aerosol particles, and $d\boldsymbol{v} = dv_1 dv_2 ... dv_c$ for the different variables representing the particle density function. The functions for the different processes will be described in more detail later in this chapter.

Compared to equation (1), this GDE is much more complex with the inclusion of charge effects. Equation (4) also uses realistic expressions for the different functions of the processes involved, making it impossible to get analytical solutions and very difficult to get numerical ones with methods like the sectional technique. However, it is possible to simulate this problem with the DSMC method without making a lot of assumptions that compromise the accuracy of the results. Throughout the rest of this chapter, we will consider the particle density function as $n_p(\boldsymbol{v},t)$ because only the volumes of the different particle components are saved in the particle list. Moreover, an additional list is available with the densities of each component, so masses can be easily obtained.

3.1 Initial particle list

The description of the DSMC program we created for this work is as follows. Each particle is represented by an element in a list, and each of these elements is in a sublist which contains the volumes for the different components of the particle including an extra component to keep track of the volume gained by condensation, and the number of electric charges in that particle. Figure 1 shows a representation of a simulated particle made up of three different components besides water and a charge level of −q.

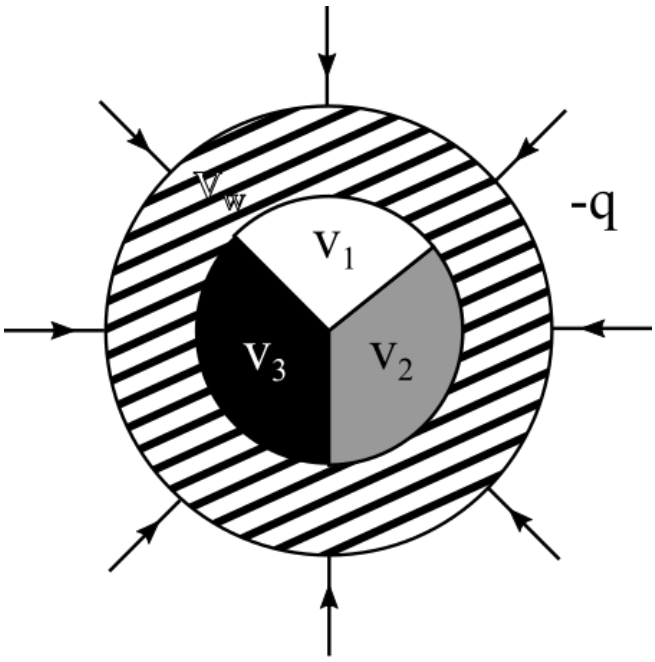

Figure 1. Depiction of a simulated particle representing the volumes of 3 components (V_1, V_2, and V_3) surrounded by water (stripes) and a negative charge level q.

The initial particle list for the simulation can be obtained from measurements of size and charge distributions, like those obtained from a TDMA (Simones et al., 2011; Simones and Loyalka, 2015) or by sampling from a known distribution using the inversion method. Creating an initial particle list extracted from experimental data is necessary when one wants to compare measurements with simulations. In the system developed by Simones and Loyalka (2015), one obtains a number distribution for every charge level (positive, negative, and neutral) considered in the experiment. Each bin in these distributions have the frequency (per unit of volume) for the different particle sizes (in 20 different size bins) measured by the instruments. After adding all frequencies for the different size bins, we obtained the total number of particles. Due to computer's memory and speed limitations, simulations cannot run with the large number of particles found in experiments (~ 10^{11}), a smaller number of simulated particles must be used

instead (~ 10^5). A factor relating to the actual number of particles in the aerosol and the number of simulated particles, $f = N_{real} / N_{sim}$, is used to scale down the data in the measured distributions to the desired number of simulated particles. For this work, data from the particle number distributions measured from a spark generated graphite aerosol was fitted to lognormal distributions, as shown in equation (5), because these functions represent the data very well. Values for the mean x and the standard deviation σ were obtained from the number distribution corresponding to the different charge levels measured.

$$f(x) = \frac{1}{\sqrt{2\pi}x\sigma} \mathrm{e}^{-\frac{(-\mu+\log[x])^2}{2\sigma^2}} \tag{5}$$

Using these parameters, mean, and standard deviation, values for diameters of particles can be sampled from the lognormal distributions by acceptance-rejection. Mathematica® has a dedicated command to perform this task, which is referred to as RandomVariate (Wolfram Research Inc., 2018). Also, it is important to consider the fraction of the total particles that is in every charge level in order to reproduce this in the simulation. So, the fraction of total particles in every charge level was calculated from the measurements, and it was used to determine the number of particles for a specific size that are going to be created for the simulation. Each particle generated is associated with its corresponding charge level. The range of particle sizes falls between the smallest and largest size bin used in the measurements, and these depend on specific parameters of the TDMA (i.e., sheath flow, polydisperse aerosol flow, etc.). As previously mentioned, the particle parameters saved in the list are component volumes and the number of charges. With each particle diameter obtained by acceptance-rejection, one can calculate the total

volume of the particle but not the volume or mass of its components since data obtained from measurements with a TDMA do not include any information about the components or their proportions. Thus, assumptions need to be made based on previous knowledge about the experimental setup for the generation of the aerosol or according to the particle composition we want to test. At our laboratory, a spark generator is used to produce nanoparticles; thus, a simple way to generate a two-species aerosol is to use electrodes (i.e., material of interest for nanoparticle generation) of different materials in the device or alloyed electrodes with known mass fractions. Another approach is to use two separate spark generators (each one generating a specific material) and then mix their streams into one. However, it is difficult to measure how much of each component is being injected into the aerosol mainly because the particles produced are very small (from 6 nm to approximately 230 nm). The next chapter will have more information about generation and characterization of particles; thus, as mentioned earlier, an assumption is made for the particle composition based on the mass fraction of each component (e.g., fifty percent of the total mass for each component) to calculate their volumes in the particle list. It is also possible to use a certain distribution for the particle composition, which was evident when the particles generated by spark discharge notably had a distribution of composition rather than a uniform composition (Tabrizi et al., 2008b; Tabrizi et al., 2010). Finally, as many particles as indicated by the product of the fraction particles for each charge level and the total number of simulated particles are created for each charge considered. Volumes for each component are assigned based on the particle diameter chosen in the acceptance-rejection process and on the assumptions about particle composition. This process is applied using lognormal functions representing particle number distributions

for the different charge levels in the aerosol. The format of the particle list for a problem considering aerosol particles with two components and water is shown in Figure 2. This list represents the aerosol, and it is modified at each time step by all the processes mentioned above either by deleting particles or by modifying their component volumes and charge. Each row in the left column of Figure 2 (particle list) represents a particle.

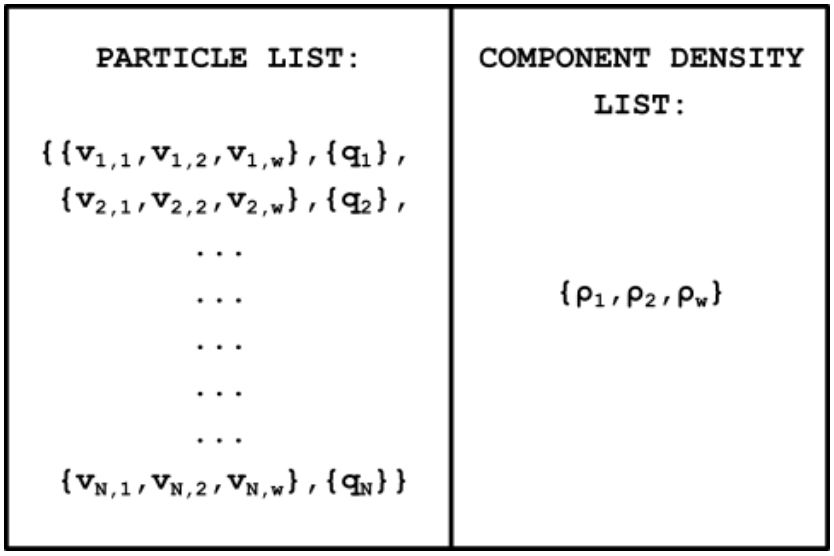

Figure 2. Format for particle and component density lists used in a DSMC simulation considering aerosol particles made up of two components and water.

The particle list stores the volumes of the different components for each particle and its charge. The first subscript in the v values and the q values indicate the particle number with N being the total number of simulated particles. The second subscript in the v values represents the component number, and w is water. The subscripts of the component density list represent component number.

After the creation of the initial particle list, one can choose the processes to run in the simulation, the time step, and the number of runs or total time. Also, other parameters like temperature, pressure, etc., are given as inputs to match experimental conditions. The

density of the different components is given as a list with the length of the number of components plus one, with the last element being the density of water, as shown in Figure 2. The order in which the different processes run and modify the particle list is: electrostatic dispersion, deposition, coagulation, and condensation. This order is chosen to ensure that slower physical processes are not overshadowed by faster ones.

3.2 Electrostatic Dispersion

The main module of this DSMC program applies the different processes mentioned above using physical models to track the fate of aerosol particles represented by elements in a list. The main module covers all the required tasks to run during a time steps (Δt) starting with electrostatic dispersion. In this process all particles are tested for potential removal comparing their electric charge to the net charge of the aerosol. The dispersion model applied in the GDE is:

$$\frac{dn_p(\boldsymbol{v},t)}{dt} = -B(\boldsymbol{v})\frac{e^2}{\varepsilon_0} n_p(\boldsymbol{v},t)\, p \sum_{q=-\infty}^{\infty} q \int_0^{\infty} n_q(\boldsymbol{u},t)\, d\boldsymbol{u} \tag{6}$$

where:

$$B(\boldsymbol{v}) = \frac{C}{3\pi\mu d}$$

$$C = 1 + \mathrm{Kn}\left[1.37 + 0.4\exp\left(-1.1/\mathrm{Kn}\right)\right]$$

$$\mathrm{Kn} = 2\lambda / d$$

$$\lambda = \lambda_{ref}\left(\frac{P_{ref}}{P_\infty}\right)\left(\frac{T_\infty}{T_{ref}}\right)\left(1+\frac{T_s}{T_{ref}}\right)\Big/\left(1+\frac{T_s}{T_\infty}\right)$$

$B(\boldsymbol{v})$ is the mobility of a particle whose total volume is given by $\sum_{c=1}^{N} v_c$, and this volume is used to get the particle diameter assuming a spherical shape; *e* is the elementary electric charge; ε_0 is the permittivity of free space; *p* is the number of charges of the particle being tested; *q* takes the value of the different electrical charge levels in the aerosol; *C* is the Cunningham correction factor; μ is the viscosity of the suspending gas; *d* is the diameter of the particle; Kn is the Knudsen number; λ is the gas mean free path at temperature T_∞ , and pressure P_∞ ; T_{ref} and P_{ref} are reference temperature and pressure; and T_s is the Sutherland's constant.

Net charge is represented by $\sum_{q=-\infty}^{\infty} q\int_0^\infty n_q(\boldsymbol{u},t)\,d\boldsymbol{u}$. Equation (6) can be simplified to:

$$\frac{dn_p(\boldsymbol{v},t)}{dt} = -\alpha\, n_p(\boldsymbol{v},t)\, p \tag{7}$$

where $\alpha = -B(\boldsymbol{v})\frac{e^2}{\varepsilon_0}\sum_{q=-\infty}^{\infty} q\int_0^\infty n_q(\boldsymbol{u},t)\,d\boldsymbol{u}$, and it is taken as a constant for a specific particle. Equation (7) has the following solution:

$$n_p(\boldsymbol{v},t) = n_p(\boldsymbol{v},0)\exp(-\alpha\, p\, t) \tag{8}$$

which can be expressed as:

$$\ln[n_p(\boldsymbol{v},t+\Delta t)/n_p(\boldsymbol{v},t)] = -\alpha\, p\,\Delta t \tag{9}$$

From the above expression, a selection-rejection technique is implemented, and the program removes particles which satisfy the two following conditions:

$$\Delta t > \frac{-\ln[Random(0,1)]}{\alpha\, p\, f} \quad \text{and} \quad \alpha\, p\, f > 0 \tag{10}$$

where $Random(0,1)$ is a pseudorandom real number in the range of 0 to 1.

The second condition in equation (10) is satisfied when the net charge of the aerosol and the particle charge being tested have the same polarity (which results in repulsion). Before deleting the particles selected to be dropped, the number of particles to be removed, their mean diameter and their most common charges are stored for further analysis. The factor *f* is needed here again to scale the number of particles in the simulation to the total number of particles in an experiment. Thus, the removal of particles lost by electrostatic dispersion is the first modification to the particle list, and it is followed by the process of deposition.

3.3 Deposition

The next process is deposition, which is much like electrostatic dispersion in the test used to decide if a particle is dropped, using the deposition rate, the natural logarithm of a pseudorandom number, and the time step. The model used to calculate the deposition rate considers two processes, gravitational settling and convection-diffusion. Larger particles settle more readily because of gravity while smaller particles undergo deposition primarily by convection-diffusion (Park, 1988). The deposition rate is given by the following equation:

$$R(\boldsymbol{v}) = R_{gravity} + R_{diffusional} = \left(-\frac{A_{floor} V_T}{V_{chamber}} \right) + \left(-\frac{D}{\Delta} \left(\frac{A_{wall}}{V_{chamber}} + \frac{A_{floor}}{V_{chamber}} + \frac{A_{ceiling}}{V_{chamber}} \right) \right)$$

(11)

where:

$$D = \frac{k_B T C}{3\pi d \eta \chi}$$

$$V_T = \frac{\rho_p g\, d^2 C}{18\eta\chi}$$

where A_{floor}, A_{wall}, and $A_{ceiling}$ are the floor, wall, and ceiling surface areas of the chamber containing the aerosol; V_T is the particle settling velocity; $V_{chamber}$ is the volume of the chamber; D is the particle diffusivity or diffusion coefficient; Δ is the diffusion boundary layer thickness; k_B is the Boltzmann constant; T is the absolute temperature; C is the Cunningham correction factor; d is the diameter of the particle considering a sphere with a volume equal to $\sum_{c=1}^{N} v_c$; η is the gas viscosity; χ is the dynamic shape factor; ρ_p is the particle density calculated as $\sum_{c=1}^{N} v_c \rho_c \Big/ \sum_{c=1}^{N} v_c$; and g is the acceleration due to gravity.

Considering deposition alone in the GDE, we have a differential equation parallel to the radioactive decay equation:

$$\frac{dn_p(\boldsymbol{v},t)}{dx} = -R(\boldsymbol{v})\, n_p(\boldsymbol{v},t) \tag{12}$$

Using a procedure similar to electrostatic dispersion (equations (7) to (10)), the following condition is established to test particles for removal. All particles are tested and if the following condition is true, they are removed from the particle list:

$$\Delta t > \frac{-\ln[Random(0,1)]}{R(\boldsymbol{v})} \tag{13}$$

The number of particles removed, their mean diameter and their most common charges are stored for further analysis.

3.4 Coagulation

The next process is coagulation, and the first step in the simulation of coagulation is to calculate the number of pairs of particles which interact in an interval of time Δt. This number is obtained using the NTC method. First developed by Bird (1994) to simulate rarefied molecular gas dynamics, the NTC method has also been used in the simulation of aerosols (Campbell and Loyalka, 2015; Palaniswaamy and Loyalka, 2007a; Palsmeier and Loyalka, 2013). The number of collisions is given by the following equation:

$$n_{pairs} = \frac{1}{2} f N_{sim}^2 K_{\max} \Delta t \tag{14}$$

where *f* is the ratio of the number of real particles in the aerosol to the number of particles in the simulation ($f = N_{real} / N_{sim}$), $K_{\max}$ is the maximum value for the coagulation rate found so far in the simulation, and Δt is the time step considered for the simulation step. Note that not all collisions result in particles coalescing. An initial estimation of the maximum coagulation rate is made (K_{ini}) at the start of the simulation, based on a sample of 100 randomly selected particles. This results in a value that is a good approximation of $K_{\max}$ that is not too slow and thus underestimating the coagulation rate.

K_{ini} and $K_{\max}$ are calculated using a coagulation kernel, which estimates the rate of coalescence of two particles based on its size and charge among other properties. Several factors lead to the collision of two particles like the Brownian motion of particles, gravitational and turbulence effects, acoustics, etc. Brownian diffusion is dominant for the particle size range considered in this work (Hidy and Brock, 1972); hence, we consider only Brownian motion ($\beta_{Brownian}$), as described in the MAEROS

manual (Gelbard, 1982), and a multiplier, which considers the electric charge effects in coagulation ($\beta_{p,q}$) (Adachi et al., 1981; Fuchs, 1964; Vemury et al., 1997), as shown in the model for the coagulation kernel described below:

$$K_{p,q}\left(\boldsymbol{u},\boldsymbol{v}\right)=\beta_{Brownian}\beta_{p,q} \tag{15}$$

$$\beta_{Brownian}=\frac{2\pi\left(D_i+D_j\right)\left(\gamma_i d_i+\gamma_j d_j\right)}{\left(\dfrac{d_i+d_j}{d_i+d_j+2\sqrt{g_{di}^2+g_{dj}^2}}+\dfrac{8\left(D_i+D_j\right)}{\sqrt{V_i^2+V_j^2}\left(d_i+d_j\right)}\right)} \tag{16}$$

$$\beta_{p,q}=\begin{cases}\dfrac{\lambda_{p,q}}{\exp\left(\lambda_{p,q}\right)-1}, & \text{for repulsion}\\ \dfrac{\left|\lambda_{p,q}\right|}{1-\exp\left(-\left|\lambda_{p,q}\right|\right)}, & \text{for attraction}\end{cases} \tag{17}$$

where

$$D_i=\frac{k_B T C_i}{3\pi d_i \eta \chi_i},$$

$$C_i=1+\mathrm{Kn}_i\left[1.37+0.4\exp\left(-1.1/\mathrm{Kn}_i\right)\right]$$

$$\mathrm{Kn}_i=2\lambda/d_i,$$

$$\lambda=\lambda_{ref}\left(\frac{P_{ref}}{P_\infty}\right)\left(\frac{T}{T_{ref}}\right)\left(1+\frac{T_s}{T_{ref}}\right)\Big/\left(1+\frac{T_s}{T}\right)$$

$$g_{di}=\frac{1}{3D_i\ell_i}\left[\left(d_i+\ell_i\right)^3-\left(d_i^2+\ell_i^2\right)^{3/2}\right]-d_i,$$

$\ell_i=\dfrac{8d_i}{\pi V_i}$, and

$$V_i=\sqrt{\frac{8k_B T}{\pi m_i}},$$

$$\lambda_{p,q} = \frac{p\,q\,e^2}{2\pi\,\varepsilon_0 k_B T\left(d_i + d_j\right)},$$

where the subscripts *i* and *j* are the particle indices; *D* is the particle diffusion coefficient; γ is the collision shape factor; *d* is the particle diameter calculated considering the volume of a sphere equal to $\sum_{c=1}^{N} u_c$ for particle *i*, and $\sum_{c=1}^{N} v_c$ for particle *j*; g_d represents the distance between the real surface of the particle and the spherical surface enclosing the actual particle as assumed by Fuchs (1964); *V* is the particle speed; $\lambda_{p,q}$ is the ratio of electrostatic to kinetic potential energy of colliding aerosol particles; k_B is the Boltzmann constant; *T* is the absolute temperature; η is the gas viscosity; χ is the dynamic shape factor; *C* is the Cunningham correction factor for each particle; Kn is the Knudsen number; λ is the gas mean free path at temperature T, and pressure P_∞; T_{ref} and P_{ref} are reference temperature and pressure; T_s is the Sutherland's constant; ℓ is the apparent mean free path of the particle; m is the particle mass calculated by $\sum_{c=1}^{N} u_c \rho_c$ for particle *i*, and $\sum_{c=1}^{N} v_c \rho_c$ for particle *j*; *p* and *q* are the numbers of elementary charges of the *i*th and *j*th particles interacting; *e* is the elementary electrical charge; and ε_0 is the permittivity of free space.

The number of collisions calculated (n_{pairs}) might require more than the remaining number of particles in the simulation when it has been run for a long time, so the program only runs if the number of collisions is less than half the number of simulated particles (two particles per collision). After the number of collisions is calculated by equation (14), the same number of pairs of particles are randomly selected.

Then, for every pair (potential collision), the coagulation rate is determined using equations (15) to (17). The pairs that actually collide and generate new particles must satisfy the following condition:

$$\frac{K_{p,q}}{K_{\max}} \geq Random(0,1) \tag{18}$$

where $K_{\max}$ is the maximum coagulation rate found so far in the ongoing iterations of the simulation. It takes the value of K_{ini} at the beginning of the simulation, and it is updated when a larger value is found. If the condition in equation (18) is met, the properties of the pairs of particles selected are added; then, the volumes of like components and the amount of electrical charges are summed and saved as new particles in a new list dedicated to this purpose. The number of new particles and their mean diameter as well as the most common charges of the interacting particles (whose similar component volumes and charges were added) are saved. Then the interacting particles are deleted from the main particle list and the program checks if there is a value of $K_{p,q}$ larger than the current $K_{\max}$ in the collisions tested. If this happens, $K_{\max}$ is updated. The new and bigger particles resulting from coagulation are not included in the particle list yet; instead, they are saved in a separate list which will be joined to the main particle list once the steps for the condensation process (next process) are applied. Saving them in separate list is to keep these particles from undergoing both coagulation and condensation in the same time step (Δt). Values of n_{pairs} and $K_{\max}$ are also saved at each time step for further analysis.

3.5 Condensation

The last and fastest of the processes (physically, but not in the simulation) is condensation; here, particles grow based on the humidity of the system. We use a generalization of Mason's formula to calculate the volume gained per time (also referred to as the condensation rate), which is dependent on particle size. It is shown in the following equation which includes Knudsen effects but Kelvin and solute effects are neglected (Saldivar, 2018):

$$\psi(\boldsymbol{v}) = 4\pi\left(\frac{3\boldsymbol{v}}{4\pi}\right)^{1/3} D_v \rho_s \left[(S-1)\right] \frac{f_c\left(\mathrm{Kn}_c\right) f_h\left(\mathrm{Kn}_h\right)}{\left(\frac{L\,D_v}{K}\right)\rho_s \beta\, f_c\left(\mathrm{Kn}_c\right) + f_h\left(\mathrm{Kn}_h\right)} \tag{19}$$

where

$$f_c\left(\mathrm{Kn}_c\right) = \left[1 + \mathrm{Kn}_c\left(\frac{\left(F_{cont}/F_{fm}\right)_c \xi_c + \zeta_c}{\mathrm{Kn}_c \xi_c + 1}\right)\right]^{-1}$$

$$f_h\left(\mathrm{Kn}_h\right) = \left[1 + \mathrm{Kn}_h\left(\frac{\left(F_{cont}/F_{fm}\right)_h \xi_h + \zeta_h}{\mathrm{Kn}_h \xi_h + 1}\right)\right]^{-1}$$

$$\mathrm{Kn}_c = \frac{\lambda_D}{r_i}, \quad \mathrm{Kn}_h = \frac{\lambda_t}{r_i}$$

$$\left(\frac{F_{cont}}{F_{fm}}\right)_c = \sqrt{\pi}\mathrm{Kn}_c, \quad \left(\frac{F_{cont}}{F_{fm}}\right)_h = \frac{5}{4}\sqrt{\pi}\mathrm{Kn}_h$$

$$\lambda_D = 2D_v\left(\frac{m_v}{2k_B T_\infty}\right)^{1/2}, \quad \lambda_t = \frac{4}{5}\frac{K\,T_\infty}{P_\infty}\left(\frac{m_g}{2k_B T_\infty}\right)^{1/2}$$

$$\xi_c = 1.333, \quad \xi_h = 1.9234$$

$$\zeta_c = 1.0161, \quad \zeta_h = 1.1759\frac{5}{8}\sqrt{\pi}$$

$$\beta = \frac{L m_v}{k_B T_\infty^2}$$

where $\boldsymbol{v}$ is the sum of the volumes of the different components in the particle $\left(\sum_{c=1}^{N} v_c\right)$; D_v is the diffusion coefficient of the vapor; ρ_s is the saturation density of vapor at ambient conditions $\left(T_\infty\right)$; S is the saturation ratio; factors $f_c\left(\mathrm{Kn}_c\right)$ and $f_h\left(\mathrm{Kn}_h\right)$ account for the Knudsen effects (Loyalka and Park, 1988); r_i is the radius of the spherical particle corresponding to volume $\sum_{c=1}^{N} v_c$; m_v is the vapor molecular mass; k_B is the Boltzmann constant; T_∞ is the ambient temperature; K is the thermal conductivity of the mixture; P_∞ is the ambient pressure; m_g is the background gas molecular mass; and L is the latent heat of vaporization.

The condensation rate is calculated for all simulated particles except for the new particles generated by coagulation in the current time step. The volume added to each of these particles is equal to $\psi\left(\boldsymbol{v}\right)\Delta t$. This volume gained is added to the last element of the particle's sublist, which is dedicated to tracking the amount of water in the particle. The total volume of water added at each time step is saved for further analysis.

3.6 Final processing

After the volume gained from condensation has been added to each element of the main particle list, the separate list with the particles generated from coagulation and the main particle list are joined. This task concludes the activities that modify the particle list in a single time step. Finally, the program prints the information to track the evolution of

the aerosols as: initial and final number of particles, initial and final volume, number of particles dropped by electrostatic dispersion, mean diameter and most common charges of those particles, number of particles dropped by deposition, mean diameter and most common charges of those particles, number of pairs tested for coagulation, number pairs that actually collided and formed new particles, mean diameter and most common charges of the particles coalescing, the current value of $K_{\max}$, and the total volume added by condensation in the time step.

The steps described in sections 3.2 to 3.6 are repeated until the number of iterations selected (based on the total time for simulation) is reached. A particle list is saved at the end of each time step, these lists are used to create tables with data such as mean aerosol particle diameter, mean mass of each particle component, mean particle density, and relative frequency of particles in the different charge levels. Also, these particle lists are used to make plots of number and component mass distributions with and without discrimination of charge levels to study the evolution of the aerosol.

3.7 Simulations of Carbon-Silver Aerosols

Using the program described above, we considered the problem of modeling the evolution of carbon-silver aerosols with different particle compositions including the processes of electrostatic dispersion, deposition, coagulation and condensation. The initial particle lists for these simulations were obtained from TDMA measurements of size and charge distribution from graphite nanoparticles, using constants and parameters equal to those used in these simulations (which will be presented later in this section). The neutral, positively, and negatively charged size distributions of the experiment were

fitted to lognormal distributions (equation (5)) and then the particle diameters were sampled from them. The values for the mean and the standard deviation of these distributions are shown in Table 2. Four distributions of positive charge levels and four of negative charge levels plus the distribution for neutral particles were used: −4, −3, −2, −1, 0, +1, +2, +3, and +4. The distributions for graphite show asymmetry between negative and positive charge levels with the same number of charges (i.e., +1 and −1, +2 and −2, etc.), with positive charges having more particles. The total number of particles measured in the experiment where these distributions were obtained was 1.9×10^{11}. With the purpose of creating around 100,000 particles for the simulation, pseudorandom variates for the particle diameter were obtained from these distributions. The number of particles in the simulation for each charge level agree with the fraction of the total number of particles for the different charges shown in Table 2. These fractions were obtained from the measurements mentioned previously. From the sampled particle diameter and the desired component mass fractions (particle composition), the volume for the different components was determined. For a problem involving two components, their volumes are calculated by the following equations:

$$v_1 = \frac{mf\ v_T}{mf + (1-mf)\dfrac{\rho_1}{\rho_2}} \tag{20}$$

$$v_2 = \frac{(1-mf)\,v_T}{(1-mf) + mf\dfrac{\rho_2}{\rho_1}} \tag{21}$$

where v_1 and v_2 are the volumes of components 1 and 2, respectively; mf is the fraction of the total mass of the particle assigned to component 1, leaving component 2 with a fraction of $(1-mf)$; v_T is the total volume of the particle (obtained from its diameter

considering a spherical shape); and $\rho 1$ and $\rho 2$ are the densities of components 1 and 2, respectively.

Table 2. Values for the mean, standard deviation and fraction of total particles in the lognormal distributions used to generate the initial particle list.

Charge level	Mean (μ)	Standard deviation (σ)	Fraction of total number of particles
−4	4.37071	0.292887	0.00003
−3	4.15887	0.27829	0.00030
−2	3.93296	0.299941	0.00472
−1	3.8275	0.435026	0.07166
0	3.83999	0.433734	0.71597
+1	3.78437	0.374704	0.12828
+2	3.99336	0.326592	0.04938
+3	4.15115	0.312869	0.01995
+4	4.24606	0.295176	0.00970

Two problems with different particle compositions were chosen for simulation: one aerosol with particles made up of 90% graphite and 10% silver and the other aerosol made up of particles having 10% graphite and 90% silver (in mass). Considering graphite as component one and silver as component two, the first problem corresponds to mf = 0.9, and the second problem to mf = 0.1 (equations (20) and (21)). The purpose of simulating these two problems is to explore how particle composition affects the evolution of aerosols having different proportions of graphite and silver in the particles (different particle density). The lognormal distributions shown in Table 2 are better suited for Problem 1 since they were obtained from pure graphite, but for Problem 2 (where silver mass dominates) one would expect more symmetrical charge distributions as shown by Simones et al. (2011) and Simones and Loyalka (2015). Nevertheless, in the absence of lognormal functions fitted to measurements of silver aerosols and with the purpose of having the same initial size distributions in both problems, the functions in Table 2 are also used for Problem 2.

The initial particle lists in both problems have a total of 71,597 neutral particles, 20,731 positively charged particles and 7,671 negatively charged particles. These add to a total of 99,999 particles, which leaves a scaling factor, *f*, of around 1.9×10^{6}. The various parameters and values used in the simulations are listed in Table 3.

Table 3. Simulation parameters and their values.

Parameter	Symbol	Value	Units
Graphite density	ρ_1	2,100	kg/m^3
Silver density	ρ_2	10,490	kg/m^3
Ambient temperature	$T,\ T_\infty$	296.15	K
Ambient pressure	P_∞	95,000	Pa
Reference temperature	T_{ref}	293	K
Reference pressure	P_{ref}	101,300	Pa
Sutherland's constant (air)	T_s	110.4	K
Reference gas mean free path	λ_{ref}	6.73×10^{-8}	m
Boltzmann Constant	k_B	1.38065×10^{-23}	J/K
Air viscosity @ ~300 K	μ	1.83245×10^{-5}	kg m^{-1} s^{-1}
Gravitational acceleration	g	9.81	m s^{-2}
Permittivity of free space	ε_0	$8.854187818\times10^{-12}$	F/m
Elementary electric charge	e	1.6019×10^{-19}	C
Ratio of floor area to volume (aerosol chamber)	$\frac{A_{floor}}{V_{chamber}}$	1.07	m^{-1}
Ratio of ceiling area to volume (aerosol chamber)	$\frac{A_{ceiling}}{V_{chamber}}$	1.07	m^{-1}
Ratio of walls area to volume (aerosol chamber)	$\frac{A_{wall}}{V_{chamber}}$	2.29	m^{-1}
Diffusion boundary layer thickness	Δ	10^{-5}	m
Saturation density of vapor @ 25°C	ρ_s	23×10^{-3}	kg/m^3
Diffusion coefficient of vapor	D_v	0.289×10^{-4}	m^2/s
Saturation ratio	S	1.0000001	dimensionless
Thermal conductivity of a gas-vapor mixture	K	2.7×10^{-2}	W m^{-1} K^{-1}
Latent heat of vaporization	L	2.257×10^{6}	J/kg
Vapor molecular mass	m_v	2.989×10^{-26}	kg
Gas molecular mass	m_g	4.65×10^{-26}	kg

3.7.1 Problem 1: Particle composition of 90% graphite and 10% silver

For this problem particle composition was chosen to be 90% graphite and 10% silver (in mass). A time step of 50 seconds was chosen because it allows enough time for significant activity in the different ongoing processes without having too many interactions, which would yield poorer results. The simulation was run for 30 time steps to reach a total time of 1500 seconds. Starting with general information about the number of particles and aerosol volume, Table 4 shows the initial and final number of simulated particles and the initial and final volume of the aerosol (no scaling) for all times considered. Total volume is increased in all time steps, starting with a gain of 15% from the initial value at the beginning of the simulation and decreasing steadily to 6% (relative to the initial total volume at each time step) in the end. This may be due to the change in composition of the aerosol as particles get more water causing their density to change (see Table 5), and to the reduction in the number of particles by various processes. However, condensation more than compensated for the volume lost, increasing the volume of the aerosol by around one order of magnitude at the end of the simulation. In terms of total number of particles, its reduction from the initial quantity in the first time step is around 10% and it decreased to 2% by the time of 750 seconds, then slowly went down to 1.2% at the final time step.

To identify some of the particles' properties from the population that remains suspended in the aerosol, Table 5 shows the mean particle diameter, the mean mass of each component and the mean density of the aerosol particles for each time step. The mean diameter is constantly increasing as a result of condensation, the removal of small particles by convection-diffusion and electrostatic dispersion, and by the effect of

coagulation. The mean masses for each component also increase as a result of small-sized particle removal and coagulation. The mean masses of graphite and silver per particle slowly and steadily grow while the growth of water mass is more pronounced. The ratio of graphite mass to silver mass is kept as 9 at all times, but these two materials which made up 100% of the particles' mass at the beginning, end up making up only 10% of the mean particle mass (9% graphite, 1% silver) while the rest (90%) is water in the final time step. This change in particle composition decreases the mean particle density, which is shown in the last column of Table 5. It starts with a value very close to graphite density declining rapidly to a value near water density. This phenomenon is produced only by condensation; however, it affects other processes in which particle density is a factor needed to determine the rate of interaction.

To get more details about the workings of each one of the active processes in the simulation, Tables 6, 7, and 8 show data of the particles interacting by electrostatic dispersion, deposition and coagulation, respectively. This information clarifies the evolution of the aerosol, principally on how the removal of particles takes place (for the first two processes) and what kind of particles are coalescing. These tables show the percentage of particles lost by each process relative to the total number of particles lost in each time step, the mean diameter of the particles interacting and their most common charges. For coagulation, Table 8 also shows the number of pairs of particles to be tested and the values of $K_{\max}$ for each time step. Note that the number of new particles resulting from coagulation represent at the same time a reduction in the number of particles at that time step because two particles coalesce to become one. Some of the values from these

tables need to be scaled to the whole aerosol population and this is indicated in the column title as "(no scaling)" or as a note at the end of the table.

Table 4. Number of particles and volumes for the different time steps of the simulation in Problem 1.

Time (s)	Initial number of particles	Final number of particles	Total initial volume (m^3)	Total final volume (m^3)	Total water volume gained (m^3) by condensation
50	99999	90063	1.20E−17	1.38E−17	2.19E−18
100	90063	83158	1.38E−17	1.58E−17	2.40E−18
150	83158	78035	1.58E−17	1.80E−17	2.62E−18
200	78035	73879	1.80E−17	2.04E−17	2.85E−18
250	73879	70436	2.04E−17	2.30E−17	3.09E−18
300	70436	67537	2.30E−17	2.58E−17	3.33E−18
350	67537	65090	2.58E−17	2.89E−17	3.58E−18
400	65090	62930	2.89E−17	3.22E−17	3.83E−18
450	62930	61028	3.22E−17	3.57E−17	4.10E−18
500	61028	59374	3.57E−17	3.95E−17	4.37E−18
550	59374	57905	3.95E−17	4.36E−17	4.64E−18
600	57905	56556	4.36E−17	4.79E−17	4.93E−18
650	56556	55294	4.79E−17	5.25E−17	5.21E−18
700	55294	54144	5.25E−17	5.74E−17	5.50E−18
750	54144	53079	5.74E−17	6.25E−17	5.79E−18
800	53079	52069	6.25E−17	6.79E−17	6.09E−18
850	52069	51184	6.79E−17	7.36E−17	6.39E−18
900	51184	50358	7.36E−17	7.96E−17	6.70E−18
950	50358	49498	7.96E−17	8.58E−17	6.99E−18
1000	49498	48717	8.58E−17	9.24E−17	7.30E−18
1050	48717	48026	9.24E−17	9.93E−17	7.62E−18
1100	48026	47343	9.93E−17	1.06E−16	7.94E−18
1150	47343	46675	1.06E−16	1.14E−16	8.25E−18
1200	46675	46016	1.14E−16	1.22E−16	8.57E−18
1250	46016	45363	1.22E−16	1.30E−16	8.87E−18
1300	45363	44823	1.30E−16	1.38E−16	9.21E−18
1350	44823	44243	1.38E−16	1.47E−16	9.52E−18
1400	44243	43702	1.47E−16	1.56E−16	9.83E−18
1450	43702	43137	1.56E−16	1.65E−16	1.01E−17
1500	43137	42626	1.65E−16	1.74E−16	1.05E−17

Note: Values for number of particles and volumes need to be scaled.

Table 5. Mean diameter, mean mass of each component and mean density of aerosol particles for each time step in Problem 1.

Time (s)	Mean particle diameter, *d* (nm)	Mean mass of graphite (kg)	Mean mass of silver (kg)	Mean mass of water (kg)	Mean particle density (kg/m^3)
0	61	2.47E−19	2.75E−20	0.00E+00	2283
50	66	2.65E−19	2.94E−20	2.44E−20	2079
100	71	2.79E−19	3.10E−20	5.42E−20	1916
150	76	2.89E−19	3.22E−20	8.95E−20	1784
200	81	2.99E−19	3.32E−20	1.30E−19	1676
250	85	3.07E−19	3.41E−20	1.77E−19	1587
300	90	3.14E−19	3.49E−20	2.29E−19	1513
350	95	3.20E−19	3.56E−20	2.88E−19	1451
400	99	3.26E−19	3.62E−20	3.52E−19	1398
450	104	3.31E−19	3.68E−20	4.24E−19	1354
500	108	3.36E−19	3.73E−20	5.02E−19	1315
550	113	3.40E−19	3.78E−20	5.87E−19	1282
600	117	3.45E−19	3.83E−20	6.80E−19	1254
650	122	3.49E−19	3.88E−20	7.80E−19	1229
700	126	3.53E−19	3.92E−20	8.88E−19	1208
750	131	3.56E−19	3.96E−20	1.00E−18	1189
800	136	3.60E−19	4.00E−20	1.13E−18	1172
850	140	3.63E−19	4.03E−20	1.26E−18	1158
900	144	3.65E−19	4.06E−20	1.40E−18	1144
950	149	3.69E−19	4.10E−20	1.55E−18	1133
1000	154	3.72E−19	4.13E−20	1.72E−18	1122
1050	158	3.75E−19	4.17E−20	1.89E−18	1113
1100	163	3.78E−19	4.20E−20	2.07E−18	1105
1150	167	3.81E−19	4.23E−20	2.25E−18	1097
1200	172	3.84E−19	4.26E−20	2.45E−18	1091
1250	176	3.87E−19	4.30E−20	2.67E−18	1085
1300	180	3.90E−19	4.33E−20	2.89E−18	1079
1350	185	3.93E−19	4.36E−20	3.12E−18	1074
1400	189	3.96E−19	4.40E−20	3.37E−18	1069
1450	194	3.99E−19	4.44E−20	3.63E−18	1065
1500	198	4.02E−19	4.47E−20	3.89E−18	1061

Table 6. Results from the interaction of particles by electrostatic dispersion (ED) in Problem 1.

Time (s)	Particles dropped by ED (no scaling)	Percentage of particles lost by ED	Mean diameter of particles lost by ED (nm)	Most common charges in particles dropped by ED
50	185	1.9%	50	+1, +2, +3, +4
100	112	1.6%	62	+1, +2, +4, +3
150	68	1.3%	60	+1, +2, +3, +4
200	62	1.5%	67	+1, +2, +3, +4
250	43	1.2%	74	+2, +1, +4, +3
300	32	1.1%	85	+1, +2, +3, +4, +6
350	27	1.1%	91	+4, +1, +2, +3
400	26	1.2%	98	+1, +2, +3
450	25	1.3%	103	+1, +2, +4, +3
500	25	1.5%	103	+1, +2, +4, +3, +5
550	19	1.3%	99	+1, +2, +3, +4
600	18	1.3%	110	+2, +1, +3, +4
650	12	1.0%	106	+1, +3, +2, +4
700	14	1.2%	120	+1, +2, +3, +4
750	16	1.5%	129	+1, +2, +4
800	16	1.6%	125	+1, +2, +4
850	11	1.2%	134	+2, +1, +4, +3
900	11	1.3%	151	+3, +2, +4, +1
950	4	0.5%	147	+2, +1
1000	6	0.8%	152	+2, +3, +1
1050	9	1.3%	147	+1, +2
1100	7	1.0%	144	+1, +2
1150	2	0.3%	161	+2, +1
1200	6	0.9%	155	+1, +2, +4
1250	5	0.8%	168	+1, +4, +2
1300	2	0.4%	163	+2, +1
1350	8	1.4%	182	+2, +3, +4, +1
1400	2	0.4%	203	+3, +2
1450	6	1.1%	179	+2, +1
1500	5	1.0%	177	+2, +1, +3

Table 7. Results from the interaction of particles by deposition (DEPO) in Problem 1

Time (s)	Particles dropped by DEPO (no scaling)	Percentage of particles lost by DEPO	Mean diameter of particles lost by DEPO (nm)	Most common charges in particles dropped by DEPO
50	8620	86.8%	45	0, +1, −1, +2, +3, −2, +4, −3
100	5821	84.3%	51	0, +1, −1, +2, +3, −2, +4, −3
150	4244	82.8%	58	0, +1, −1, +2, +3, +4, −2, −4
200	3397	81.7%	63	0, +1, −1, +2, +3, +4, −2, +5, −3
250	2771	80.5%	68	0, +1, −1, +2, +3, +4, −2, −3
300	2275	78.5%	75	0, +1, −1, +2, +3, +4, −2, −3
350	1891	77.3%	79	0, +1, −1, +2, +3, +4, −2, −3
400	1648	76.3%	85	0, +1, −1, +2, +3, +4, −2, +5
450	1410	74.1%	89	0, +1, −1, +2, +3, +4, −2
500	1210	73.2%	96	0, +1, −1, +2, +3, +4, −2
550	1049	71.4%	100	0, +1, −1, +2, +3, +4, −2
600	962	71.3%	104	0, +1, −1, +2, +3, +4, −2
650	878	69.6%	111	0, +1, −1, +2, +3, +4, −2, −3
700	801	69.7%	115	0, +1, −1, +2, +3, +4, −2
750	728	68.4%	119	0, +1, −1, +2, +3, −2, +4
800	706	69.9%	124	0, +1, −1, +2, +3, −2, +4
850	577	65.2%	130	0, +1, −1, +2, +3, +4, −2
900	545	66.0%	137	0, +1, −1, +2, +3, +4, −2, −3
950	545	63.4%	136	0, +1, −1, +2, +3, −2, +4, +5
1000	469	60.1%	143	0, +1, −1, +2, +3, +4, −2
1050	399	57.7%	147	0, +1, −1, +2, +3, −2, +4
1100	406	59.4%	153	0, +1, −1, +2, +3, +4, −3
1150	397	59.4%	160	0, +1, −1, +2, +3, +4, −2
1200	406	61.6%	160	0, +1, −1, +2, +3, −2, +4, −3
1250	364	55.7%	163	0, +1, −1, +2, +3, +4, −2
1300	304	56.3%	171	0, +1, −1, +2, +3, −2, +4
1350	320	55.2%	176	0, +1, −1, +2, +3, +4, +5, −2
1400	279	51.6%	177	0, +1, −1, +2, +3, +4, −2
1450	278	49.2%	182	0, +1, −1, +2, +3, +4, +5, −2
1500	270	52.8%	189	0, +1, −1, +2, +4, +3

Table 8. Results from the interaction of particles by coagulation and data of particles coalescing in Problem 1

Time (s)	Pairs of particles tested	New particles (no scaling)	Contribution to reduction in number of particles	Mean diameter (nm)	Most common charges	K_{max}
50	3525	1131	11%	69	0, +1, −1, +2, +3, +4, −2	4.66E−14
100	15693	972	14%	76	0, +1, −1, +2, +3, +4, −2, −3	4.66E−14
150	13783	811	16%	79	0, +1, −1, +2, +3, +4, −2, −4, −3, +5	4.66E−14
200	12331	697	17%	83	0, +1, −1, +2, +3, +4, −2, −4, −3	4.66E−14
250	11197	629	18%	89	0, +1, −1, +2, +3, +4, −2, −3	4.66E−14
300	10291	592	20%	92	0, +1, −1, +2, +3, +4, −2, +5	4.66E−14
350	9547	529	22%	99	0, +1, −1, +2, +3, +4, −2	4.66E−14
400	8917	486	23%	101	0, +1, −1, +2, +3, +4, −2	4.66E−14
450	8384	467	25%	103	0, +1, −1, +2, +3, +4, −2, +6	4.66E−14
500	7927	419	25%	111	0, +1, −1, +2, +3, +4, −2	4.66E−14
550	7537	401	27%	115	0, +1, −1, +2, +3, +4, −2, +5	4.66E−14
600	7185	369	27%	120	0, +1, −1, +2, +3, +4, −2, −3	4.66E−14
650	6870	372	29%	124	0, +1, −1, +2, +3, +4, −2	4.66E−14
700	6580	335	29%	129	0, +1, −1, +2, +3, +4, −2	4.66E−14
750	6322	321	30%	136	0, +1, −1, +2, +3, +4, −2	4.66E−14
800	6078	288	29%	138	0, +1, −1, +2, +3, −2, +4, −3	4.66E−14
850	5876	297	34%	144	0, +1, −1, +2, +3, +4, −2	4.66E−14
900	5683	270	33%	147	0, +1, −1, +2, +3, +4, −2	4.66E−14
950	5501	311	36%	154	0, +1, −1, +2, +3, +4, −2	4.66E−14
1000	5328	306	39%	159	0, +1, −1, +2, +3, +4, −2, +5	4.66E−14
1050	5174	283	41%	164	0, +1, −1, +2, +3, +4, −2, −3, +5	4.66E−14
1100	5026	270	40%	169	0, +1, −1, +2, +3, +4, −2, +5	4.66E−14
1150	4886	269	40%	175	0, +1, −1, +3, +2, +4, −2, +5	4.66E−14
1200	4745	247	37%	177	0, +1, +2, −1, +3, −2, +4, +6	4.66E−14
1250	4620	284	43%	178	0, +1, −1, +2, +3, +4, −2	4.66E−14
1300	4501	234	43%	188	0, +1, −1, +2, +3, +4, +5, +6	4.66E−14
1350	4390	252	43%	190	0, +1, −1, +2, +3, −2, +4, +6	4.66E−14
1400	4285	260	48%	194	0, +1, −1, +2, +3, +4, −2, +6, −4	4.66E−14
1450	4180	281	50%	197	0, +1, −1, +2, +3, +4, −2, +6	4.66E−14
1500	4073	236	46%	204	0, +1, −1, +2, +3, −2, +4, +5, +6	4.66E−14

The main contributor to the removal of particles is deposition over the entire simulation. However, deposition is more prominent at the beginning, dropping 87% of the particles versus 11% from coagulation. The contribution from deposition decreases to

53% over time resulting in an increase of the contribution from coagulation (46%). Electrostatic dispersion has a minor contribution to the removal ranging from 0.3% to 1.9%. In general, interactions by all processes decrease as time goes by, reducing the amount of aerosol particles suspended; however, deposition declines more dramatically. To analyze the interacting particles interacting we compare their mean diameter and most common charges (as shown in Tables 6, 7, and 8) to the mean diameter of all aerosol particles at each time step shown in Table 5 and to the relative frequency of particles in the different charge levels shown in Table 9.

Table 6 shows the electrostatic dispersion's minor contribution to the particles lost during the evolution of the aerosol. The mean diameter of these particles is smaller than the mean diameter of the total aerosol population for every time step. The reason for this is that small and light particles are more likely to be pushed by electrostatic forces. The charges of these dropped particles have a positive sign in all cases because the net charge of the aerosol is positive. Two factors affect the likelihood of particles with a specific charge being rejected: 1) the relative frequency of particles in each charge level and 2) the number of positive charges in the particles (higher positive charges are more likely to be rejected). These two influences can explain the numbers in the fifth column from the left in Table 6; thus, the order of charges agree with the frequency of particles with those charge levels for the first time steps (those with more particles dropped), but later particles with higher positive charges are chosen despite their lower frequency (as shown in Table 9). Note that in that column the charges of the particles being removed are ordered by their frequency from most to less frequent.

Table 7 shows that deposition is the main contributor to the reduction of the number of particles in the aerosol. In Table 5, the mean diameter of the particles dropped by this process start at around 16 nm smaller than the mean aerosol particle diameter at the beginning of the first time step and ends approaching the mean aerosol particle diameter by the last time step with a difference of only 5 nm. This suggest that mostly smaller particles are being dropped at the beginning, and with time, larger particles start to be removed along with the smaller ones. This is due to the strong contribution of convection-diffusion to the removal rate, which is higher than that of the gravitational settling for most of the particles in the aerosol given the size range considered in the simulation. The abundance of very small particles makes deposition very strong in the first time steps of the simulation. Furthermore, as these particles are removed, the contribution of deposition is reduced. Another factor responsible for the reduction in activity for deposition is the effect of condensation and coagulation; thus, as particles grow larger the component of the removal rate from convection diffusion gets smaller. Meanwhile, the gravitational settling does not grow significantly (for the particle size range in this simulation). This behavior will be seen more clearly in later figures showing the particle number distributions for selected time steps. The influence of coagulation on deposition was confirmed by a simulation with the same initial particle list where condensation was not active. This reduction in the particles deposited because of condensation, is a clear example of the synergistic nature of these processes. Condensation also reduced the mean particle density, which affected the deposition rate. Regarding the most common charges of the particles removed by deposition, these agree with the relative frequency of particles in the different charge levels shown in Table 9.

This is expected because the deposition rate is only influenced by the size and composition of the particle and not by the number of charges or polarity and because the initial particle number distributions for all charge levels (Table 2) have similar values in their mean and standard deviation (i.e., similar fractions of small-sized particles). If these distributions had different mean values, deposition could favor those with a higher population of either very small or very large sized particles.

Coagulation starts with an initial value for K_{max} of 8.91×10^{-15} and is updated in the first time step to 4.66×10^{-14}; this value remains for the rest of the simulation, as shown in Table 8. The small initial value results in fewer pairs selected for testing in that iteration, but the number of pairs passing the test for coagulation is not smaller than the values in the next time steps (it is actually larger). The number of pairs coalescing declines in every time step. Coagulation is the second contributor to the reduction in total number of particles (after deposition) at all time steps. However, the decline in the number of particles coalescing is much slower than the reduction of interactions by deposition. By the last time step, coagulation has almost the same contribution as deposition to the reduction in the number of particles. The mean diameter of particles coalescing is larger (4 to 13 nm) than the mean diameter of the aerosol particles. This means that on average, larger (heavier) particles are coalescing. The charges involved agree mostly with the relative frequency of particles in the different charge levels; however, this order is disrupted in some time steps showing a preference for larger or less frequent charges. The difference is presumably due to the high likelihood of coalescing for pairs of particles in which each particle has a high number of charges and different polarities. The selection of the pairs to test is random but when the particles selected

satisfy the conditions mentioned, it is very likely that they coalesce. Coagulation rate is also influenced by other processes. When deposition is strong the number of particles is reduced quickly lowering the coagulation rate, and as previously mentioned, deposition can be enhanced or diminished by coagulation (changing particle sizes). The effect of a changing mean particle density (Table 5) will be understood better when this simulation is compared with a problem where denser particles are used, in the next section.

Changes in the relative frequency of particles at every charge level during the simulation are shown in Table 9. Neutral particles are the only ones whose fraction is reduced most likely from the coagulation of neutral particles with charged particles as the new particle becomes charged. The fractions of particles at both positive and negative charge levels increase, but the fractions corresponding to negatively charged particles show a higher gain. This is expected since the aerosol has a positive net charge that will reject only positively charged particles by electrostatic dispersion. Although unlikely, there is coalescence between particles with the same polarity (positive) giving rise to a few particles with charges higher than +4 (+5, +6, +7, +8, and +9). This is not happening with negatively charged particles because their low fractions make these interactions even less likely.

Table 9. Relative frequency of particles in each charge level ordered by largest from left to right, except for the last column (Problem 1).

Time (s)	Charge level									
	0	+1	−1	+2	+3	+4	−2	−3	−4	> +4
0	0.72	0.13	0.072	0.049	0.020	0.010	0.0047	3.0E−04	3.0E−05	0
50	0.71	0.13	0.072	0.051	0.021	0.010	0.0048	3.1E−04	3.3E−05	1.1E−05
100	0.71	0.13	0.072	0.052	0.022	0.011	0.0049	3.0E−04	3.6E−05	4.8E−05
150	0.71	0.13	0.072	0.053	0.023	0.011	0.0050	3.1E−04	2.6E−05	6.4E−05
200	0.71	0.13	0.072	0.054	0.023	0.011	0.0051	3.0E−04	1.4E−05	9.5E−05
250	0.71	0.13	0.072	0.054	0.023	0.011	0.0052	3.0E−04	1.4E−05	1.7E−04
300	0.70	0.13	0.072	0.055	0.024	0.011	0.0052	2.8E−04	1.5E−05	2.1E−04
350	0.70	0.13	0.072	0.055	0.024	0.011	0.0053	2.9E−04	1.5E−05	2.6E−04
400	0.70	0.13	0.073	0.055	0.025	0.012	0.0053	3.0E−04	1.6E−05	3.0E−04
450	0.70	0.13	0.073	0.056	0.025	0.012	0.0055	3.1E−04	1.6E−05	3.6E−04
500	0.70	0.13	0.073	0.056	0.025	0.012	0.0055	3.2E−04	1.7E−05	4.2E−04
550	0.70	0.13	0.074	0.057	0.025	0.012	0.0056	3.6E−04	1.7E−05	5.2E−04
600	0.70	0.13	0.074	0.057	0.025	0.012	0.0056	3.7E−04	1.8E−05	5.7E−04
650	0.69	0.13	0.074	0.057	0.025	0.012	0.0057	3.6E−04	1.8E−05	6.1E−04
700	0.69	0.13	0.074	0.058	0.026	0.012	0.0058	3.7E−04	1.8E−05	7.0E−04
750	0.69	0.13	0.074	0.058	0.026	0.012	0.0058	3.8E−04	1.9E−05	7.3E−04
800	0.69	0.13	0.075	0.058	0.026	0.012	0.0058	3.8E−04	3.8E−05	7.7E−04
850	0.69	0.13	0.075	0.059	0.026	0.012	0.0059	3.9E−04	3.9E−05	8.2E−04
900	0.69	0.13	0.075	0.059	0.026	0.012	0.0059	3.8E−04	4.0E−05	8.7E−04
950	0.69	0.13	0.075	0.059	0.027	0.013	0.0058	3.8E−04	4.0E−05	9.1E−04
1000	0.69	0.13	0.075	0.060	0.027	0.013	0.0059	3.9E−04	4.1E−05	9.4E−04
1050	0.69	0.13	0.075	0.060	0.027	0.013	0.0059	4.2E−04	4.2E−05	9.8E−04
1100	0.68	0.13	0.075	0.060	0.027	0.013	0.0060	4.2E−04	4.2E−05	9.9E−04
1150	0.68	0.13	0.075	0.061	0.027	0.013	0.0060	4.3E−04	4.3E−05	1.0E−03
1200	0.68	0.13	0.075	0.061	0.027	0.013	0.0060	4.1E−04	4.3E−05	1.0E−03
1250	0.68	0.13	0.075	0.062	0.028	0.013	0.0061	4.2E−04	4.4E−05	1.1E−03
1300	0.68	0.13	0.075	0.062	0.028	0.013	0.0061	4.2E−04	4.5E−05	1.2E−03
1350	0.68	0.13	0.075	0.062	0.028	0.013	0.0061	4.5E−04	4.5E−05	1.2E−03
1400	0.68	0.13	0.075	0.062	0.028	0.014	0.0062	4.6E−04	4.6E−05	1.2E−03
1450	0.68	0.13	0.075	0.062	0.028	0.014	0.0062	4.6E−04	4.6E−05	1.2E−03
1500	0.68	0.14	0.075	0.063	0.028	0.014	0.0063	4.7E−04	4.7E−05	1.3E−03

Besides the data shown in the tables, several types of plots are presented to visualize aerosol evolution in terms of number and mass distributions, with and without discrimination by charge level. Distributions are obtained for four evenly spaced time steps along the simulation. The vertical lines show the limits of the 20 different size bins considered and the points indicate the number of particles for every size bin. Note that the lines connecting the points are just to improve visualization of the distributions, but the

points indicate discrete values for the regions comprised in a size bin. Also, note that the number of particles and masses shown in the following figures represent only the particles in the simulation, they are not scaled to the number of particles in the aerosol. To scale them, one simply needs to multiply the number of particles by the factor *f*. Figure 3 shows the particle number distributions without discrimination of charge levels. Particle diameters are shown to grow rapidly and almost evenly for all size bins, presumably due to condensation and to a lesser degree to coagulation, as is shown in Table 5. The apparent narrowing of the distribution as time passes is due to the logarithmic scale in the x-axis. The removal of small-sized particles by convection-diffusion is noticeable in the transition from 0 to 500 seconds as the distribution not only shifted to the right (condensation) but its left tail was shortened.

Figures 4, 5, and 6 show the component mass distributions of graphite, silver, and water respectively at 0, 500, 1000, and 1500 seconds without discrimination of charge. These show the total mass of each component in the aerosol per size bin. The shape of the distributions is the same for graphite and silver, but the mass of graphite is 9 times the mass of silver in all the size bins. There is no mass distribution for water at 0 seconds because the aerosol is dry at the beginning of the simulation; however, at 500, 1000, and 1500 seconds, one can see the rapid growth of this component surpassing the mass of graphite in the particles.

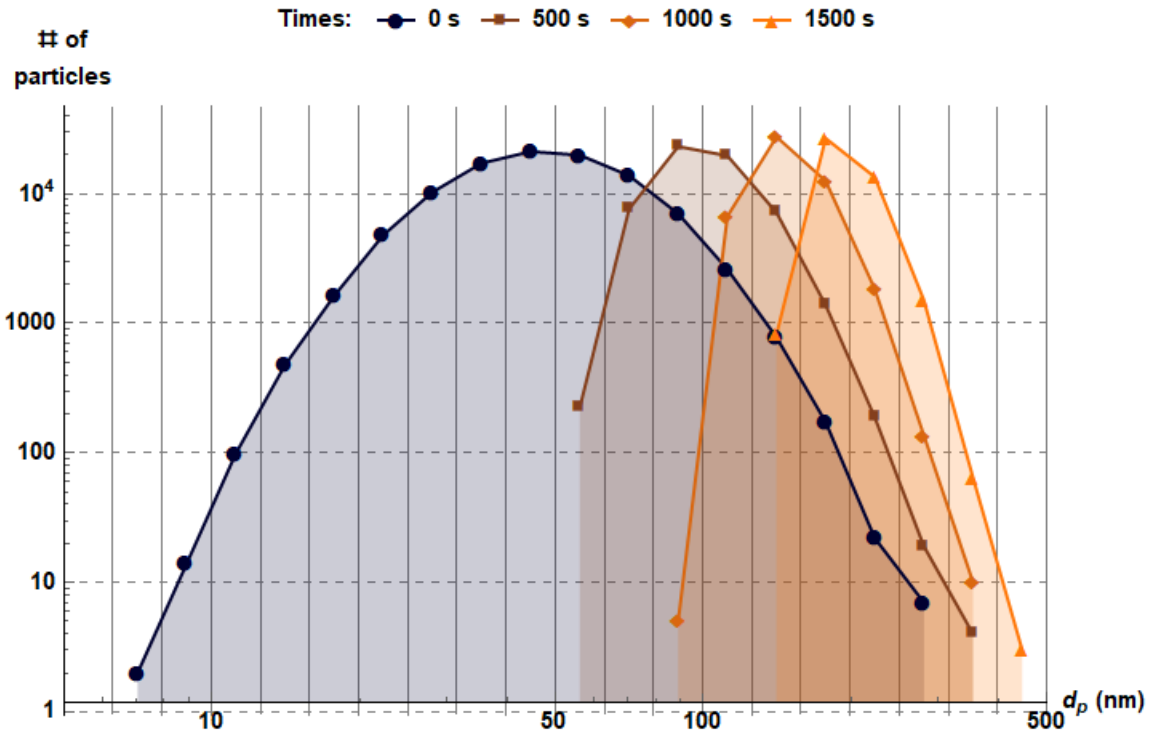

Figure 3. Particle number distributions for Problem 1 at 0, 500, 1000 and 1500 seconds.

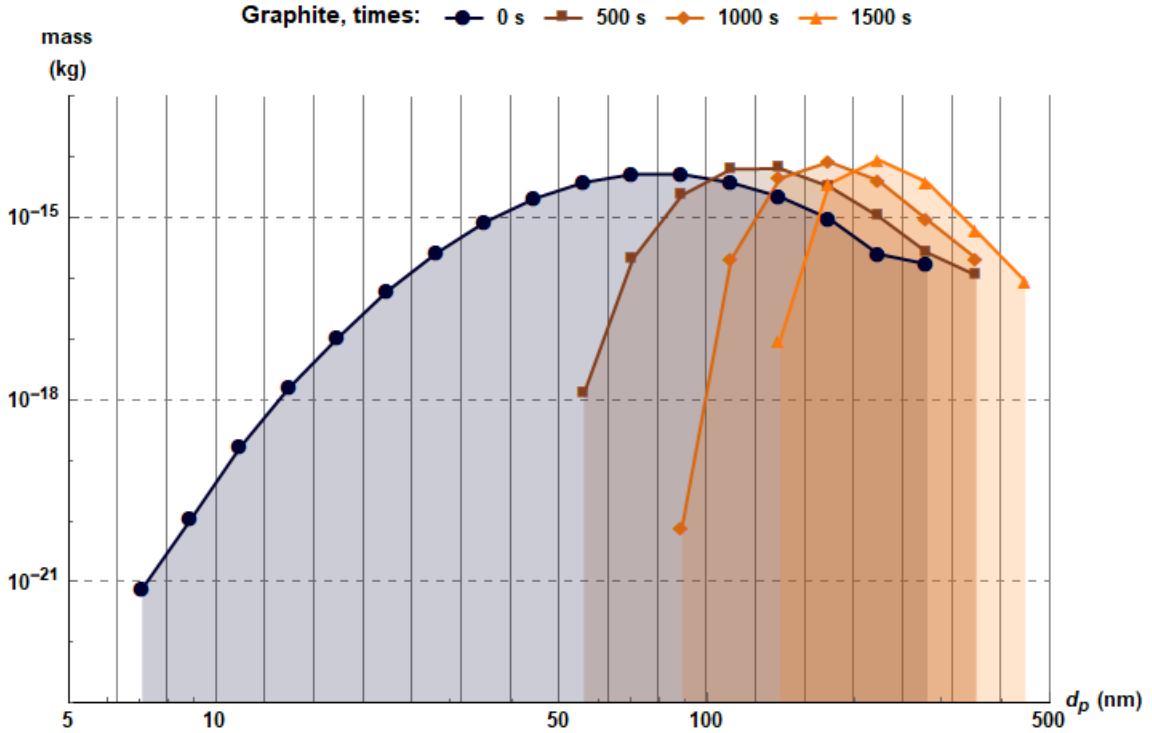

Figure 4. Mass distribution of graphite for Problem 1 at 0, 500, 1000 and 1500 seconds.

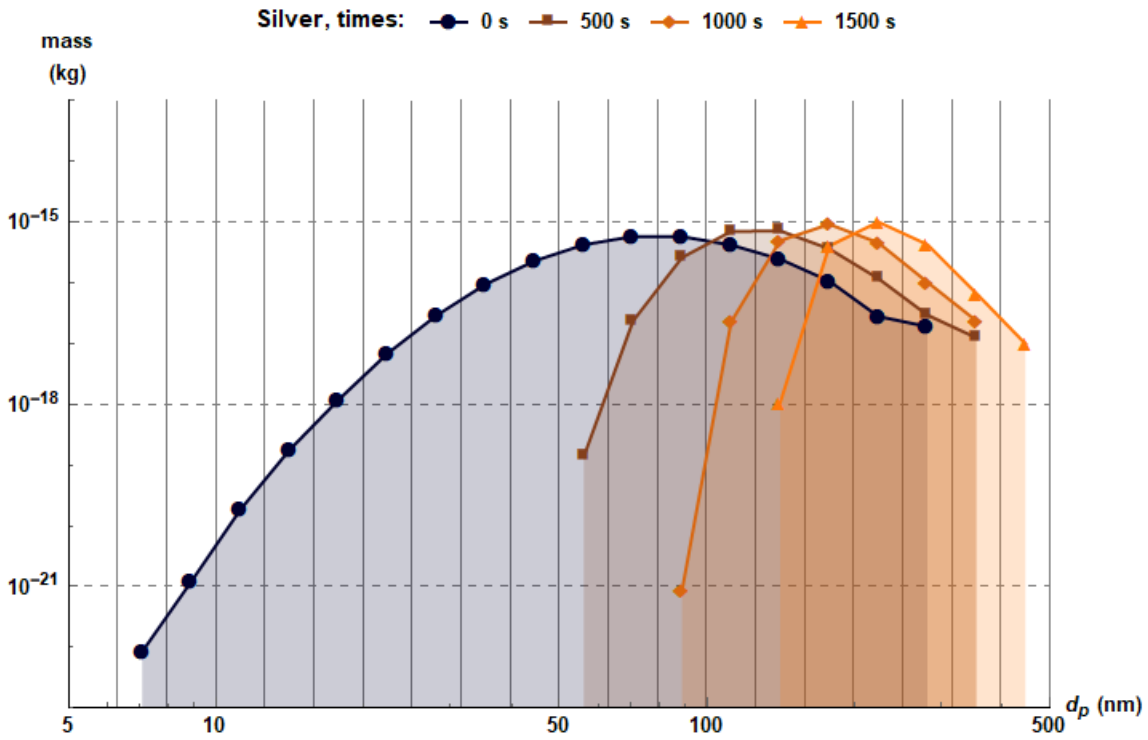

Figure 5. Mass distribution of silver for Problem 1 at 0, 500, 1000 and 1500 seconds.

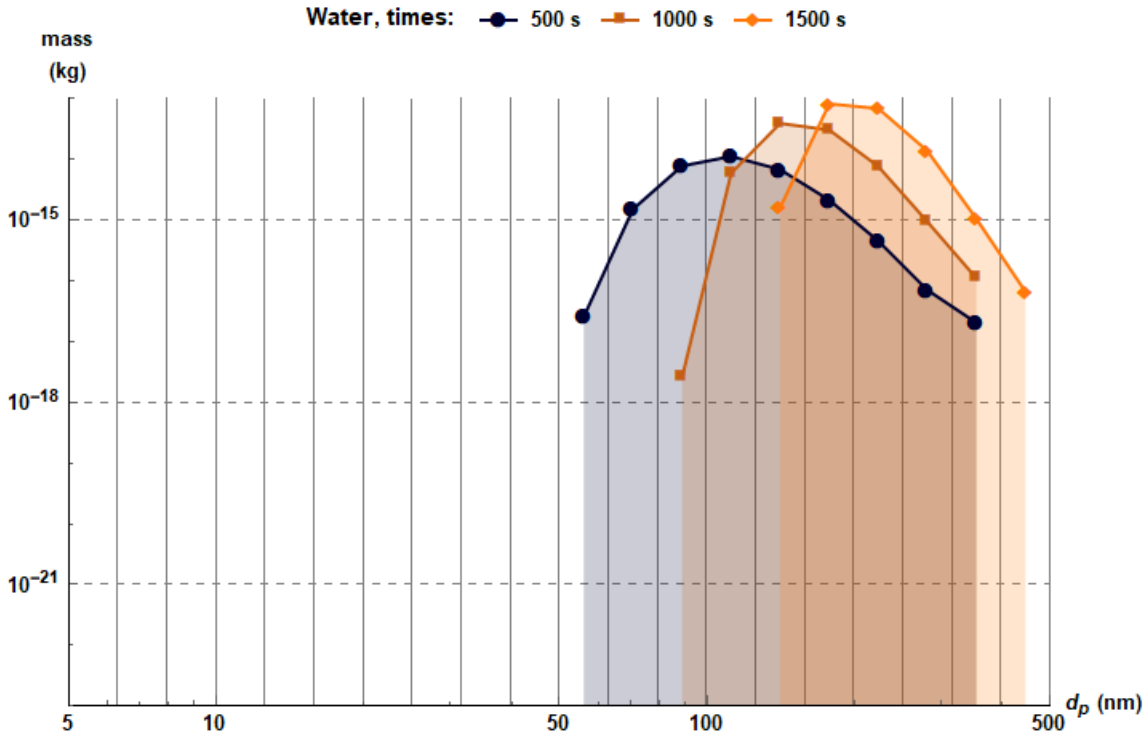

Figure 6. Mass distribution of water for Problem 1 at 500, 1000 and 1500 seconds.

Particle number distributions with discrimination of charges are shown in Figures 7, 8, 9, and 10 for times of 0, 500, 1000, and 1500 seconds, respectively. These allow us to see the evolution of the aerosol with more detail than in Figure 3 since one can observe how the particles in the different charge levels change in size. These figures show that both neutral and charged small-sized particles are being removed (as shown in Tables 6 and 7), that distributions of negative charges approach their positive counterparts as time passes (due to electrostatic dispersion of particles), and that the neutral distribution gets closer to the charged distributions as their fraction of particles is diminished (due to coagulation). Also, as these distributions are shifted to larger particle diameters, their mean values seem to become more alike, but it is difficult to tell with the logarithmic scale.

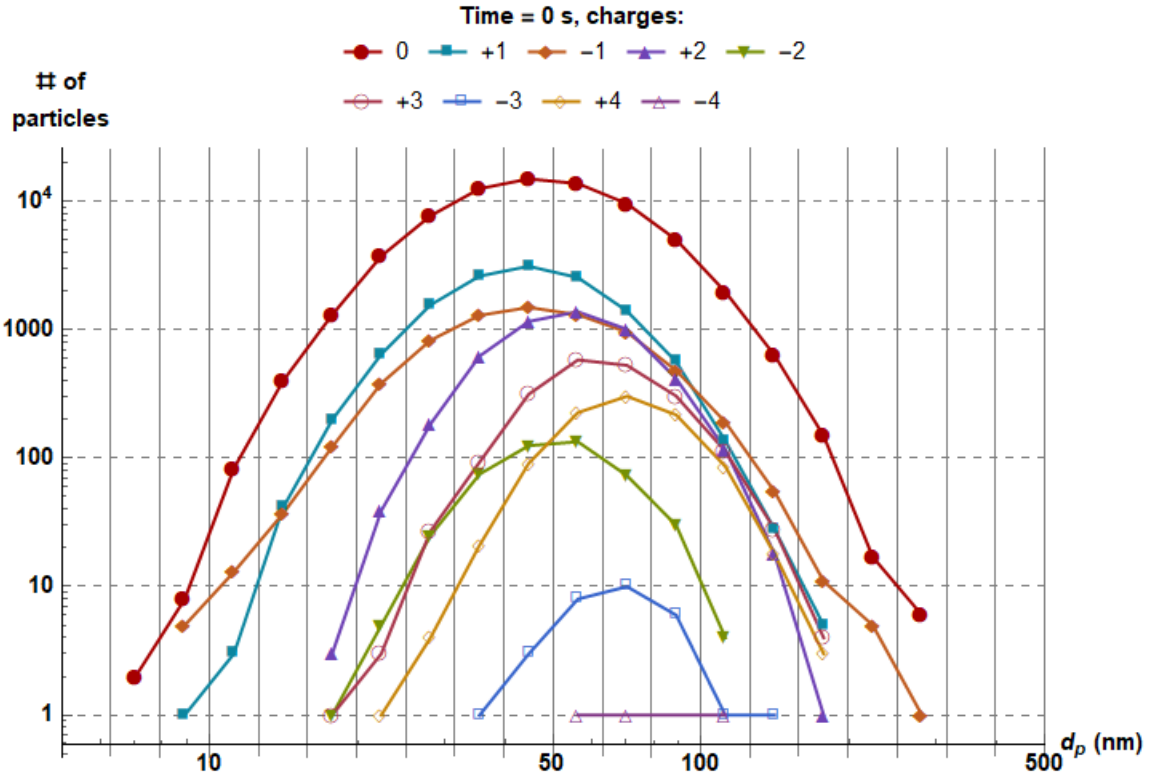

Figure 7. Particle number distribution for Problem 1 with discrimination of charge at 0 seconds.

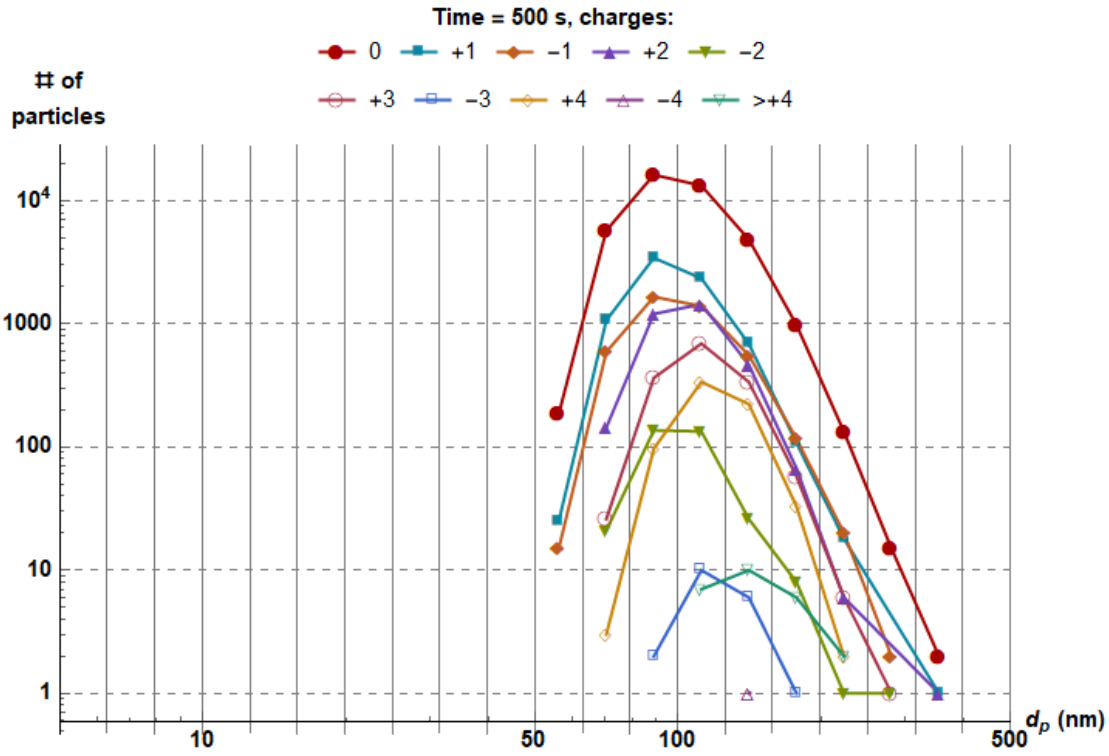

Figure 8. Particle number distribution for Problem 1 with discrimination of charge at 500 seconds.

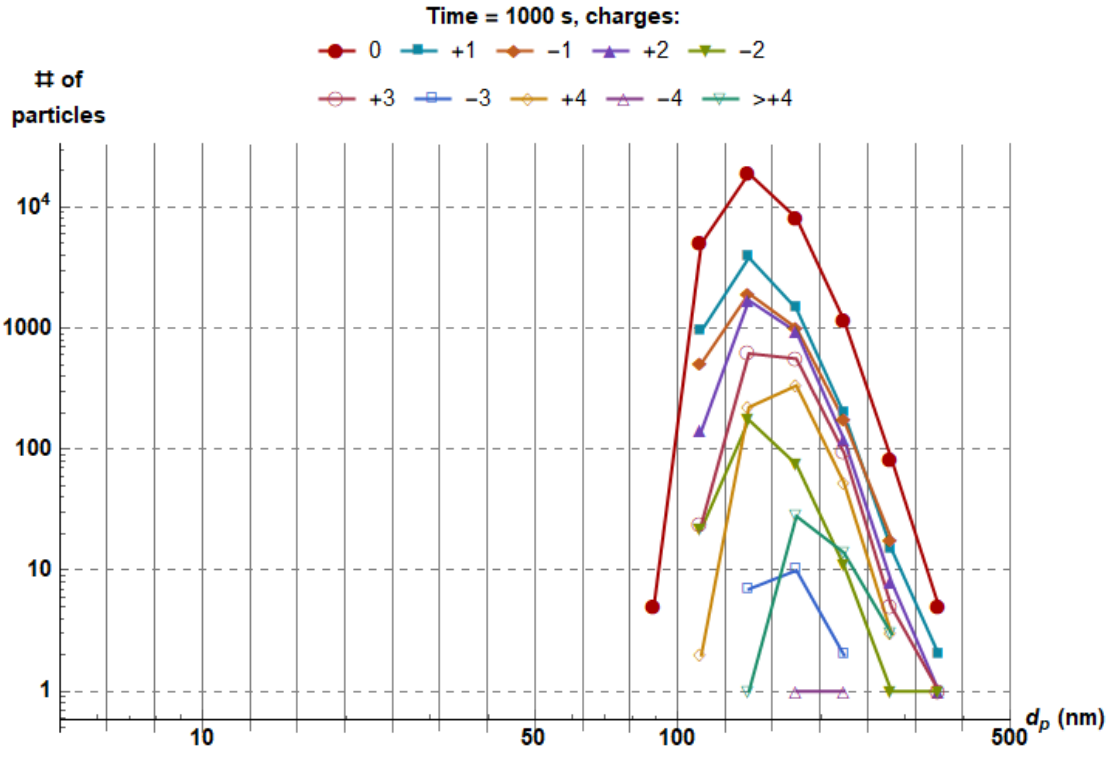

Figure 9. Particle number distribution for Problem 1 with discrimination of charge at 1000 seconds.

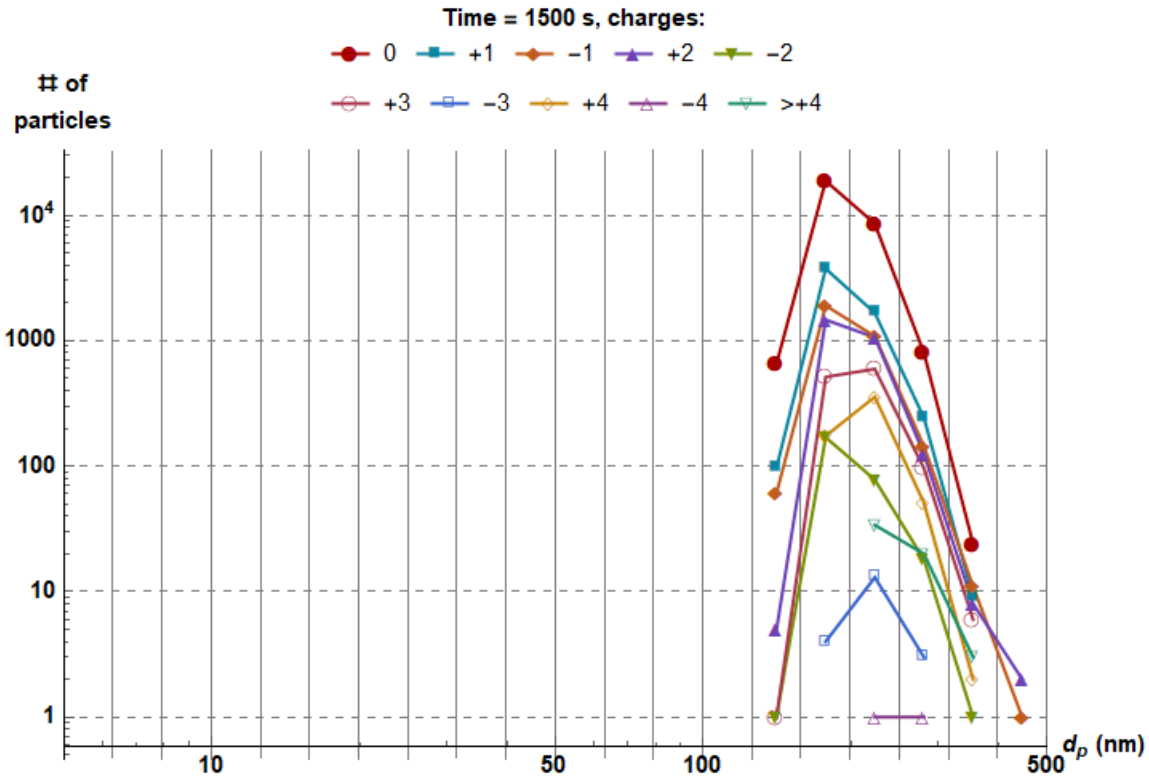

Figure 10. Particle number distribution for Problem 1 with discrimination of charge at 1500 seconds.

Figures 11 to 21 show mass distributions for every charge level of the components making up the aerosol particles. These correspond to the same time steps considered in the previous figures (0, 500, 1000, and 1500 seconds). In the initial distributions the particles have no water in them, so no mass distribution of water is shown at this time. The distributions for graphite and silver at the different charge levels have the same shape, mean and standard deviation in each time step, the only difference is that the masses of graphite are 9 times greater than those of silver. Conversely, water mass distributions differ from their equivalent of graphite and silver in each time step. This is due to the process by which particles gain water during the simulation.

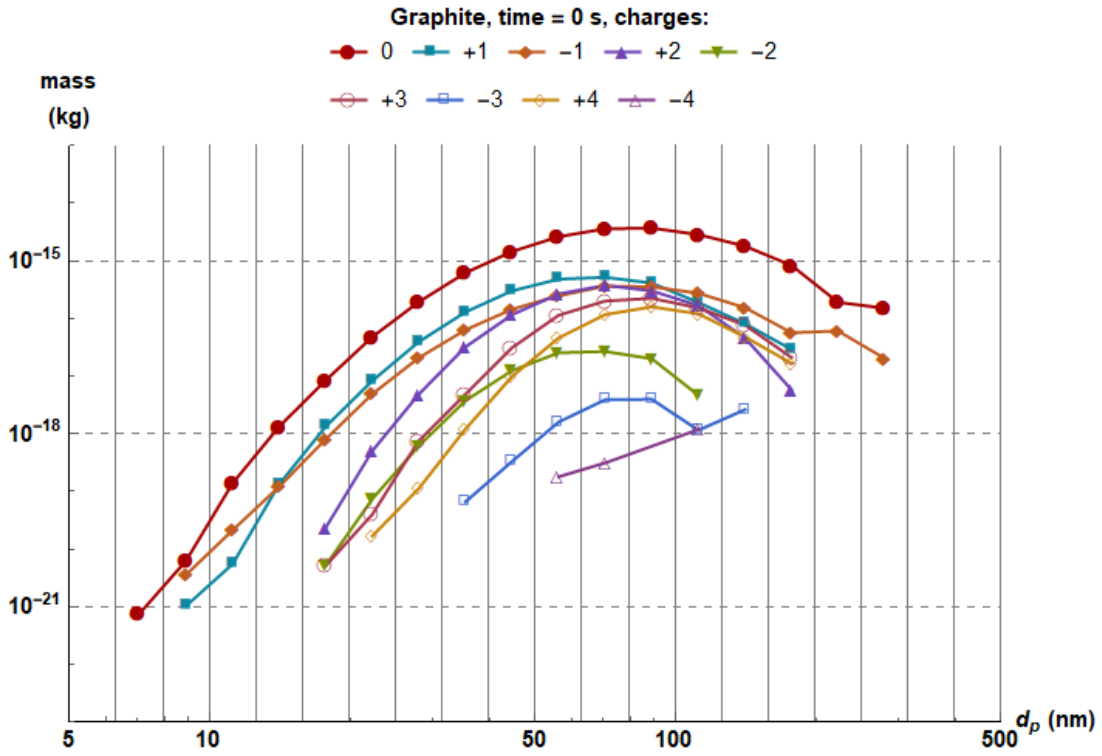

Figure 11. Mass distribution of graphite for Problem 1 with discrimination of charge at 0 seconds.

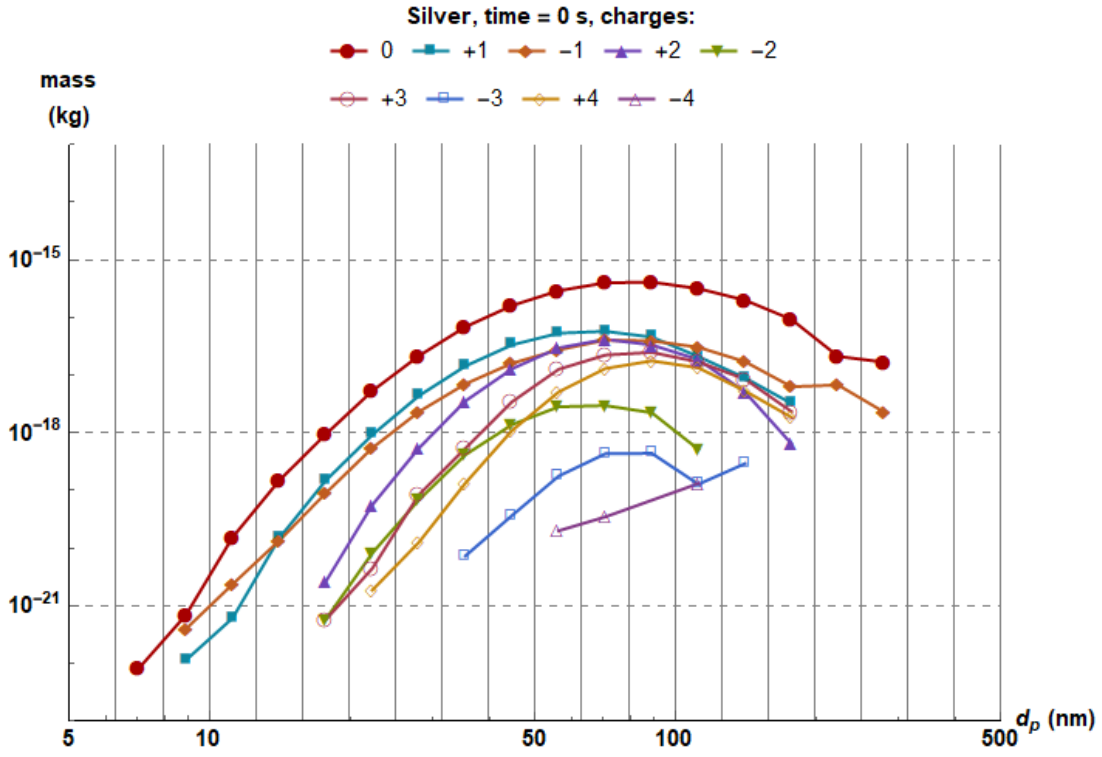

Figure 12. Mass distribution of silver for Problem 1 with discrimination of charge at 0 seconds.

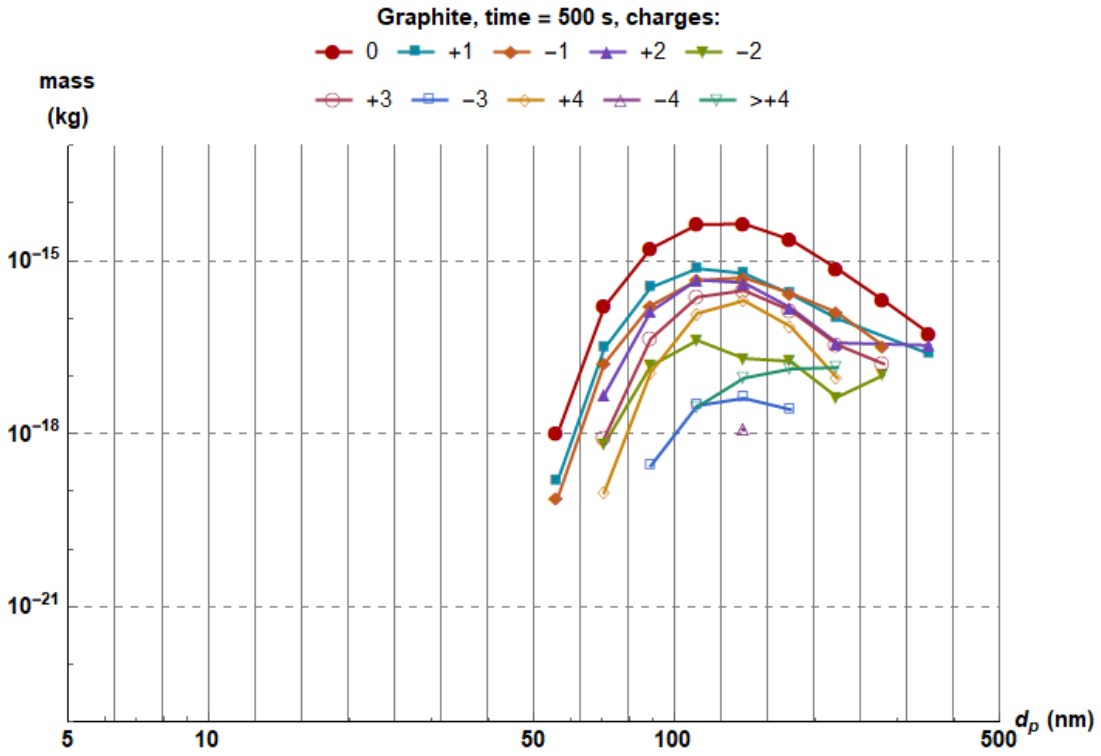

Figure 13. Mass distribution of graphite for Problem 1 with discrimination of charge at 500 seconds.

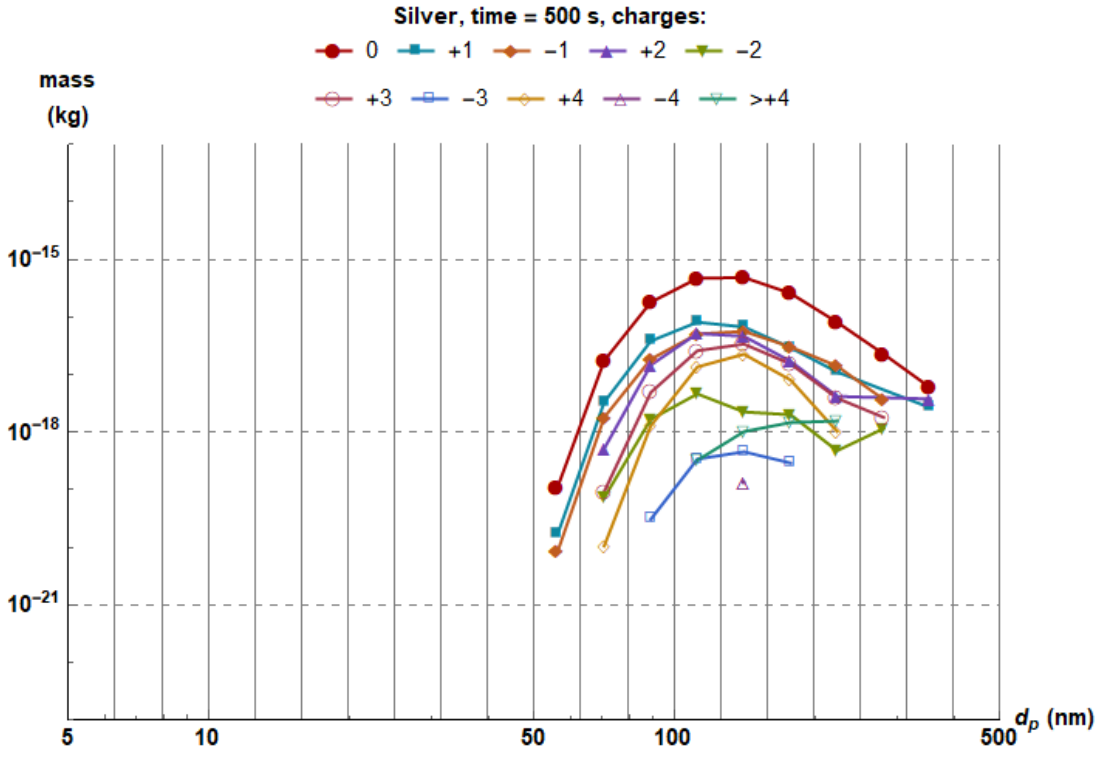

Figure 14. Mass distribution of silver for Problem 1 with discrimination of charge at 500 seconds.

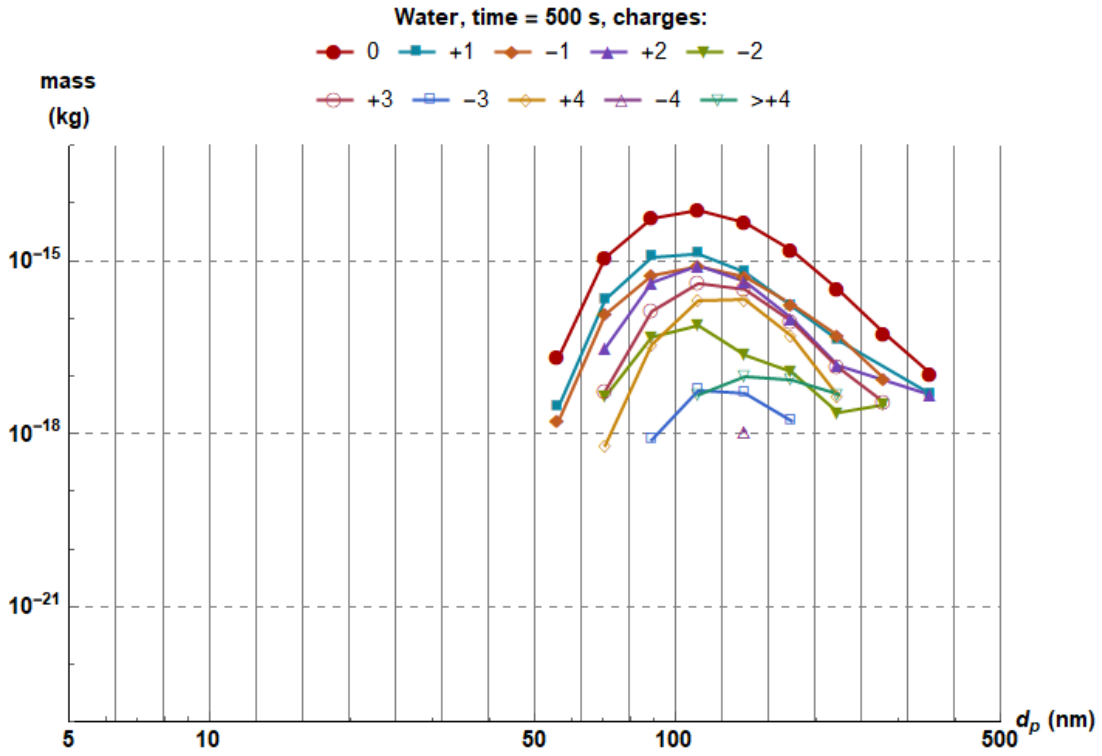

Figure 15. Mass distribution of water for Problem 1 with discrimination of charge at 500 seconds.

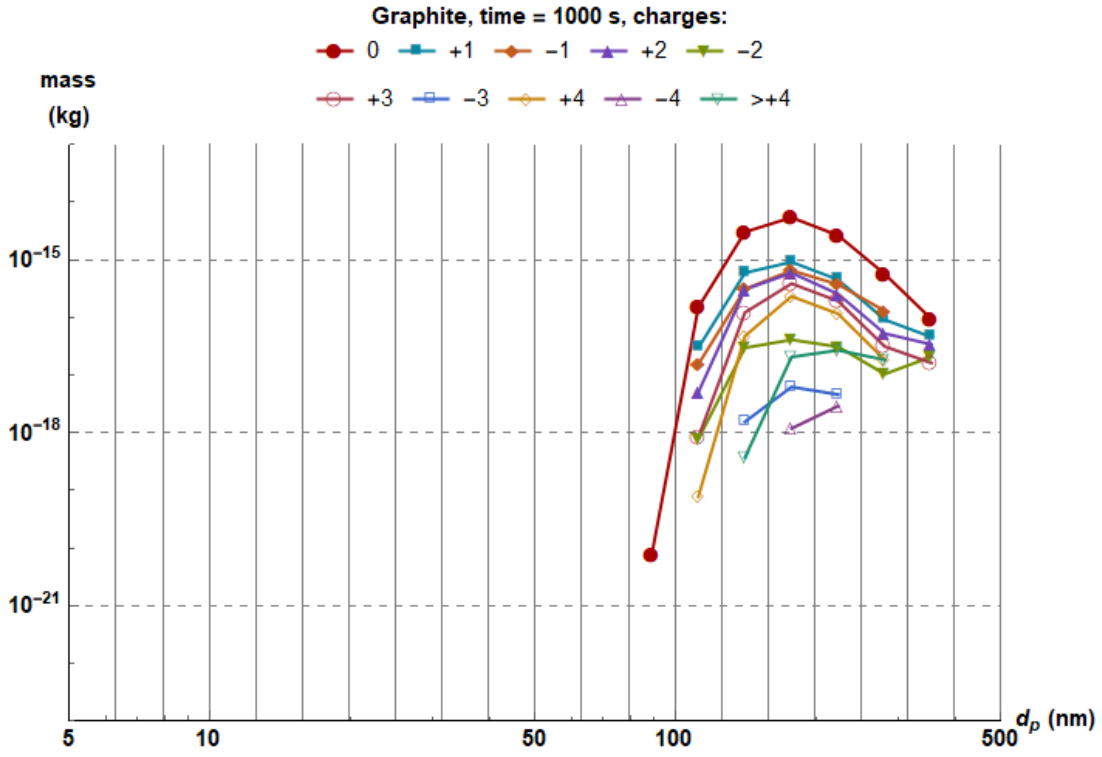

Figure 16. Mass distribution of graphite for Problem 1 with discrimination of charge at 1000 seconds.

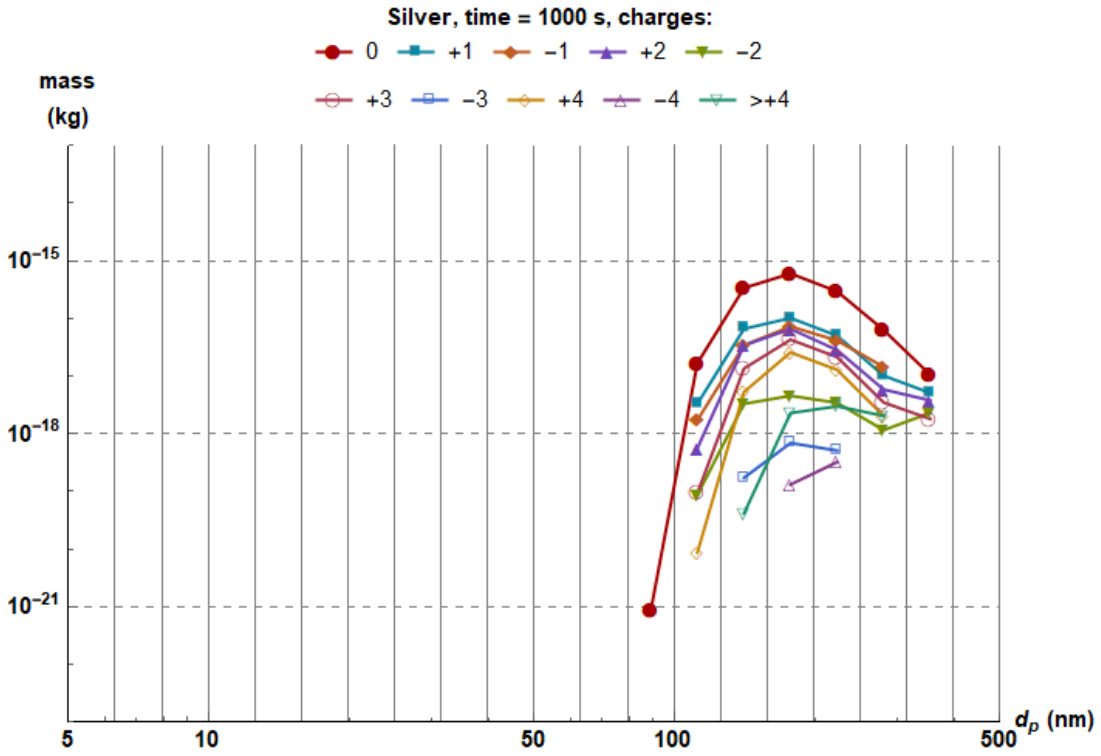

Figure 17. Mass distribution of silver for Problem 1 with discrimination of charge at 1000 seconds.

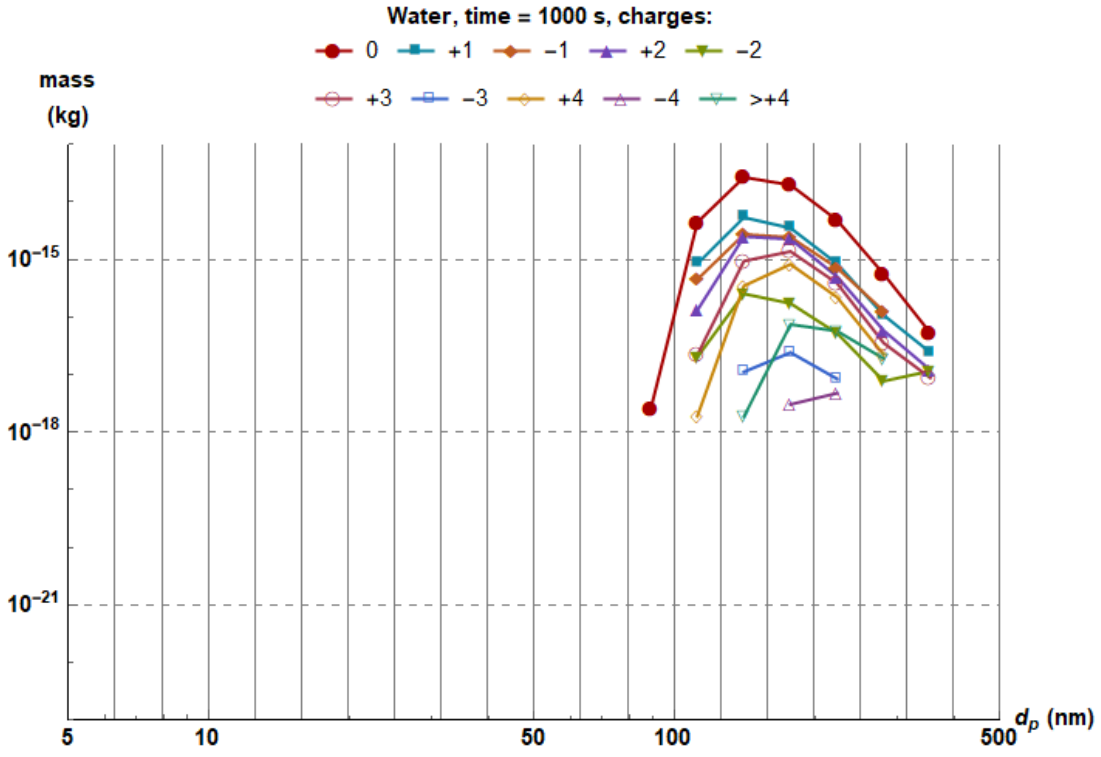

Figure 18. Mass distribution of water for Problem 1 with discrimination of charge at 1000 seconds.

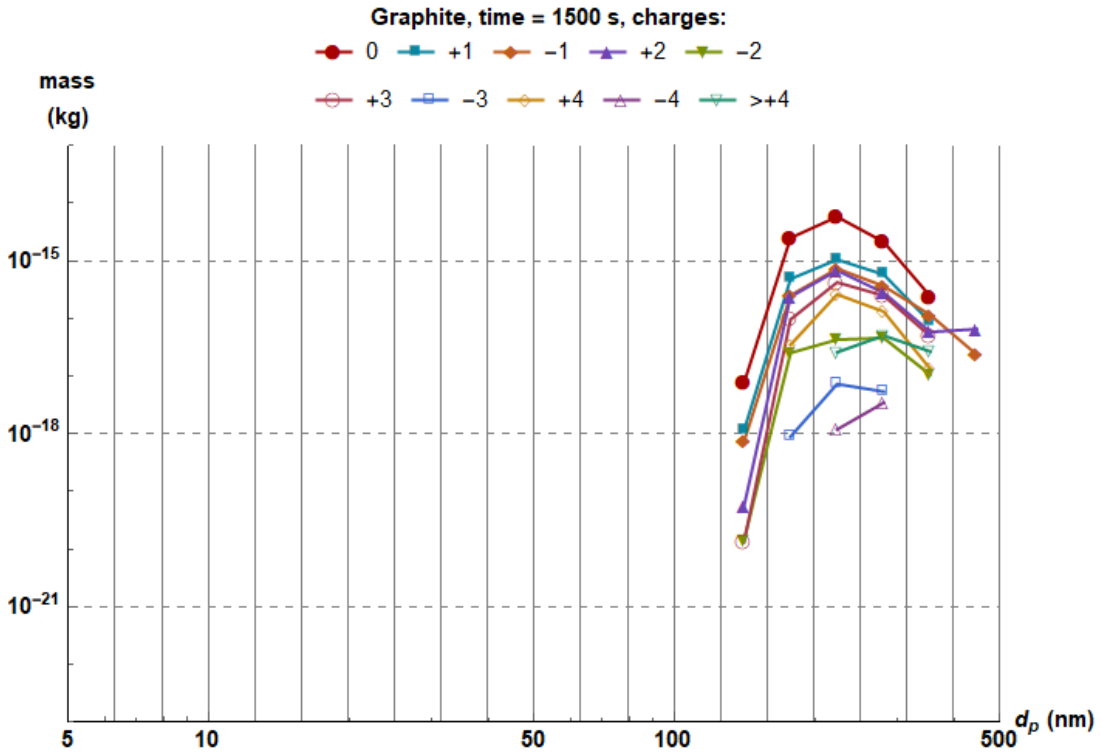

Figure 19. Mass distribution of graphite for Problem 1 with discrimination of charge at 1500 seconds.

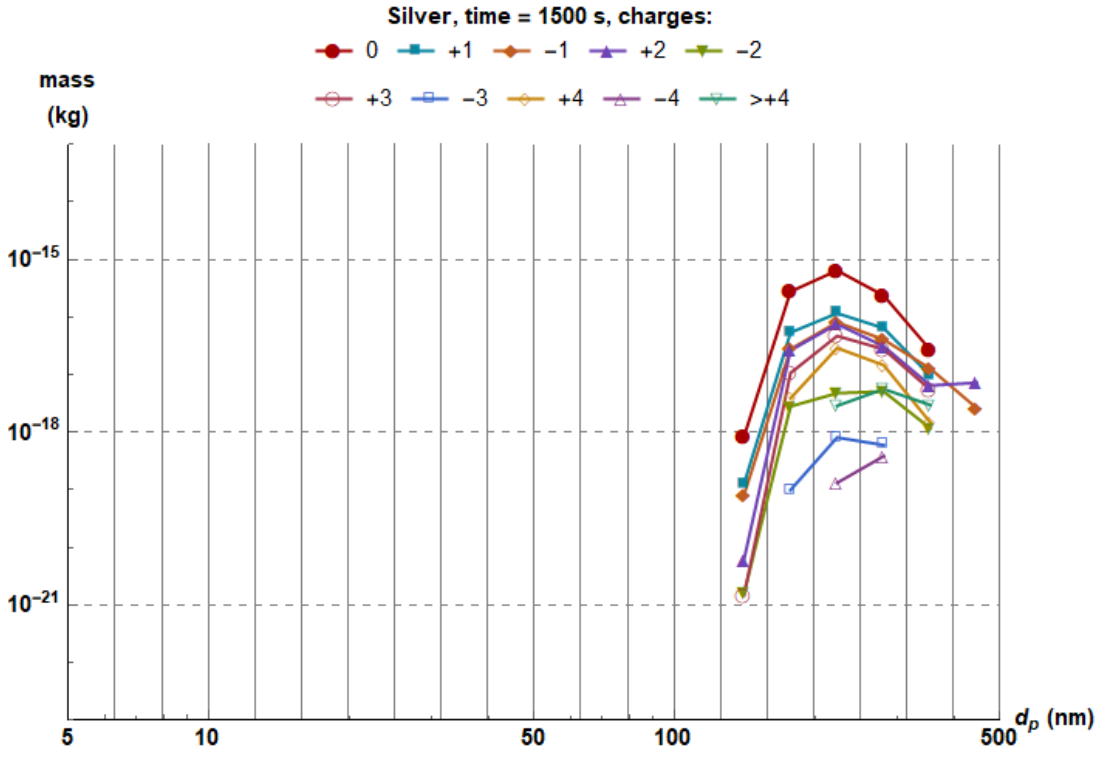

Figure 20. Mass distribution of silver for Problem 1 with discrimination of charge at 1500 seconds.

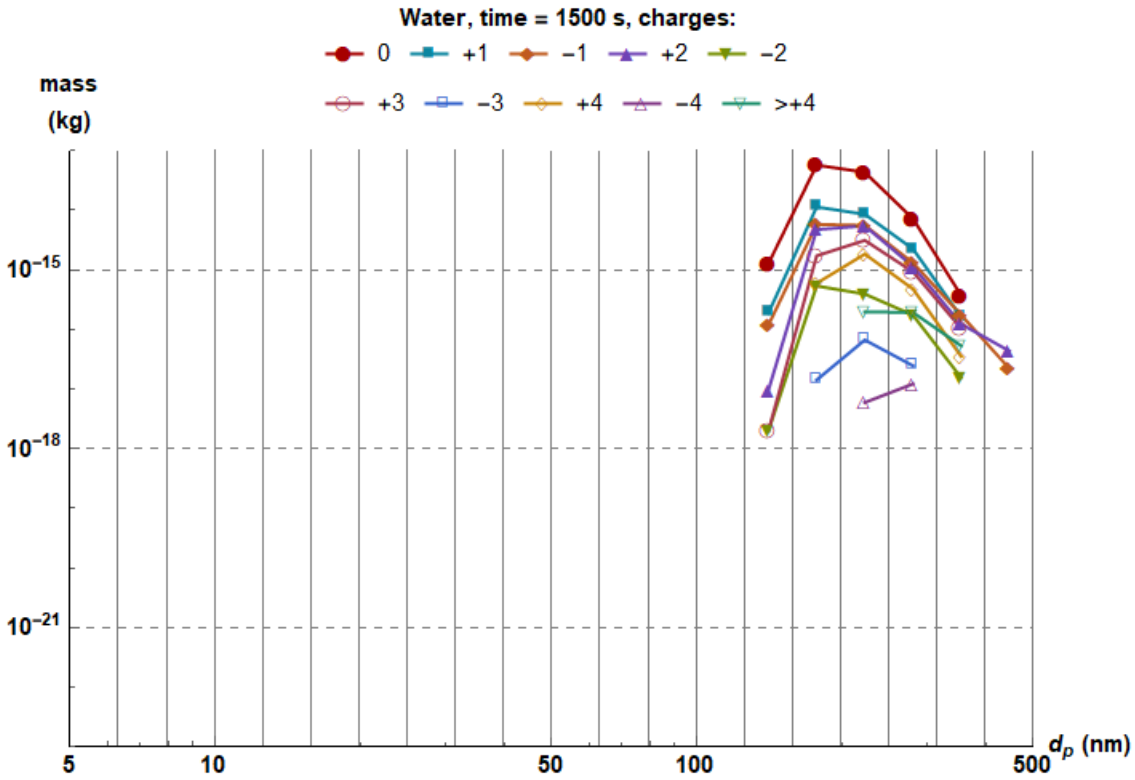

Figure 21. Mass distribution of water for Problem 1 with discrimination of charge at 1500 seconds.

3.7.2 Problem 2: Particle composition of 10% graphite and 90% Silver

The particle composition for this problem is given as 10% graphite and 90% silver (mf = 0.1), with much denser particles than Problem 1, but with the same size distribution. The same values for the time step (50 seconds), and number of iterations (30) with 1500 seconds of total time were used for Problem 2 since they provide a good number of interactions in all processes and allowed us to make comparisons with Problem 1. Table 10 shows information about the aerosol such as number of particles, total volume and volume gained at each time step. Table 11 shows properties of the aerosol particles such as mean diameter, mean component masses, and mean density. Total volume is increased in all the time steps in a very similar way to Problem 1, starting with a gain of 15% and decreasing steadily to a value of 6% (relative to the initial volume

at each time step). However, a slightly lesser amount of volume is gained by condensation at each time step. Meanwhile, more particles are removed during this simulation with denser particles. The overall reduction in number of particles is more pronounced than in Problem 1, starting with 10% of the total in the first time step; then, reducing to 2% at 850 seconds and to 1.5% at the final time step.

Some characteristics of the aerosol particles which remain suspended at different times are shown in Table 11. These are mean particle diameter, mean mass of each component, and mean particle density. The mean diameter is constantly growing, more than in Problem 1. The last time step of Problem 2 has a mean particle diameter that is 4 nm larger than its equivalent in Problem 1. The mean mass of graphite and silver per particle grows slowly, while the mass of water increases faster. However, at the final time step, the mean water mass is 70% while in the previous simulation it was 90%. The ratio of graphite to silver mass is maintained at 0.1 at all times. This composition results in a larger mean particle density starting at 7,495 kg/m^3 and dropping to 1,334 kg/m^3 (final time step) as more water is added to the particle. This parameter is the main factor for the differences between the two simulations presented, since initial size distributions are equal in both cases.

To analyze more carefully what kind of particles are being removed or are coalescing and how the different processes influence the aerosol, Tables 12, 13 and 14 show data about the interactions by electrostatic dispersion, deposition, and coagulation, respectively. This will shed more light on why particles are reduced in number faster and why mean diameter is larger for Problem 2. These tables show the percentage of particles lost by each process relative to the total number of particles lost in each time step as well

as the mean diameter of the particles interacting and their most common charges. For coagulation, the number of particles pairs to be tested and the values of $K_{\max}$ for each time step are also shown. Note that the number of new particles resulting from coagulation represent at the same time a reduction in the number of particles at that time step because two particles coalesce into one. Some of the values from these tables need to be scaled to the whole aerosol population and this is indicated in the column title as "(no scaling)" or as a note at the end of the table.

Table 10. Number of particles and volumes in the different time steps of the simulation in Problem 2.*

Time (s)	Initial number of particles	Final number of particles	Total initial volume (m^3)	Total final volume (m^3)	Total water volume gained (m^3) by condensation
50	99999	89899	1.22E−17	1.40E−17	2.19E−18
100	89899	82754	1.40E−17	1.60E−17	2.38E−18
150	82754	77206	1.60E−17	1.81E−17	2.59E−18
200	77206	72910	1.81E−17	2.05E−17	2.82E−18
250	72910	69280	2.05E−17	2.31E−17	3.04E−18
300	69280	66351	2.31E−17	2.59E−17	3.28E−18
350	66351	63687	2.59E−17	2.89E−17	3.51E−18
400	63687	61420	2.89E−17	3.21E−17	3.76E−18
450	61420	59401	3.21E−17	3.56E−17	4.01E−18
500	59401	57606	3.56E−17	3.93E−17	4.26E−18
550	57606	55929	3.93E−17	4.33E−17	4.51E−18
600	55929	54399	4.33E−17	4.75E−17	4.77E−18
650	54399	52930	4.75E−17	5.18E−17	5.03E−18
700	52930	51682	5.18E−17	5.66E−17	5.30E−18
750	51682	50472	5.66E−17	6.15E−17	5.57E−18
800	50472	49376	6.15E−17	6.67E−17	5.84E−18
850	49376	48387	6.67E−17	7.22E−17	6.13E−18
900	48387	47392	7.22E−17	7.79E−17	6.39E−18
950	47392	46524	7.79E−17	8.40E−17	6.68E−18
1000	46524	45659	8.40E−17	9.02E−17	6.95E−18
1050	45659	44851	9.02E−17	9.68E−17	7.24E−18
1100	44851	44093	9.68E−17	1.04E−16	7.53E−18
1150	44093	43295	1.04E−16	1.11E−16	7.79E−18
1200	43295	42612	1.11E−16	1.18E−16	8.09E−18
1250	42612	41941	1.18E−16	1.25E−16	8.36E−18
1300	41941	41299	1.25E−16	1.33E−16	8.65E−18
1350	41299	40648	1.33E−16	1.41E−16	8.92E−18
1400	40648	40016	1.41E−16	1.50E−16	9.20E−18
1450	40016	39448	1.50E−16	1.58E−16	9.48E−18
1500	39448	38866	1.58E−16	1.67E−16	9.75E−18

*Note: Values for number of particles and volumes need to be scaled.

Table 11. Mean diameter, mean mass of each component and mean density of aerosol particles for each time step in Problem 2.

Time (s)	Mean particle diameter, *d* (nm)	Mean mass of graphite (kg)	Mean mass of silver (kg)	Mean mass of water (kg)	Mean particle density (kg/m^3)
0	62	9.17E−20	8.25E−19	0.00E+00	7495
50	67	9.85E−20	8.87E−19	2.44E−20	6478
100	72	1.04E−19	9.36E−19	5.43E−20	5669
150	77	1.09E−19	9.78E−19	8.97E−20	5011
200	81	1.13E−19	1.01E−18	1.31E−19	4470
250	86	1.16E−19	1.05E−18	1.78E−19	4023
300	91	1.19E−19	1.07E−18	2.31E−19	3649
350	95	1.22E−19	1.10E−18	2.90E−19	3333
400	100	1.25E−19	1.12E−18	3.57E−19	3066
450	105	1.27E−19	1.14E−18	4.30E−19	2837
500	109	1.29E−19	1.16E−18	5.10E−19	2640
550	114	1.32E−19	1.18E−18	5.98E−19	2474
600	119	1.34E−19	1.20E−18	6.94E−19	2328
650	123	1.36E−19	1.22E−18	7.98E−19	2202
700	128	1.38E−19	1.24E−18	9.11E−19	2091
750	133	1.40E−19	1.26E−18	1.03E−18	1995
800	137	1.42E−19	1.28E−18	1.16E−18	1910
850	142	1.44E−19	1.29E−18	1.30E−18	1834
900	146	1.46E−19	1.31E−18	1.45E−18	1767
950	151	1.47E−19	1.32E−18	1.61E−18	1707
1000	156	1.49E−19	1.34E−18	1.78E−18	1653
1050	160	1.51E−19	1.36E−18	1.96E−18	1605
1100	165	1.52E−19	1.37E−18	2.15E−18	1562
1150	170	1.54E−19	1.39E−18	2.35E−18	1523
1200	174	1.56E−19	1.40E−18	2.56E−18	1488
1250	179	1.57E−19	1.42E−18	2.78E−18	1456
1300	183	1.59E−19	1.43E−18	3.02E−18	1426
1350	188	1.61E−19	1.45E−18	3.26E−18	1400
1400	193	1.62E−19	1.46E−18	3.52E−18	1376
1450	197	1.64E−19	1.48E−18	3.79E−18	1354
1500	202	1.66E−19	1.49E−18	4.08E−18	1334

Table 12. Results from the interaction of particles by electrostatic dispersion (ED) in Problem 2.

Time (s)	Particles dropped by ED (no scaling)	Percentage of particles lost by ED	Mean diameter of particles lost by ED (nm)	Most common charges in particles dropped by ED
50	187	1.9%	49	+1, +2, +3, +4
100	107	1.5%	55	+1, +2, +3, +4
150	82	1.5%	61	+1, +2, +3, +4
200	56	1.3%	68	+1, +2, +4, +3
250	49	1.3%	72	+1, +2, +4, +3
300	32	1.1%	84	+1, +2, +3, +4
350	35	1.3%	87	+2, +1, +3, +4
400	20	0.9%	96	+1, +2, +3, +4
450	20	1.0%	96	+1, +2, +3
500	23	1.3%	107	+2, +1, +3, +4, +5
550	15	0.9%	103	+1, +2, +4, +5, +3
600	11	0.7%	113	+1, +4, +3, +2
650	9	0.6%	124	+2, +1, +6, +4, +3
700	16	1.3%	128	+1, +3, +5, +2
750	14	1.2%	129	+2, +3, +1, +4
800	10	0.9%	135	+1, +4, +3, +2
850	7	0.7%	128	+3, +2, +1
900	8	0.8%	135	+2, +1, +3
950	3	0.3%	159	+4, +2, +1
1000	14	1.6%	165	+2, +1, +4, +3
1050	7	0.9%	149	+2, +1
1100	8	1.1%	156	+1, +2, +3
1150	4	0.5%	142	+1, +3
1200	8	1.2%	153	+1, +4, +3, +2
1250	5	0.7%	188	+2, +1, +4
1300	4	0.6%	176	+2, +4, +1
1350	1	0.2%	163	+1
1400	8	1.3%	182	+1, +2, +3
1450	7	1.2%	241	+2, +3, +1
1500	2	0.3%	182	+2

Table 13. Results from the interaction of particles by deposition (DEPO) in Problem 2.

Time (s)	Particles dropped by DEPO (no scaling)	Percentage of particles lost by DEPO	Mean diameter of particles lost by DEPO (nm)	Most common charges in particles dropped by DEPO
50	8717	86.3%	45	0, +1, −1, +2, +3, +4, −2, −3
100	5865	82.1%	51	0, +1, −1, +2, +3, +4, −2, −3
150	4399	79.3%	58	0, +1, −1, +2, +3, +4, −2
200	3308	77.0%	63	0, +1, −1, +2, +3, +4, −2, −3
250	2676	73.7%	68	0, +1, −1, +2, +3, −2, +4, −3
300	2097	71.6%	75	0, +1, −1, +2, +3, −2, +4, +6, −3
350	1871	70.2%	81	0, +1, −1, +2, +3, +4, −2, −3
400	1543	68.1%	84	0, +1, −1, +2, +3, +4, −2, −3
450	1342	66.5%	91	0, +1, −1, +2, +3, −2, +4, −3, +5
500	1176	65.5%	96	0, +1, −1, +2, +3, +4, −2, +6
550	1047	62.4%	99	0, +1, −1, +2, +3, +4, −2, +5
600	907	59.3%	105	0, +1, −1, +2, +3, −2, +4
650	889	60.5%	111	0, +1, −1, +2, +3, +4, −2, +6, −3
700	706	56.6%	115	0, +1, −1, +2, +3, +4, −2, +5
750	719	59.4%	120	0, +1, −1, +2, +3, +4, −2
800	609	55.6%	124	0, +1, −1, +2, +3, −2, +4
850	548	55.4%	129	0, +1, −1, +2, +3, +4
900	508	51.1%	136	0, +1, −1, +2, +4, +3, −2
950	438	50.5%	141	0, +1, −1, +2, +3, +4, −2
1000	429	49.6%	144	0, +1, +2, −1, +3, +4
1050	400	49.5%	147	0, +1, −1, +2, +3, +4, −2
1100	384	50.7%	152	0, +1, −1, +2, +3, +4, −2
1150	386	48.4%	158	0, +1, −1, +2, +3, +4, −2
1200	325	47.6%	164	0, +1, −1, +2, +3, +4, −2
1250	310	46.2%	167	0, +1, −1, +2, +3, +4, −2
1300	292	45.5%	176	0, +1, −1, +2, +4, +3, −2, +5
1350	301	46.2%	175	0, +1, −1, +2, +3, +4, −2
1400	283	44.8%	180	0, +1, −1, +2, +3, +4
1450	243	42.8%	182	0, +1, −1, +2, +4, +3, −2
1500	251	43.1%	189	0, +1, −1, +2, +3, +4, −2, +5

Table 14. Results from the interaction of particles by coagulation, data of particles coalescing in Problem 2.

Time (s)	Pairs of parti-cles tested	New parti-cles (no scaling)	Contri-bution to reduction in number of particles	Mean dia-meter (nm)	Most common charges	K_{max}
50	6146	1196	12%	76	0, +1, −1, +2, +3, +4, −2	7.62E−14
100	25556	1173	16%	86	0, +1, −1, +2, +3, +4, −2	7.94E−14
150	23159	1067	19%	89	0, +1, −1, +2, +3, +4, −2, −3, +5	8.36E−14
200	21693	932	22%	93	0, +1, −1, +2, +3, +4, −2, +7, +5	8.36E−14
250	19597	905	25%	96	0, +1, −1, +2, +3, +4, −2, +6	8.56E−14
300	18364	800	27%	101	0, +1, −1, +2, +3, +4, −2, −3	8.61E−14
350	17017	758	28%	105	0, +1, −1, +2, +3, +4, −2, +5, −3, +6	8.77E−14
400	16119	704	31%	110	0, +1, −1, +2, +3, +4, −2, +6, −3	8.81E−14
450	15130	657	33%	114	0, +1, −1, +2, +3, +4, −2, −3, +6	8.81E−14
500	14209	596	33%	118	0, +1, −1, +2, +3, +4, −2	8.81E−14
550	13411	615	37%	125	0, +1, −1, +2, +3, +4, −2, +6	8.81E−14
600	12694	612	40%	127	0, +1, −1, +2, +3, +4, −2, −3	8.81E−14
650	12006	571	39%	134	0, +1, −1, +2, +3, +4, −2, +5, −3	8.81E−14
700	11433	526	42%	136	0, +1, −1, +2, +3, +4, −2, −3, +5	8.81E−14
750	10888	477	39%	145	0, +1, −1, +2, +3, +4, −2, +5	8.81E−14
800	10425	477	44%	148	0, +1, −1, +2, +3, +4, −2, +5	8.81E−14
850	9998	434	44%	151	0, +1, −1, +2, +3, +4, −2, +6, +5	8.81E−14
900	9612	479	48%	156	0, +1, −1, +2, +3, +4, −2, +5, +6	8.81E−14
950	9247	427	49%	161	0, +1, −1, +2, +3, −2, +4, +5, +7, +6	8.81E−14
1000	8907	422	49%	168	0, +1, −1, +2, +3, +4, −2, +5, +6	8.89E−14
1050	8668	401	50%	172	0, +1, −1, +2, +3, +4, −2, +6, +5, +7	8.89E−14
1100	8367	366	48%	179	0, +1, −1, +2, +3, +4, −2, +5, +6, +7, −3	8.89E−14
1150	8084	408	51%	181	0, +1, +2, −1, +3, −2, +4, +5, −3	9.18E−14
1200	8062	350	51%	188	0, +1, +2, −1, +3, +4, −2, +5, +7	9.22E−14
1250	7849	356	53%	194	0, +1, −1, +2, +3, +4, −2, +6, −3, +5	9.34E−14
1300	7712	346	54%	194	0, +1, +2, −1, +3, +4, −2, +5, +6, −3, +7	9.53E−14
1350	7628	349	54%	202	0, +1, −1, +2, +3, +4, −2, +5, −3, +8, +6	9.56E−14
1400	7409	341	54%	206	0, +1, −1, +2, +3, +4, −2, +6, +8, +5, +7	1.01E−13
1450	7587	318	56%	213	0, +1, −1, +2, +3, +4, +5, −2, +6	1.01E−13
1500	7370	329	57%	217	0, +1, −1, +2, +3, +4, −2, +6, +7, −3	1.01E−13

Deposition starts as the main contributor to the reduction of particles being responsible for 86% of the particles removed versus 12% from deposition and 2% from electrostatic dispersion. With time deposition becomes less active while coagulation gains relevance contributing equally to the reduction in the number of particles at approximately 1000 seconds. From that time (1000 seconds), coagulation gets more activity than deposition and at the final time step 57% of the reduction in the number of particles is due to coagulation versus 43% from deposition. This is a change from Problem 1 where the activity of coagulation did not overtake deposition. The number of particles removed at all time steps by deposition are very similar to Problem 1; however, Problem 2 starts with a slightly larger activity and ends a slightly smaller one. Meanwhile, the numbers of particles coalescing in Problem 2 is considerably larger than in Problem 1. Thus, this change is mostly due to an increase in coagulation activity instead of a decrease in deposition activity. Electrostatic dispersion maintains a small contribution with similar numbers to Problem 1. In the next three paragraphs, a more detailed analysis of the particles interacting by electrostatic dispersion, deposition and coagulation will be presented.

There is slightly less activity due to electrostatic dispersion in Problem 2 (Table 12), and it is probably a consequence of having less particles at the beginning of each time step combined with the growth of the particles. The mean diameter of particles dropped by this process is smaller than the mean diameter of particles in the whole aerosol suggesting that small sized particles are being pushed away and dropped by electrostatic forces. Their charges are positive because the net charge of the aerosol has a positive charge. The likelihood of particles with a specific charge to be rejected depends

both on the relative frequency of particles in each charge level and the number of positive charges in the particles. Higher positive charges are more likely to be rejected. These two influences explain the numbers in the fifth column from the left in Table 12 where the order of the charges agree with the frequency of particles for those charge levels in the first time steps (those with more particles dropped); however, in later time steps particles with higher positive charges are chosen in spite of their lower frequency (shown in Table 15). Note that, in that column (fifth from the left in Table 12), the charges of the particles being removed are ordered by their frequency from most to less frequent.

In this simulation, deposition (as shown in Table 13) behaves similarly to Problem 1 except for the fact that the deposition starts with slightly more activity and ends with less. This process is responsible for most of the reduction in the number of particles at the beginning, but decreases its activity quickly. The mean diameter of the particles dropped by this process start around 17 nm smaller than the mean aerosol particle diameter (Table 11) in the first time step, and continuously approaches the mean aerosol particle diameter having a difference of only 8 nm by the last time step. This suggests that mostly smaller particles are being dropped at the beginning, eventually larger particles start to be removed along with small ones. This behavior is explained as a strong contribution of convection-diffusion to the removal rate which is higher than that of gravitational settling for most of the particles in the aerosol given the size range considered in the simulation. The abundance of very small particles and possibly a high mean particle density (compared with Problem 1) make deposition very strong in the first time steps of the simulation, and as these particles are removed, the contribution of deposition is reduced. Other factors responsible for the reduction in deposition activity

are the effects of condensation and coagulation; thus, as particles grow larger, the component of the removal rate from convection-diffusion gets smaller, and gravitational settling does not grow significantly (for the particle size range in this simulation). Problem 2 shows considerably more activity in coagulation, which explains why the mean aerosol particle diameter grows larger and further reduces the population of small-sized particles, more than in Problem 1. The most common charges of the particles removed by deposition agree with the relative frequency of particles in the different charge levels shown in Table 15. Few deviations from this tendency (when fewer particles are deposited in the last time steps) can be attributed to some particles not passing the deposition test while others do.

The process most affected by the different particle composition in Problem 2 (denser particles, larger mean mass) is coagulation (Table 14). This is first seen by the larger values for $K_{\max}$, compared to those of Problem 1. They considerably increase both the number of pairs of particles to be tested and the number of pairs coalescing into larger particles. The number of pairs coalescing (new particles) declines at a much slower pace than the number of particles being removed by deposition, and the activity from coagulation surpassed deposition at 1150 seconds. This not only contributes to reducing the number of particles, but also to increasing the mean particle diameter affecting both electrostatic dispersion and deposition. The mean diameter of particles coalescing at the different time steps is 13 to 20 nm larger than the mean diameter of the aerosol particles. These values are larger than those in Problem 1; so, in this case, not only are particles larger than the mean particle diameter coalescing, but they are farther from the mean. The coagulation of larger particles favors a faster displacement of the size distribution setting

a trend towards larger diameters, which can be seen in Table 11 and in figures of number distributions to be presented in the next pages. The charges involved agree mostly with the relative frequency of particles in the different charge levels; however, sometimes larger or less frequent charges are favored. This is presumably due to the high likelihood of coalescing for pairs of particles whose elements have a high number of charges and different polarities. The pairs chosen to test coalescence are random, but when the particles selected satisfy the conditions mentioned, it is very likely that they coalesce.

The relative frequency of particles in every charge level for all the time steps of the simulation (Problem 2) is shown in Table 15. In general, the fraction of neutral particles is constantly decreasing while other charge levels increase their fractions. The fractions for particles with negative charges grow more than the positive ones because the net charge of the aerosol is positive; thus, electrostatic dispersion is rejecting only particles with positive charges. Also, for charge levels +2, +3, and +4, the higher the charge, the lesser the fraction growth. This behavior is explained by the higher probability of particles with more charges to be rejected. Up to this point everything seems very similar to Problem 1, but interestingly, the effects of stronger coagulation can be seen in this table. These effects are a faster reduction in the fraction of neutral particles accompanied by a faster increase in the fractions of charged particles. Neutral particles disappear faster as they coagulate with charged particles, causing the new particle to become charged. For this problem, coalescence also exists between particles with both positive polarities. Their fraction become significant relative to negative charge levels by the end of the simulation.

Table 15. Relative frequency of particles in each charge level ordered by largest from left to right, except for the last column (Problem 2).

Time (s)	Charge level									
	0	+1	−1	+2	+3	+4	−2	−3	−4	> +4
0	0.72	0.13	0.072	0.049	0.020	0.010	0.0047	3.0E−04	3.0E−05	0
50	0.71	0.13	0.072	0.051	0.021	0.010	0.0048	3.2E−04	3.3E−05	6.7E−05
100	0.71	0.13	0.072	0.052	0.022	0.010	0.0050	3.4E−04	3.6E−05	2.1E−04
150	0.71	0.13	0.073	0.053	0.022	0.011	0.0051	3.6E−04	3.9E−05	2.8E−04
200	0.71	0.13	0.073	0.054	0.023	0.011	0.0052	3.7E−04	4.1E−05	3.6E−04
250	0.70	0.13	0.073	0.055	0.024	0.011	0.0051	3.8E−04	4.3E−05	4.3E−04
300	0.70	0.13	0.074	0.055	0.024	0.011	0.0052	3.8E−04	4.5E−05	5.0E−04
350	0.70	0.13	0.074	0.056	0.024	0.012	0.0053	3.6E−04	4.7E−05	6.3E−04
400	0.70	0.13	0.074	0.056	0.025	0.012	0.0054	3.6E−04	4.9E−05	7.5E−04
450	0.69	0.13	0.074	0.057	0.025	0.012	0.0055	3.4E−04	5.1E−05	8.6E−04
500	0.69	0.13	0.075	0.057	0.025	0.012	0.0055	3.5E−04	5.2E−05	9.0E−04
550	0.69	0.13	0.075	0.057	0.025	0.012	0.0057	3.8E−04	5.4E−05	1.0E−03
600	0.69	0.13	0.075	0.058	0.026	0.012	0.0057	3.9E−04	5.5E−05	1.1E−03
650	0.69	0.13	0.075	0.058	0.026	0.013	0.0060	3.8E−04	5.7E−05	1.2E−03
700	0.68	0.13	0.075	0.059	0.027	0.013	0.0061	3.7E−04	5.8E−05	1.3E−03
750	0.68	0.13	0.076	0.059	0.027	0.013	0.0063	3.8E−04	5.9E−05	1.4E−03
800	0.68	0.14	0.076	0.060	0.027	0.013	0.0063	3.8E−04	6.1E−05	1.7E−03
850	0.68	0.14	0.076	0.060	0.027	0.013	0.0064	3.9E−04	6.2E−05	1.8E−03
900	0.68	0.14	0.076	0.061	0.028	0.013	0.0065	4.2E−04	6.3E−05	1.9E−03
950	0.68	0.14	0.076	0.061	0.028	0.013	0.0065	4.5E−04	6.4E−05	2.0E−03
1000	0.67	0.14	0.077	0.061	0.028	0.014	0.0067	4.6E−04	6.6E−05	2.1E−03
1050	0.67	0.14	0.077	0.062	0.028	0.014	0.0068	4.7E−04	6.7E−05	2.2E−03
1100	0.67	0.14	0.077	0.062	0.029	0.014	0.0068	4.5E−04	6.8E−05	2.3E−03
1150	0.67	0.14	0.077	0.063	0.029	0.014	0.0069	4.9E−04	6.9E−05	2.5E−03
1200	0.67	0.14	0.078	0.063	0.029	0.015	0.0069	5.2E−04	7.0E−05	2.6E−03
1250	0.67	0.14	0.078	0.064	0.029	0.015	0.0069	5.5E−04	7.2E−05	2.7E−03
1300	0.67	0.14	0.078	0.064	0.029	0.015	0.0070	5.6E−04	7.3E−05	2.8E−03
1350	0.66	0.14	0.078	0.064	0.030	0.015	0.0071	5.4E−04	9.8E−05	2.9E−03
1400	0.66	0.14	0.078	0.065	0.030	0.015	0.0072	5.5E−04	1.0E−04	3.1E−03
1450	0.66	0.14	0.078	0.065	0.031	0.015	0.0073	5.6E−04	1.0E−04	3.2E−03
1500	0.66	0.14	0.078	0.066	0.031	0.015	0.0074	5.9E−04	1.0E−04	3.4E−03

To aid in the visualization of the aerosol evolution in Problem 2, figures with number and mass distributions are presented with and without discrimination by charge level. These distributions are obtained for four evenly spaced time steps along the simulation. The vertical lines show the limits of the 20 size bins and the points indicate the number of particles for every size bin. Note that the lines connecting the points are just to improve visualization of the distributions, but the points indicate discrete values for the regions comprised in a size bin. The number of particles and the values of masses are not scaled to the whole aerosol population. Rather, they correspond to values of the simulated particles.

Figure 22 show particle number distributions along the evolution of the aerosol without the discrimination of charge levels. In this figure, one can see how particle sizes change in time irrespective of their electrical charge. Apart from the small-sized particles quickly disappearing by convection-diffusion and the general displacement of the distribution to the right by condensation, this plot shows a higher number of particles in the right tail of the distributions (especially in the final time steps) relative to Figure 3 (Problem 1). This is presumably due to coagulation since the information in Tables 4 and 10 confirmed that condensation behaves similarly in both simulations. Larger mean particle diameters are a consequence of having more particles in the right tail of the distributions.

Figures 23, 24, and 25 show the component mass distributions for graphite, silver and water respectively, without discrimination of charge. Values here correspond to the total mass of each component per size bin. The shape of the distributions is the same for graphite and silver, but the mass of silver is nine times greater than the mass of graphite

in all size bins. There is no mass distribution for water at 0 seconds because the aerosol is dry at the beginning of the simulation, but at 500, 1000, and 1500 seconds one can see the rapid growth of this component surpassing the mass of silver in the particles. The same effect (as shown in Figure 22) of the right tail of the distribution dropping less than their equivalents in Problem 1 is seen in these figures, resulting from a stronger coagulation of larger particles (as shown in Table 14).

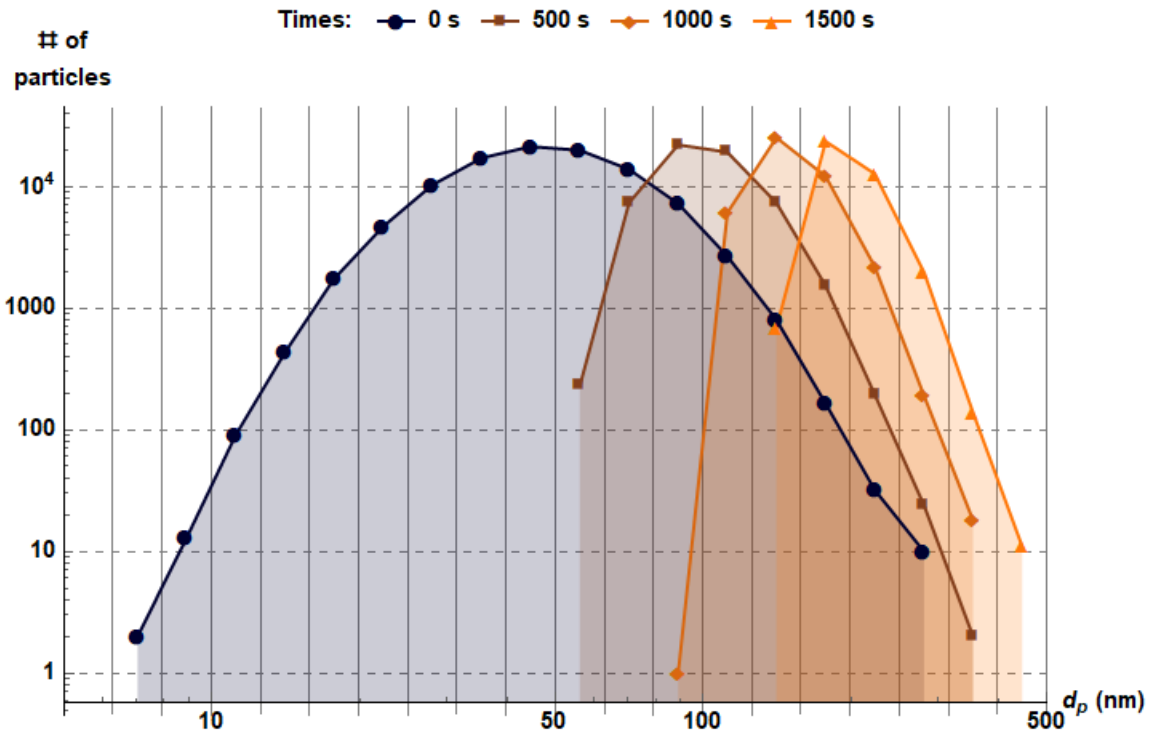

Figure 22. Particle number distributions for Problem 2 at 0, 500, 1000 and 1500 seconds.

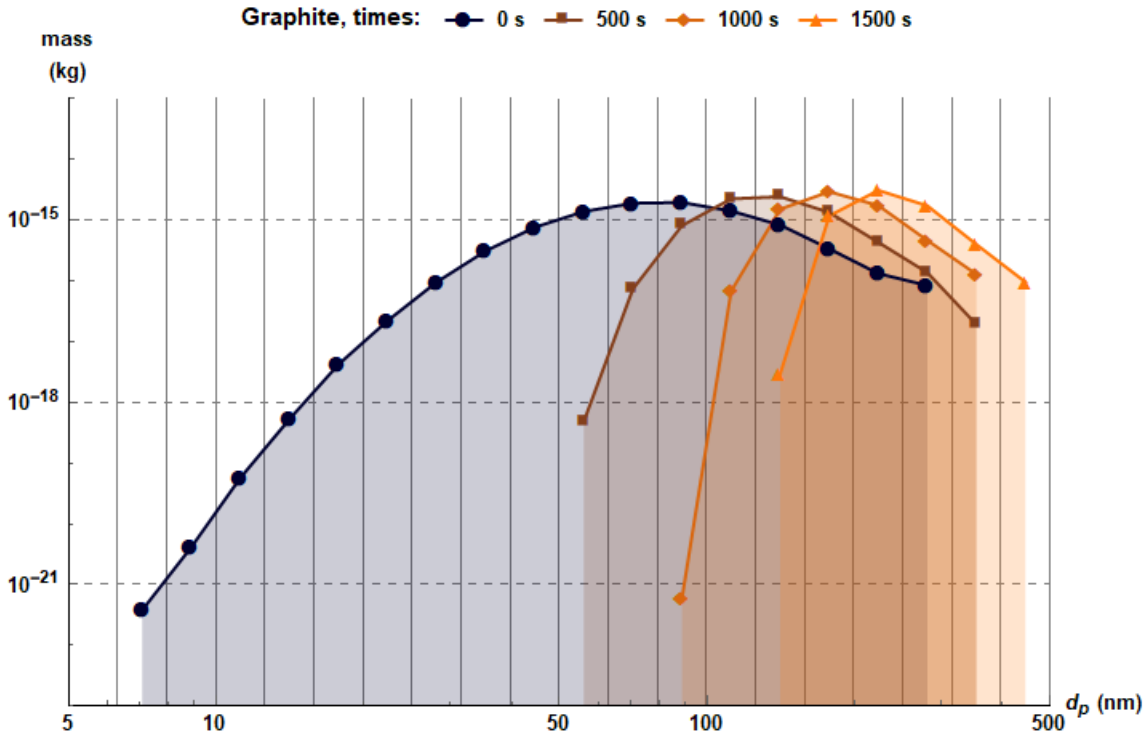

Figure 23. Mass distribution of graphite for Problem 2 at 0, 500, 1000 and 1500 seconds.

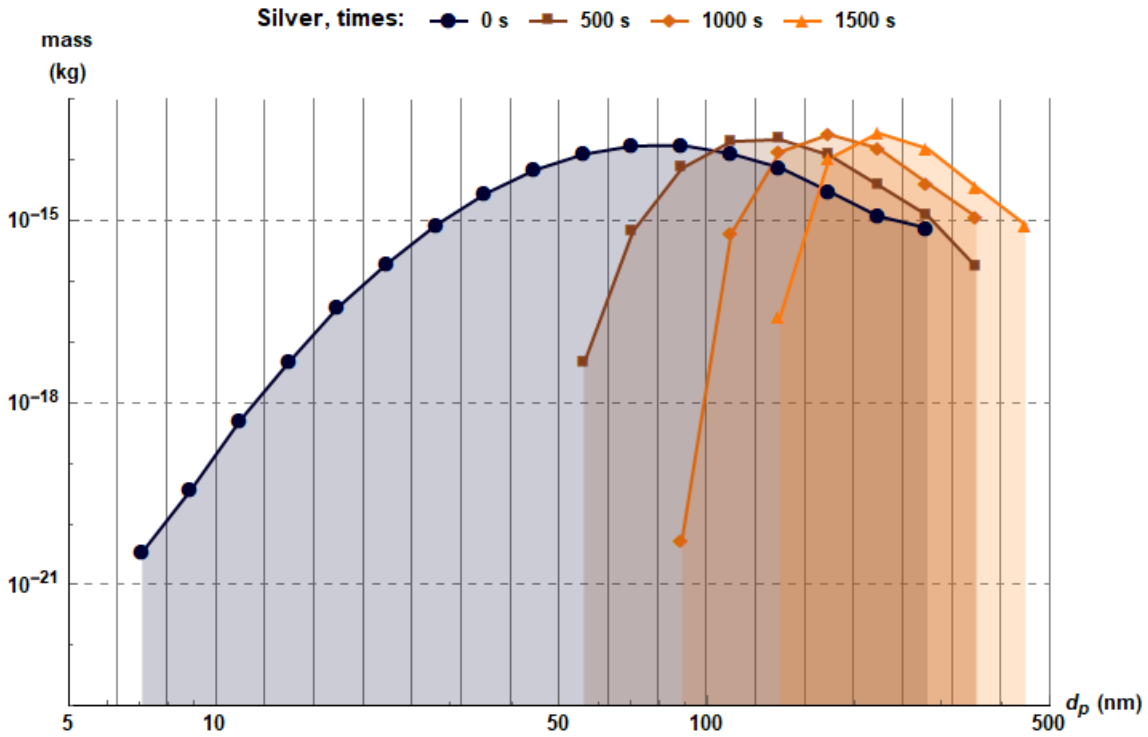

Figure 24. Mass distribution of silver for Problem 2 at 0, 500, 1000 and 1500 seconds.

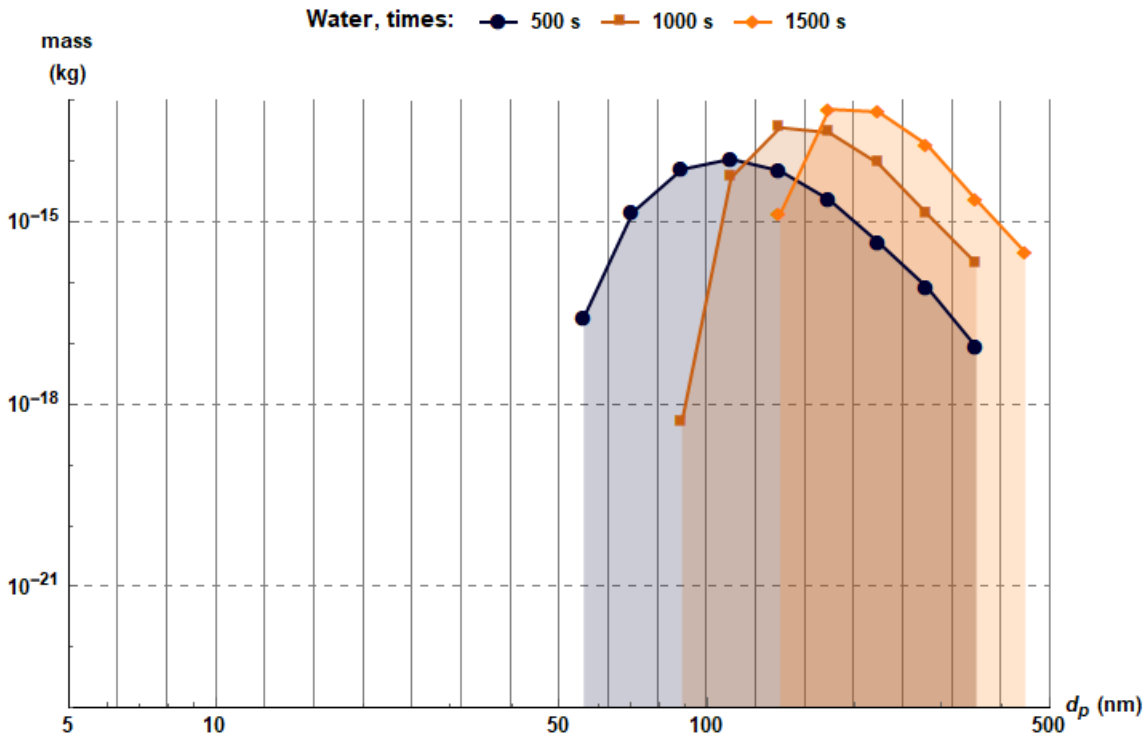

Figure 25. Mass distribution of water for Problem 2 at 500, 1000 and 1500 seconds.

Particle number distributions with discrimination of charges are shown in Figures 26, 27, 28, and 29 for times of 0, 500, 1000 and 1500 seconds, respectively. These allow us to see the evolution of the aerosol in terms of particle size within the different charge levels. These figures show that both neutral and charged small-sized particles are being removed, that distributions of negative charges approach their positive counterparts as time passes, and that the neutral distribution gets closer to charged distributions as their fraction of particles is diminished. The diminishing of the neutral particle fraction is particularly enhanced in this simulation relative to Problem 1 together with a higher number of particles in the last size bins (larger particles) for most of the distributions which are a result of a stronger coagulation activity. The mean values of the different charge levels seem to get closer with time, but it is difficult to tell in the logarithmic scale of the horizontal axis.

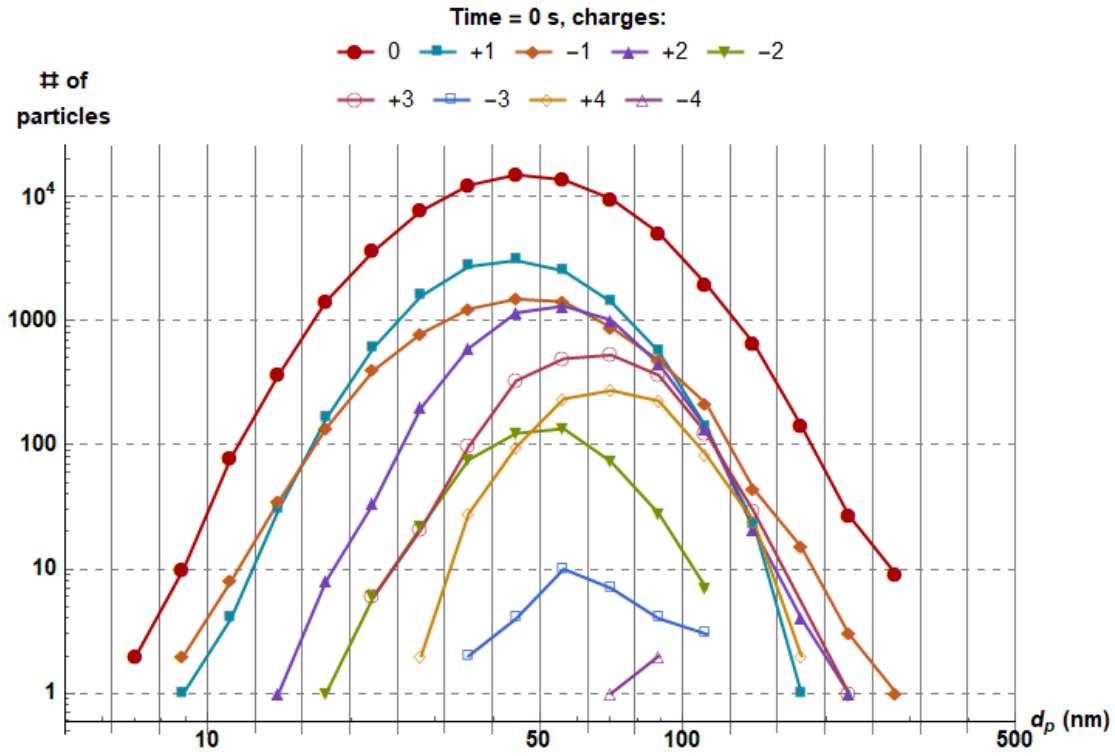

Figure 26. Particle number distribution for Problem 2 with discrimination of charge at 0 seconds.

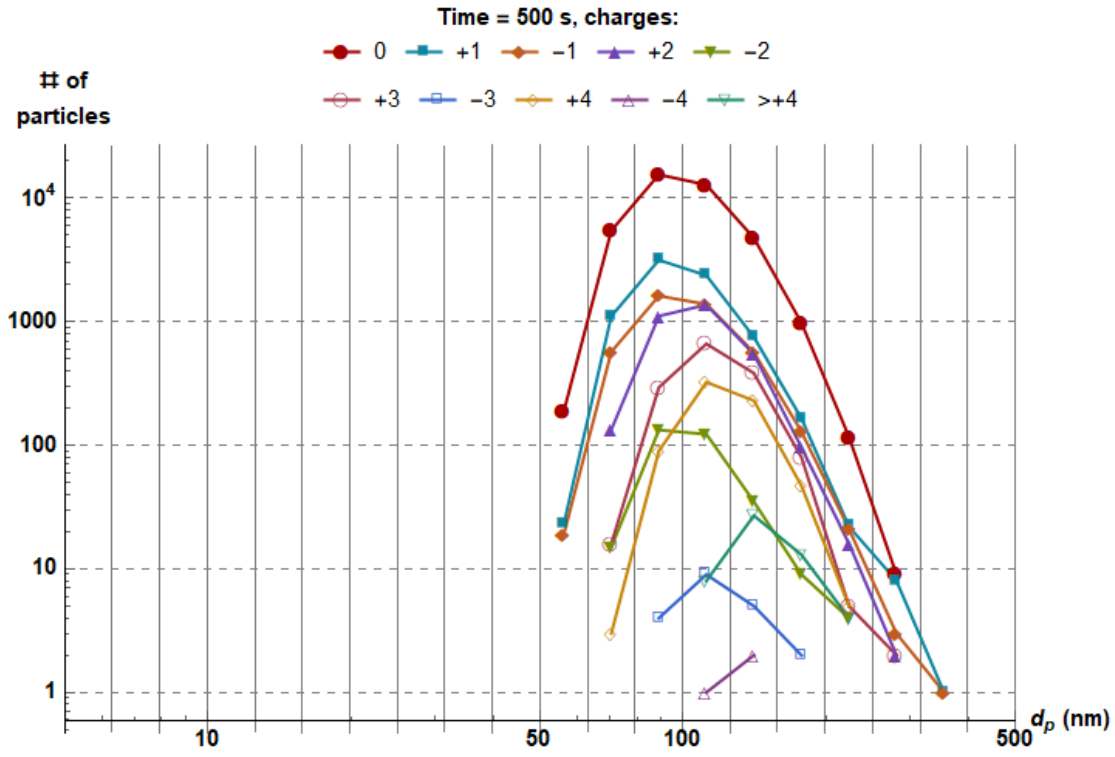

Figure 27. Particle number distribution for Problem 2 with discrimination of charge at 500 seconds.

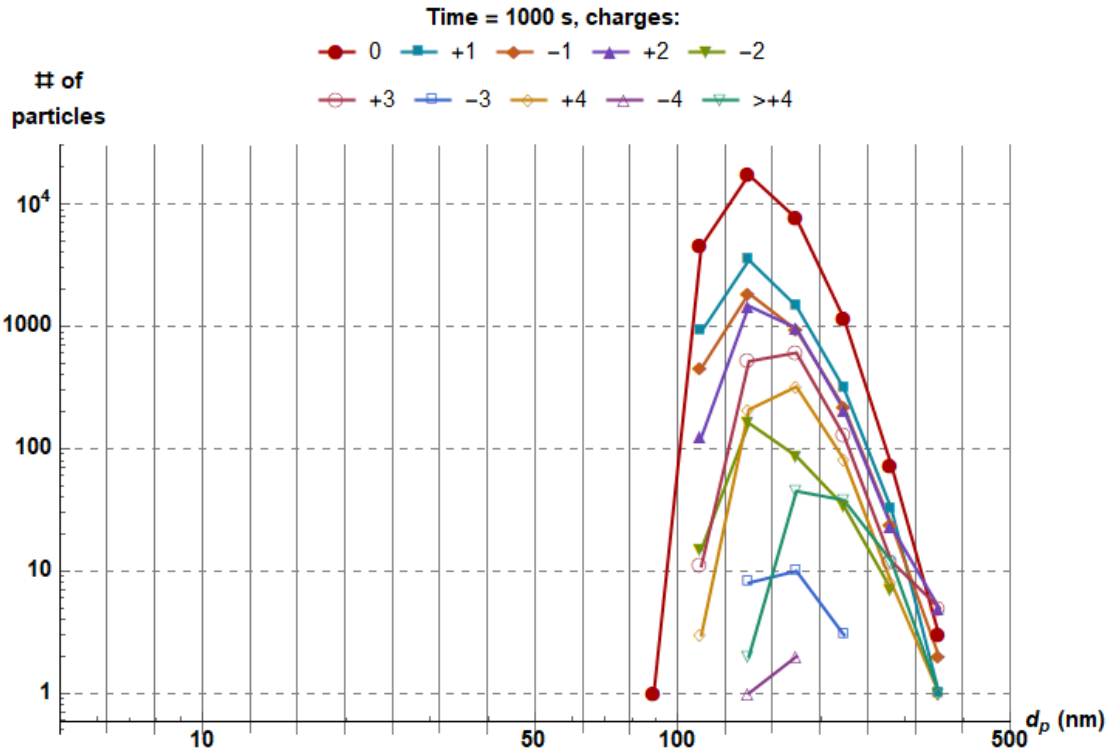

Figure 28. Particle number distribution for Problem 2 with discrimination of charge at 1000 seconds.

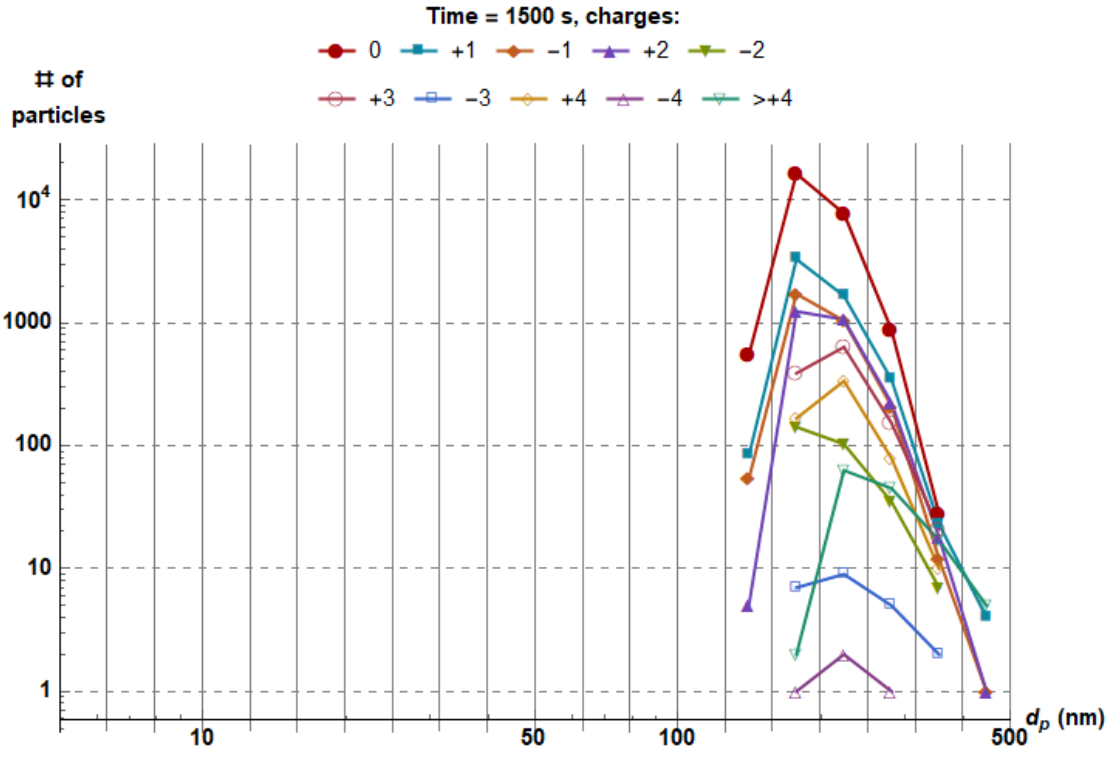

Figure 29. Particle number distribution for Problem 2 with discrimination of charge at 1500 seconds.

Mass distributions for every charge level of the components making up the aerosol particles are shown from Figures 30 to 40. These correspond to the same time steps considered in the previous figures (0, 500, 1000, and 1500 seconds). There is no mass distribution for water at time zero (starting with dry particles). The distributions for graphite and silver at different charge levels have the same shape, mean and standard deviation at each time step. The only difference is that the masses of graphite are 0.11 times that of silver. Water mass distributions do differ from those of graphite and silver because of the process by which particles gain water during the simulation. In all distributions, the right tails show more gain with time than their counterparts in Problem 1, especially in the last 3 to 5 size bins (corresponding to larger particles). The content of water in particles looks very similar to Problem 1 in terms of quantity, except more water is found in the larger particles because of the higher number of large particles. Mass distributions for neutral particles also approach the distributions of charged particles with time as was observed in number distributions. Moreover, the mean values of the mass distributions for the different charge levels seems to get closer.

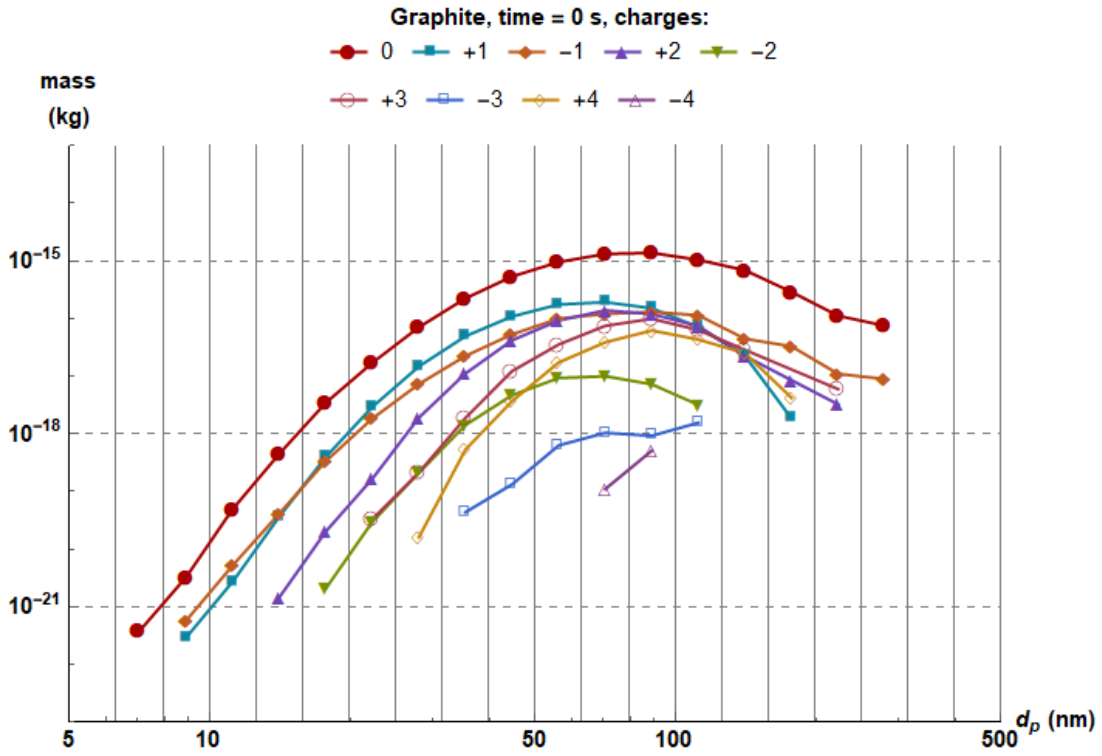

Figure 30. Mass distribution of graphite for Problem 2 with discrimination of charge at 0 seconds.

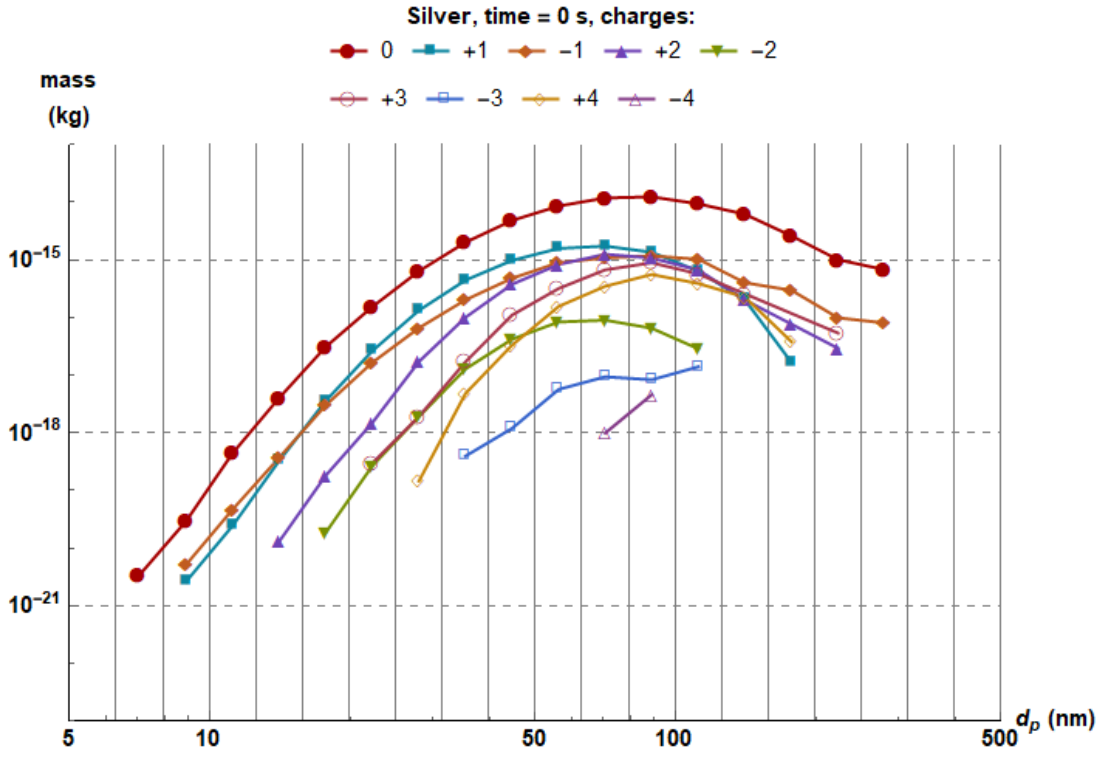

Figure 31. Mass distribution of silver for Problem 2 with discrimination of charge at 0 seconds.

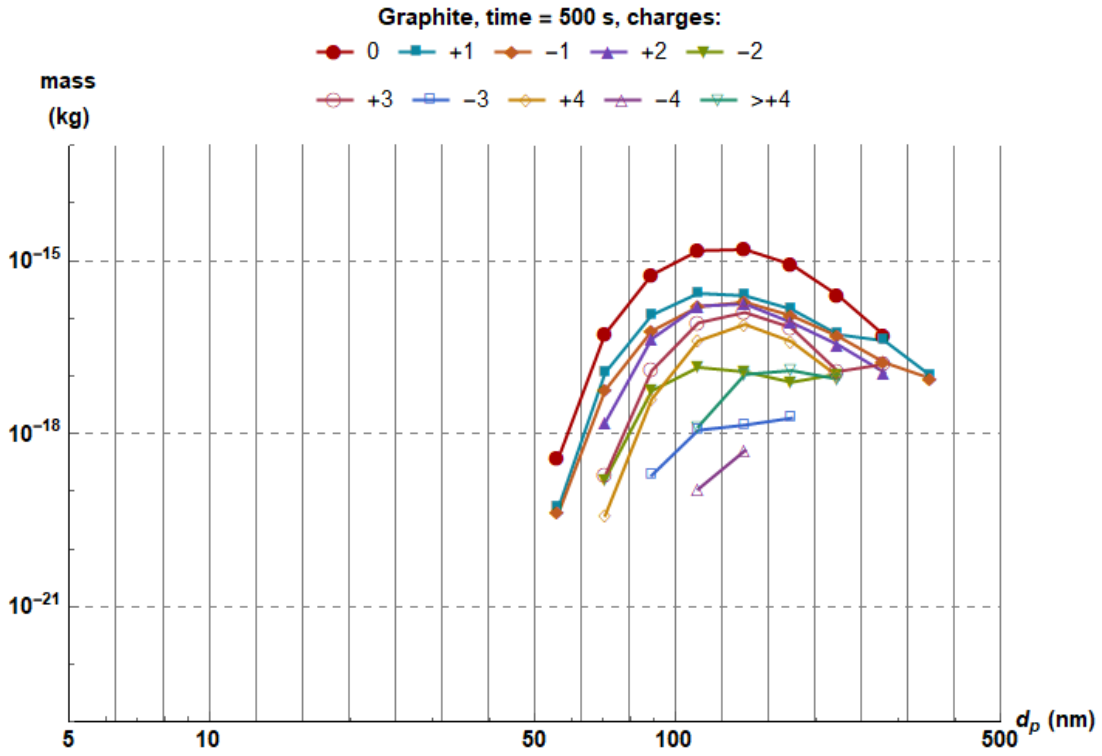

Figure 32. Mass distribution of graphite for Problem 2 with discrimination of charge at 500 seconds.

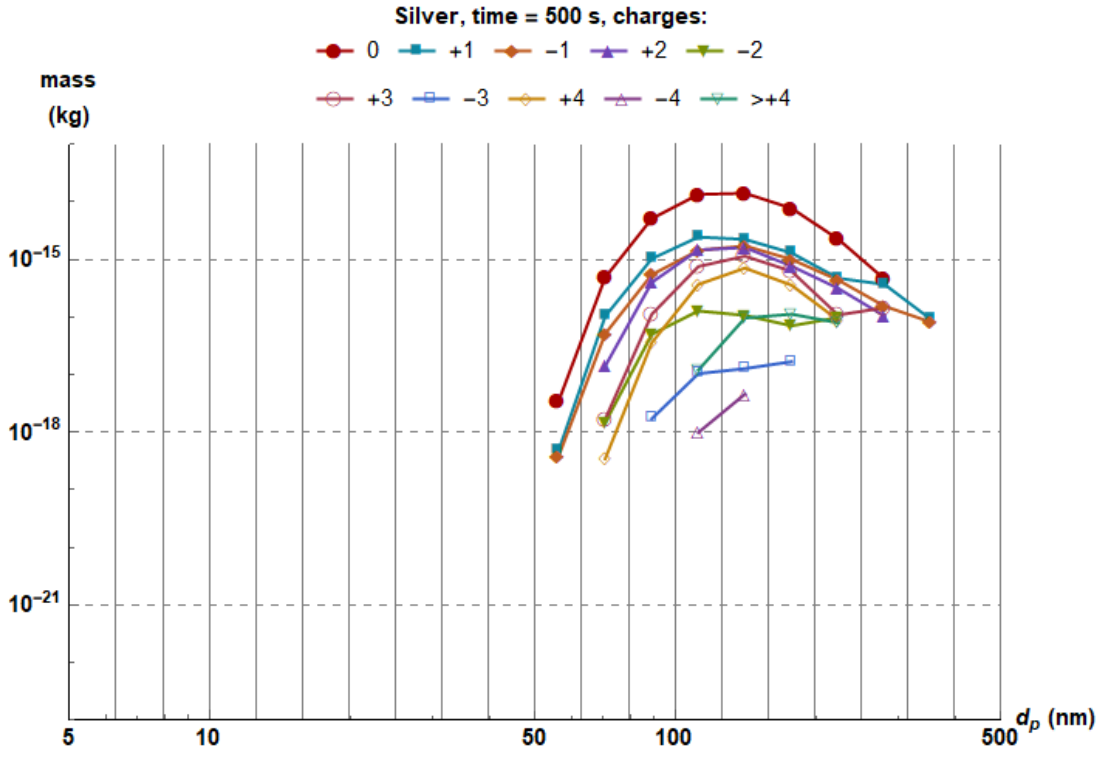

Figure 33. Mass distribution of silver for Problem 2 with discrimination of charge at 500 seconds.

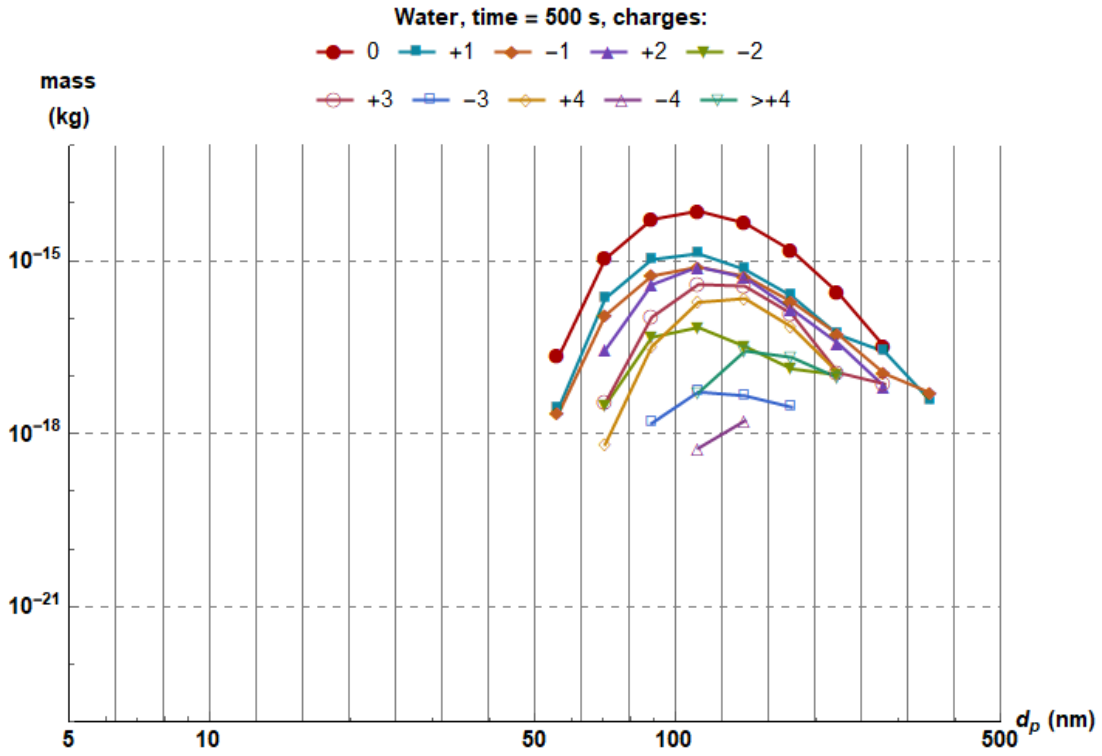

Figure 34. Mass distribution of water for Problem 2 with discrimination of charge at 500 seconds.

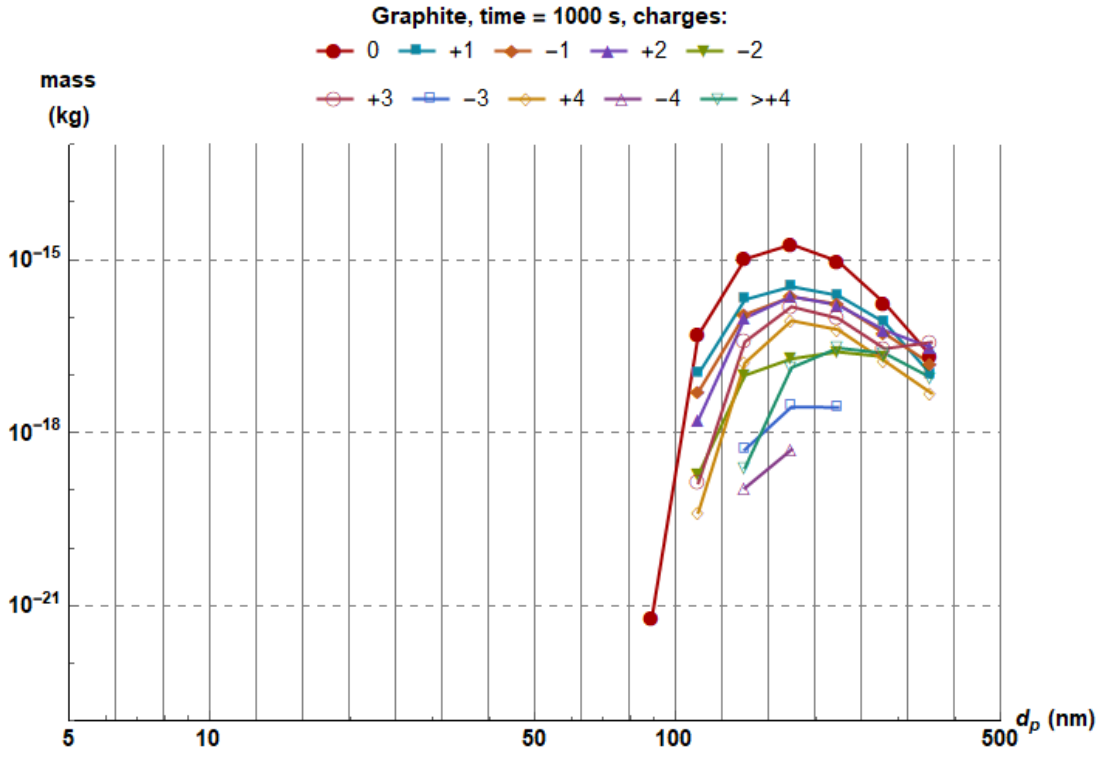

Figure 35. Mass distribution of graphite for Problem 2 with discrimination of charge at 1000 seconds.

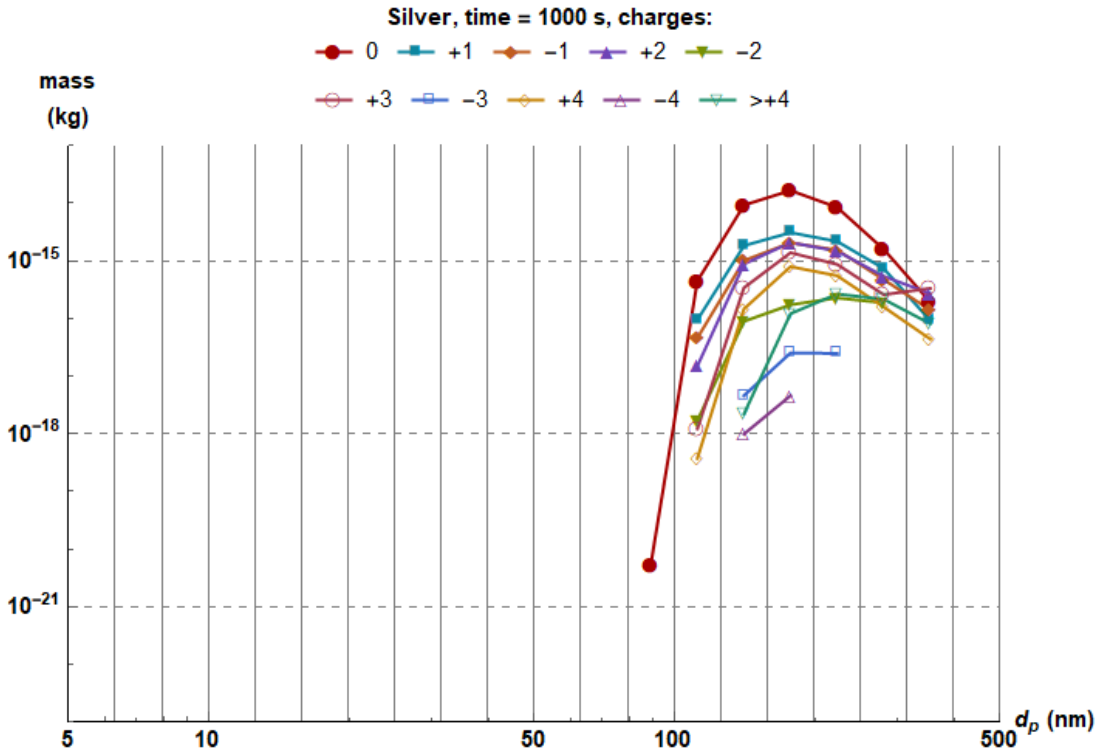

Figure 36. Mass distribution of silver for Problem 2 with discrimination of charge at 1000 seconds.

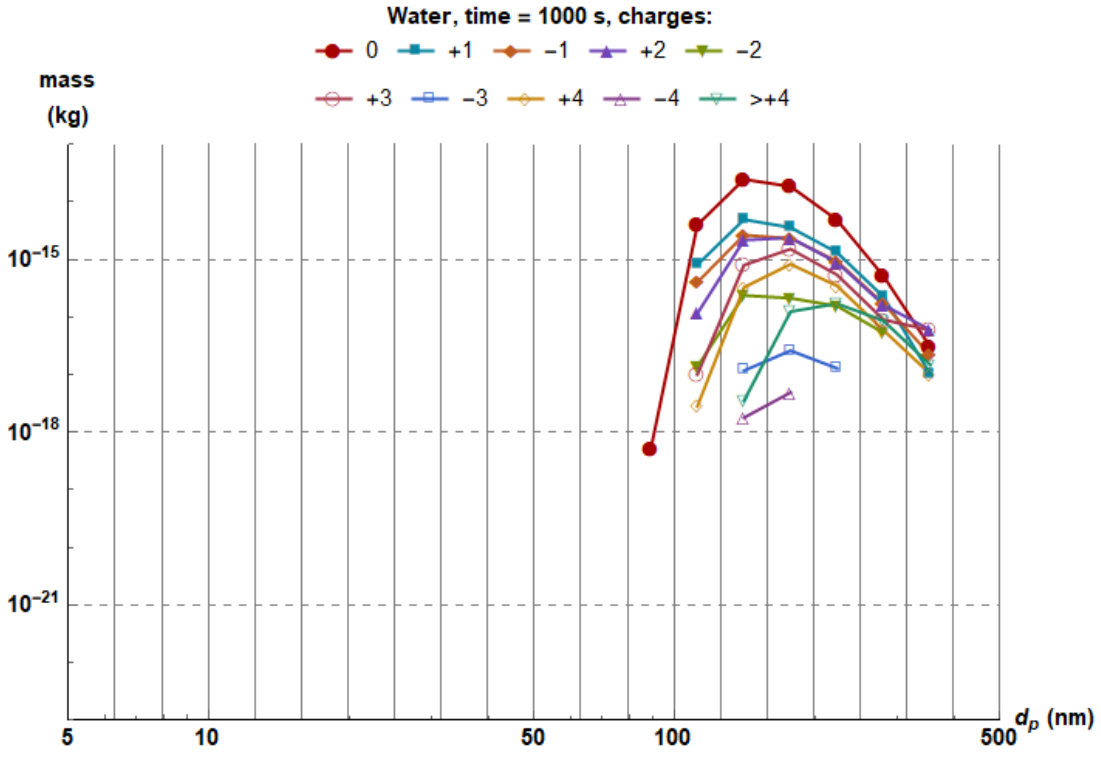

Figure 37. Mass distribution of water for Problem 2 with discrimination of charge at 1000 seconds.

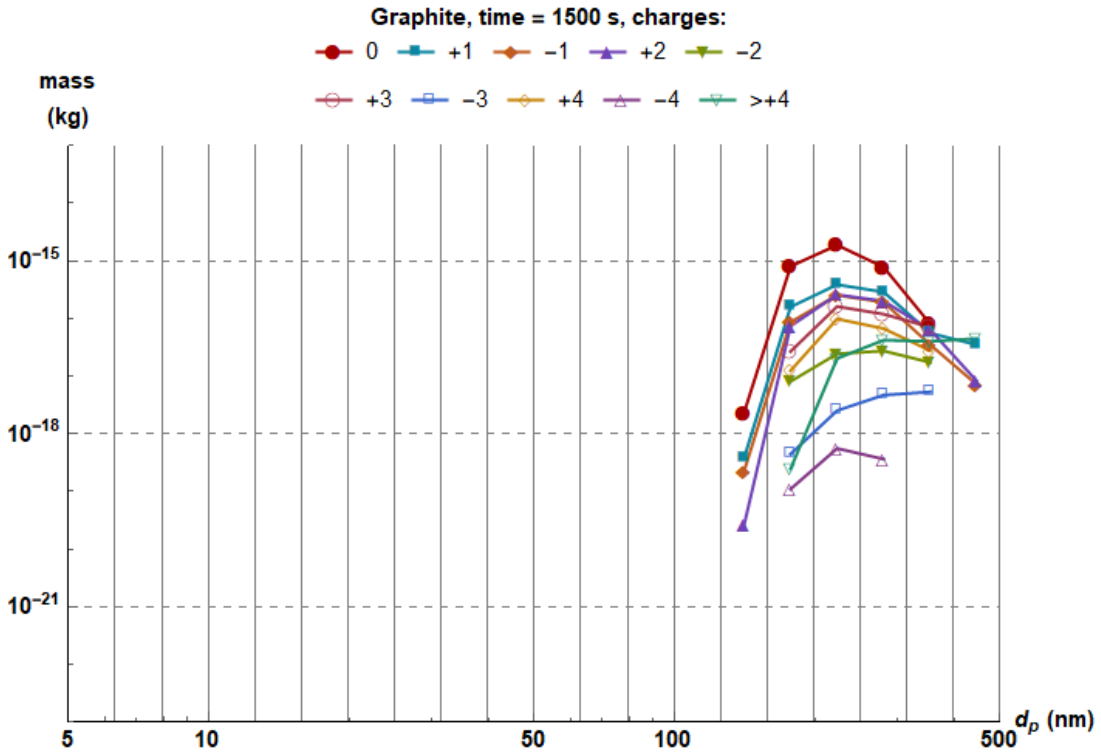

Figure 38. Mass distribution of graphite for Problem 2 with discrimination of charge at 1500 seconds.

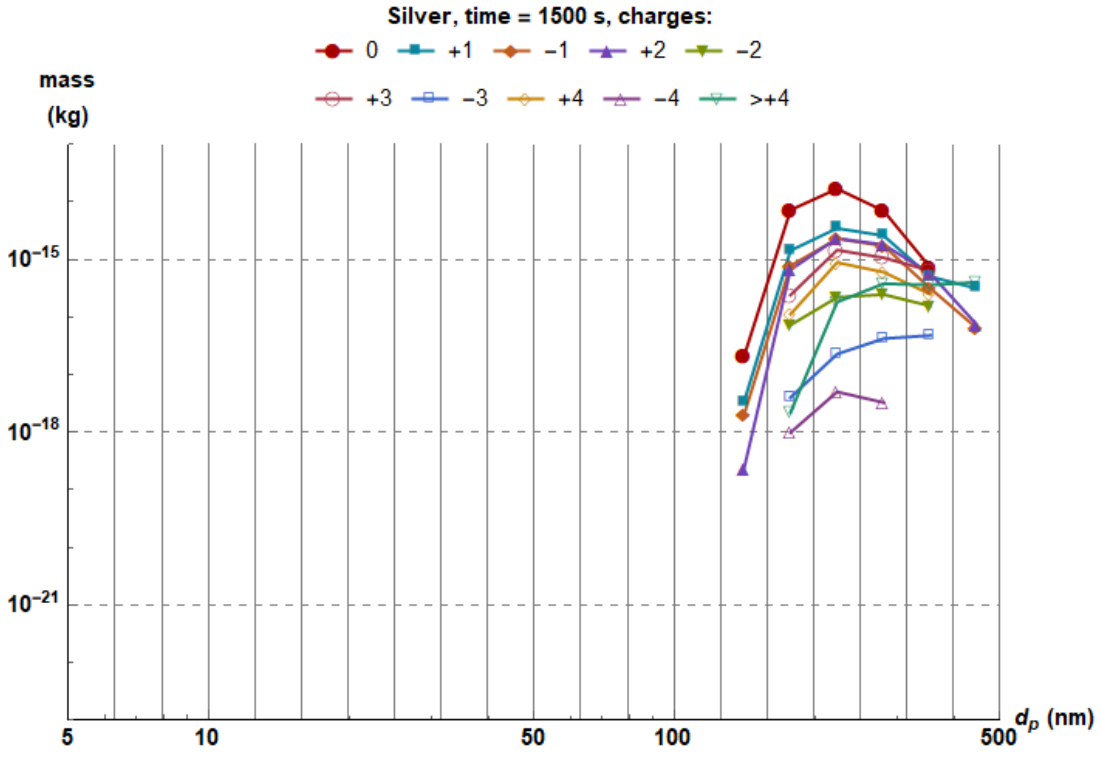

Figure 39. Mass distribution of silver for Problem 2 with discrimination of charge at 1500 seconds.

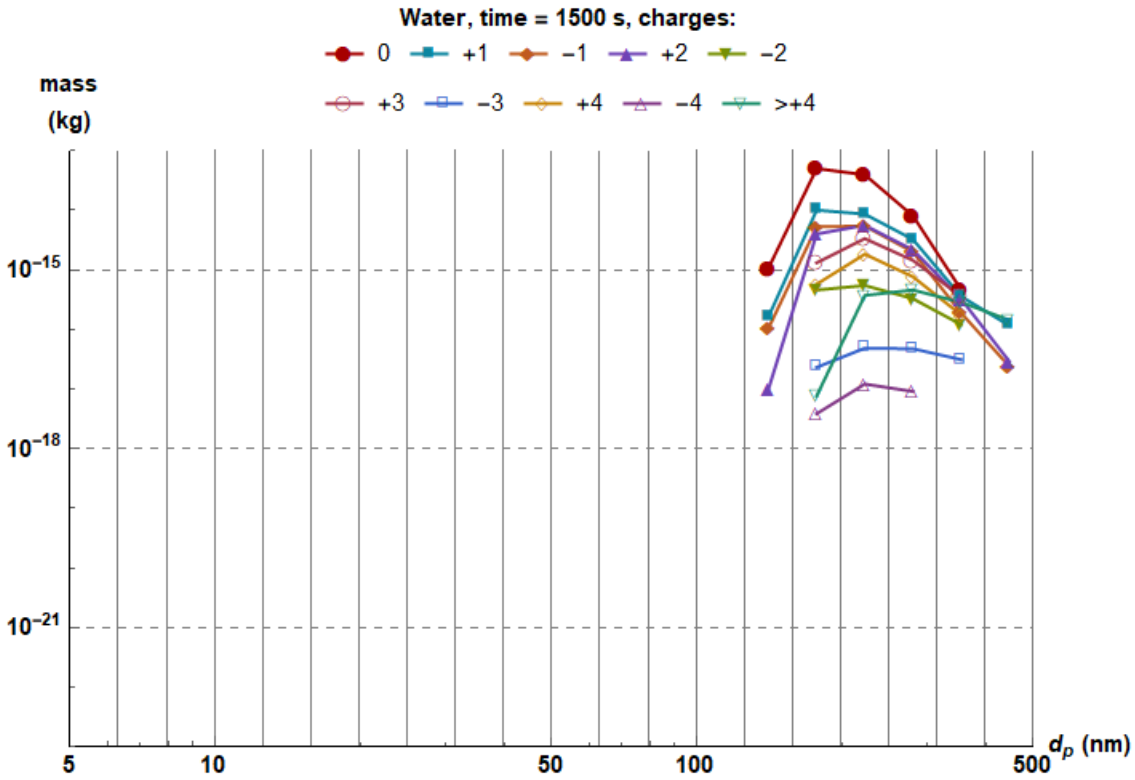

Figure 40. Mass distribution of water for Problem 2 with discrimination of charge at 1500 seconds.

3.8 Conclusions

The program developed has successfully integrated the processes of coagulation (with charge effects), deposition, condensation and electrostatic dispersion into the DSMC technique for the simulation of multi-component polydisperse aerosol evolution. Realistic physical models are used in the different processes enabling simulations which are very difficult to perform using numerical solutions. The level of complexity achievable with the DSMC technique is not limited to what has been implemented here but can grow to accommodate other particle properties or processes. Simulations and experiments can be easily compared since it is not difficult to generate particle lists representing an actual aerosol from measurements obtained with aerosol measurement equipment such as a scanning mobility particle sizer (SMPS) and a tandem differential

mobility analyzer (TDMA). These lists can be used as initial particle lists (to start a simulation) and also as a means to compare experiments and simulations at any time step. However, the particle lists obtained by SMPS and TDMA are not always adequate when it comes to giving a full account of the particle composition.

The main purpose of this program is to simulate the evolution of the aerosol changing the particle list as time goes by, but its usefulness is not limited to that. With this type of program one can perform a more detailed analysis of the particles interacting in each process thereby determining changes in the average particle size and identifying the most common charges. Besides, one can determine which process is more active, how their individual activity is influencing the other processes, and how particle composition, and electrical charge affects aerosol evolution. All this information can be used to explore their synergistic nature. The physical models used in the program have been benchmarked individually. When they are combined into a DSMC program, one can better understand the influences among them and find out more details about their combined activity. This type of analysis can give rise to new insights about the evolution of aerosols.

An interesting finding of this work is how denser particles increase the activity of coagulation. This was observed by comparing Problems 1 and 2. The simulation in Problem 2 starts with a mean particle density that is around 3.3 times higher than that of Problem 1 due to a different particle composition but with the same size distribution. This resulted in a stronger coagulation for the conditions of the simulation, while deposition and electrostatic dispersion suffered small changes. Not only did more particles undergo coagulation, but the particles coalescing had larger diameters than in Problem 1, which

was a consequence of having larger values for $K_{p,q}$ and $K_{\max}$. The higher coagulation activity resulted in a faster growth of the mean particle diameter (compared to Problem 1) and presumably caused small changes in the other processes by a faster reduction in the number of suspended particles, and possibly by the coalescing of a fraction of small particles. Having less particles affects all the processes, deposition, electrostatic dispersion and coagulation, because it reduces the amount of interactions. In condensation, it reduces the overall gain of water mass. However, it is not solely the number of particles remaining that matters; it is also important to know what kind of particles are interacting in terms of size and electrical charge. For example, coagulation in Problem 2 is targeting particles larger than the mean aerosol particle diameter, causing them to coalesce while deposition and electrostatic dispersion are removing particles smaller than the mean aerosol diameter by convection-diffusion. This circumstance somehow diminishes the impact of coagulation during these processes. However, if the size ranges of the aerosol particles are such that gravitational settling would be the main process driving deposition, then a stronger coagulation would be accompanied by stronger deposition since the new particles would have a higher likelihood of succumbing to the gravitational downward pull.

Particle composition determines the mean particle density for the aerosol. In dry particles with the same mass fractions of components, the mean particle density would have a fixed value along the entire simulation. In this case, one could think of simplifying the problem by simulating one-component particles with a density which matches their multi-component composition. However, when condensation is present, the mean particle density will change for each time step as shown in the last columns of Tables 5 and 11.

This decline in particle density might have influenced the rapid decline in particles undergoing deposition in both problems. Especially in Problem 2, where deposition initially became stronger than in Problem 1, but its activity also dropped faster. This variation in particle density, which may not be handled properly with the sectional technique, is one of the important reasons to advance in the development of the DSMC technique to simulate aerosol evolution and get more accurate results.

Future additions to this program can be the incorporation of weights to simulated particles, the use of a distribution for particle composition, a dynamic management of the order in which the different processes are applied, and the incorporation of other particle characteristics like radioactivity and shape. The use of particle weights would help to get better statistics by maintaining the number of particle volumes representing the aerosol in the particle list in processes like deposition or electrostatic dispersion; thus, particle volumes dropped would get a lower weight instead of being removed. This is explored further in chapter 5. In this work the composition of particles was fixed in the sense that all particles maintained the same ratio of graphite to silver in both problems (except for water). Although this may be a good approximation, it presumably is not the case in aerosols generated in nuclear power plants or in aerosols generated by spark discharge (as is mentioned in Section 4.1). The mass fractions of components might vary with particle size or other properties. Thus, the effect of a distribution in the particle composition needs to be explored by generating initial particle lists which account for this variation in the components' mass fractions. This will be a step forward towards getting more realistic simulations. Finally, it is advisable to implement a dynamic order for the implementation of the processes and a dynamic time step determined by the activity in

the aerosol, especially for long simulations. For the problems presented here, the order of the processes and the time step were chosen according to the activity of the processes at the beginning of the simulations. However, particles change in size, charge and composition with time and this results in different dynamics where the relevance of the different processes fluctuates. Getting the program to adapt to these changes will result in more efficient and perhaps more accurate results.

This work was focused on extending the capabilities of the simulation of aerosol evolution using the DSMC method without focusing too much on shortening simulation time. Although it is tempting to make a lot of additions to the DSMC programs in future developments, they all come at the cost of computer time. The efforts to make simulations more realistic must be accompanied by efforts to have an efficient code which saves time performing the required tasks and by implementation of parallel processing to reduce the simulation time further.

4. POSSIBLE EXPERIMENTS

Together with the development of the DSMC program, we worked on experiments to measure the evolution of two-component charged aerosols (e.g. graphite and silver) by coagulation, obtaining size and charge distributions along an open flow coagulation tube designed by Simones and Loyalka (2015). The experimental setup for measuring coagulation is shown in Figure 41. The system consists basically of a PALAS nano particle generator model DNP-3000, the coagulation tube, a TSI 3936 scanning mobility particle sizer (SMPS) spectrometer (TSI 3080 electrostatic classifier + TSI 3775 condensation particle counter), and a tandem differential mobility analyzer (TDMA) (TSI 3080 electrostatic classifier + TSI 3936 SMPS). The same SMPS is used in the TDMA. The nanoparticle generator (spark generator) is the source of the aerosol, generating particles by the ablation of electrodes made of the material of interest for the aerosol. These particles are carried out by nitrogen gas and fed into the coagulation tube which has five geometrically spaced sampling ports. Provided the carrier gas flow is constant and the current for generating particles is steady, the aerosol produced will somehow maintain a certain size and charge distribution, which is taken as the initial particle distribution (first sampling port). The coagulation tube serves as an instrument to check the evolution of the aerosol especially through coagulation, since other processes like deposition or condensation are minimized with this experimental setup.

Size and charge distributions were obtained for several single-species aerosols made of graphite, gold, silver and palladium particles (Simones et al., 2011) and the evolution by coagulation of single-species aerosols made of graphite and silver has also

been studied (Simones and Loyalka, 2015). Here, we explore the possibility of generating a two-component aerosol to measure its evolution by coagulation with the purpose of comparing the results with the program mentioned earlier in Chapter 3. The intention behind this was to eventually determine the coagulation rates of multicomponent aerosols. We have two main ways in our lab to produce this kind of aerosol: using spark generators and atomizing a solution.

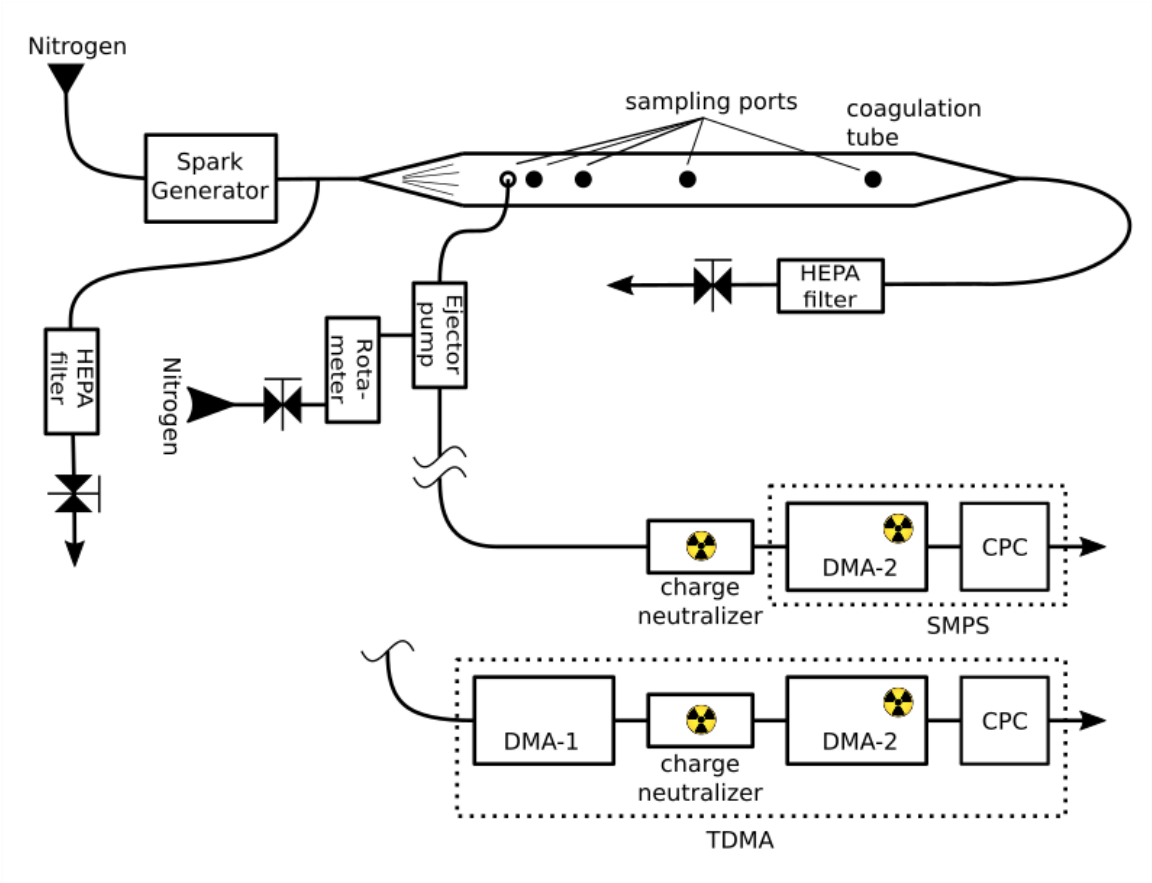

Figure 41. Schematic for the experimental setup to measure coagulation obtaining several size and charge distributions from a single component aerosol.

4.1 Two-component nanoparticles generated by spark discharge

Spark discharge is one of the most versatile techniques for generation of nanoparticles in the gas phase. It is continuous, clean, and flexible with respect to material. Furthermore, the mean particle size can be changed via the energy per spark, and the particle concentration can be varied via spark frequency. To produce a two-component aerosol by spark discharge, we consider three cases: 1) Using two spark generators, with each generator producing a different kind of nanoparticle and combining their stream, 2) using only one spark generator with electrodes of different materials installed in the cathode and anode, and 3) using one spark generator with alloyed feedstock electrodes. Figure 42 presents the mechanical arrangement of the electrodes inside a PALAS nano particle generator model DNP 3000, in the first and third option electrodes #1 and #2 would be of the same material (monometallic and alloyed, respectively). For the second option, different materials would be used. With these changes we can generate two-component aerosols, but there is still the need for characterization of the aerosols and their components at the different sampling ports.

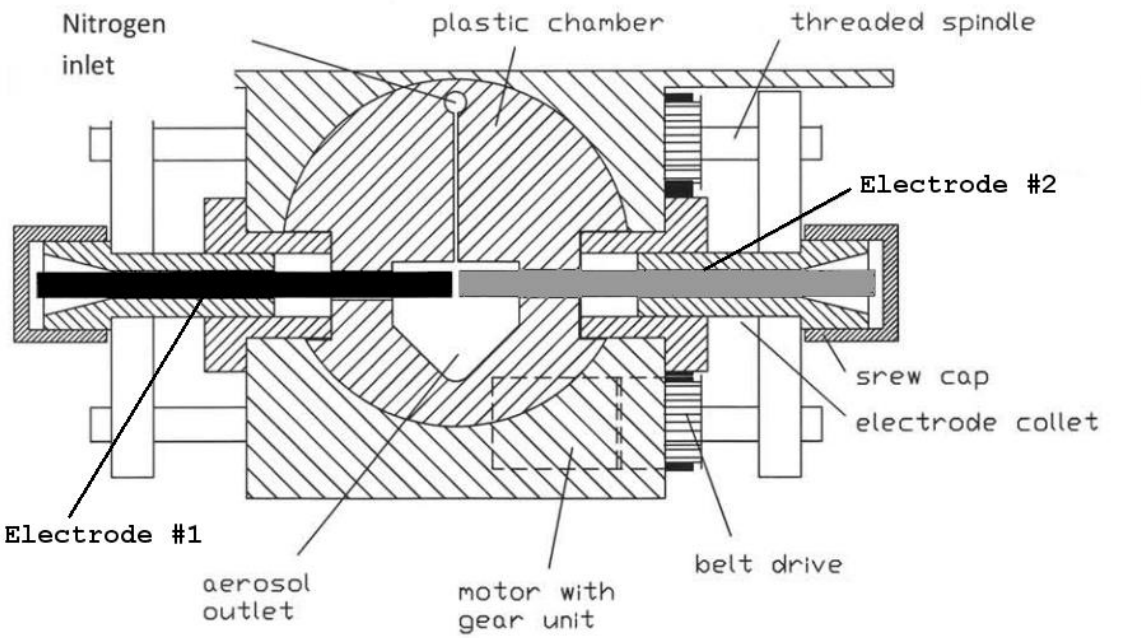

Figure 42. Mechanical arrangement of the electrode unit inside a PALAS nano particle generator model DNP 3000. Electrodes are shown in solid black and grey.

Since size and charge distributions do not provide any information about the composition of the particles, we need a way to measure the mass fractions of its components. Component distribution in particles is important because it has been shown to significantly affect the evolution of the aerosol—at least in the coagulation process (Campbell and Loyalka, 2015). The characterization of component distribution can be done using inductively coupled plasma mass spectrometry (ICP-MS) or some variant of it. Without this information, one can only compare the total number of particles and the total volume of the different size bins considered in the TDMA with the simulations. There is the possibility of making educated assumptions about the mass fractions at the creation of the aerosol but as can be seen below, these fractions vary significantly between materials. Even the polarity of the electrode affects them when using electrodes of different materials. In the next section, different alternatives to produce two-component nanoparticles will be discussed.

4.1.1 Two spark generators

When using two different spark generators, with each one generating different nanoparticles, the main concerns are characterization of the particles, achieving a good mixing of both streams and not having two-component particles in the combined streams because they would presumably have only one component (the material used in any of the spark generators). Characterization is important because aerosols coming from the two spark generators would have significantly different size distributions, even though a constant electric power and frequency is used (Byeon et al., 2008). Electrode material has a significant influence on the particle formation process as this is influenced by material properties like boiling point, evaporation enthalpy, the work function for electron emission, sputtering rate, and ionization potential (Byeon et al., 2008; Tabrizi et al., 2008a). Having particles of a single material (monometallic) might be an issue because the simulated particles in our program are represented as a combination of different materials in specific proportions, see Figure 1. The main problem in combining the stream of two spark generators might be generating an aerosol with a too diverse particle composition, which in turn results in diverse particle densities. Because density is a parameter in the models for deposition, coagulation and condensation, the simulation of the aerosol evolution must consider this varied particle composition to get accurate results. Thus, in experiments where nanoparticles are generated using two spark generators, it necessary to make the necessary changes to the initial particle list to consider monometallic particles and a varied particle composition at the beginning of the simulation.

4.1.2 Using electrodes of different materials

In several studies bimetallic nanoparticles have been generated and characterized. For example, Byeon et al. (2008) generated both monometallic (palladium, platinum, gold, and silver) and bimetallic aerosols in a spark generator (palladium–platinum, palladium–gold, and palladium –silver) characterizing the aerosols produced by SMPS, scanning electron microscopy (SEM)—energy dispersive X-ray spectroscopy (EDX), transmission electron microscopy (TEM)—selected area electron diffraction (SAED), inductively coupled plasma atomic emission spectroscopy (ICPAES), and X-ray diffraction (XRD) methods. In this study, Byeon et al. (2008) found that the monometallic particle concentrations and size distributions were different among the materials, even though a constant electric power and frequency were used (as mentioned in the previous section). In the case of bimetallic aerosols, it was found that the size distribution for any bimetal combination was between the size distribution of the two monometallic materials, that they were binary mixtures (not alloys) of two individual monometallic particles agglomerated, and that the polarity of the electrodes in each bimetal combination affected the size distribution. Table 16 shows the different mass fractions and generation rates resulting from the different combinations of electrodes and their position as either cathode or anode. Tabrizi et al. (2008a) also found that the polarity of the electrode makes a difference, observing a more intense erosion of the material in the cathode.

Tabrizi et al. (2008b) also generated bimetallic nanoparticles by spark discharge using different electrodes. They found an effective mixing of some materials mentioned in the previous study plus the combination of chromium and cobalt. An interesting

finding in the Tabrizi et al. (2008) study is that the nanoparticles they produced have a wide distribution of composition where the value obtained through ICP-MS is their average mass fraction or material ratio.

Table 16. Mass fraction and generation rates of bimetallic particles (Byeon et al., 2008)

Element (anode (+) : cathode (-))	Mass fraction	Particle generation rate (μg/min)
Pd:Ag	0.85:0.15	0.66
Ag:Pd	0.25:0.75	0.28
Pd:Pt	0.52:0.47	2.64
Pt:Pd	0.68:0.32	6.28
Pd:Au	0.59:0.41	3.78
Au:Pd	0.70:0.30	6.88

Overall, this alternative agrees with the way particles are simulated as each nanoparticle has two components from the beginning. However, without proper characterization of the nanoparticles, is difficult to make assumptions about their mass fractions. The distribution in particle composition due to this method needs to be considered in the initial particle list when simulations are run.

4.1.3 Using electrodes made of alloys

For particles produced using alloyed feedstock electrodes, Muntean et al. (2016) found

> "As there is no preferential evaporation of one of the components in the alloyed electrodes, intimate mixing of the constituent in the vapor phase occurs."

This preferential evaporation is responsible for the different mass fractions shown in Table 16. Muntean et al. (2016) studied copper, nickel, and copper-nickel alloy nanoparticles and showed that the Cu-Ni nanoparticles had almost the same composition

as the used alloyed feedstock of the electrodes, with a deviation of less than 7%. A comparison of the material ratios is found in Table 17.

Table 17. Comparison of Cu/Ni-ratios between alloyed feedstock electrodes and nanoparticles produced.

Sample	Feedstock Cu/Ni ratio, specified (mass ratio)	Nanoparticle Cu/Ni ratio (mass ratio)
Cu/Ni 80/20	4.33	4.83
Cu/Ni 60/40	1.624	1.684
Cu/Ni 40/60	0.722	0.744
Cu/Ni 20/80	0.27	0.28

This nanoparticle production method also agrees with the way particles are simulated and has the advantage that the ratio of the different materials in the nanoparticles is very close to the ratio of the materials in the alloy used to make the electrodes. This allows one to make a good assumption about the composition of the nanoparticles when methods of characterization are not readily available. In this case, particle composition matched the feedstock composition with a maximum deviation of 5%.

In any case, the best solution would be to measure the composition of the nanoparticles at the different sampling ports in the coagulation experiment. This can be accomplished connecting the stream of the aerosol (after the sampling probe) to a fiber, or membrane filter suitable to collect the nanoparticles and determine their composition with techniques like ICP-MS and their elemental distribution with techniques like STEM-EDX. This could be done before or after measuring the actual size distribution (provided the aerosol generation is steady) to associate the mass fractions measured at each sampling port with the distributions. If particle collection is done in series with size and charge distribution measurements (before the TDMA), the measurements would be

affected by the particles retained in the grid, fiber or membrane collecting particles. With the added characterization, one can take advantage of the feature of the DSMC program (in Chapter 3) to estimate the mass and volume of the different components in the aerosols and compare with measurements.

4.2 Atomized aerosols

In this method for particle generation, the material of interest for the aerosol is in a solution where the solvent can be water or alcohol. The aerosol particle size is proportional to the concentration of the solute. One advantage of this way of producing aerosols is the ease in which the two different solutes can be mixed in specific proportions to produce multi-component aerosols with known component ratios. However, we have not measured to determine if the nanoparticles produced keep these component ratios once atomized. We worked with solutions having only one solute and found it difficult to remove the solvent (water) from the particles coming out of the atomizer, even after following the recommendations from the manufacturer of the atomizer to dry them. These recommendations call for using dry air for the atomizer and diffusion driers to help to diminish the amount of water in the particles. Figure 43 shows the experimental setup we used to produce aerosols from an aqueous solution, with three diffusion dryers connected in a series and a tube surrounded by a heating strip between the first and second dryer to increase the temperature of the aerosol. The dryers consisted of an inner tube made of wire screen surrounded by silica gel or calcium sulfate (Drierite) to maintain a dry atmosphere and absorb water vapor.

Figure 43. Generation of aerosol from aqueous solution, using diffusion driers and heating strips to remove water from particles.

Apart from soluble solutes, non-soluble solid submicrometer particles can be dispersed using atomizers, but they require the use of a sonic probe or a magnetic stirrer to continuously disperse the particles in the hydrosol while atomizing. We generated aerosols with standards of polystyrene latex (PSL) particles from Bangs Laboratories, Inc. (Fishers, IN, USA) to check the calibration of the SMPS, using a TSI Model 3076 constant output atomizer (shown in Figure 43). Their size distributions (Figures 44 and 45) show a tail to the right that might be a combination of surfactant and water in the

particles. Surfactant is added to the PSL products to stabilize the small particles and keep them from agglomerating. Figure 46 shows the result of atomizing just deionized water (8 MΩ) with a significant amount of water particles present. Note that the same type of water was used in the solutions of the PSL particles, and that all size distributions were obtained using the three diffusion driers and increasing the temperature of the aerosol to 35 °C. To get the aerosol to that temperature, the temperature of the metal tubing surrounded by the heating strip becomes significantly high. We did not increase the temperature further to avoid damage to the plastic components in the system.

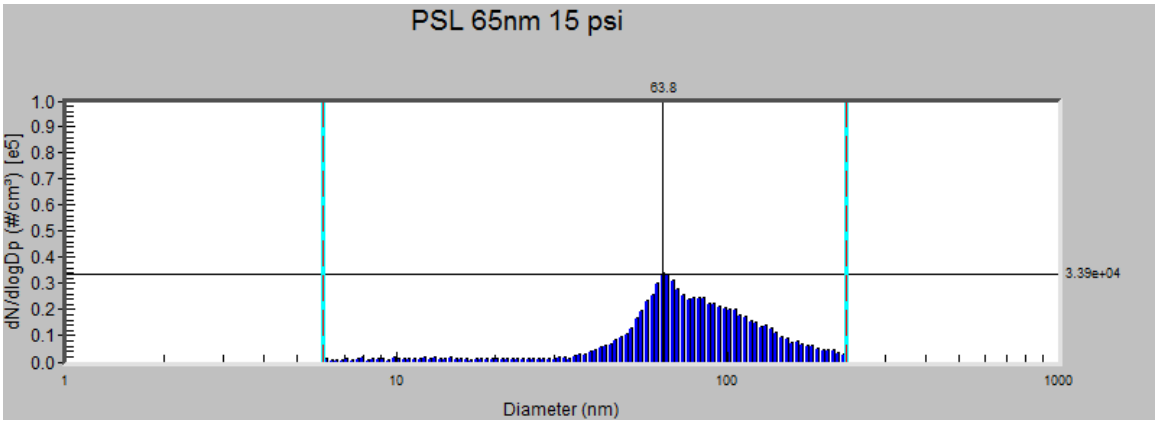

Figure 44. Size distribution of atomized 65-nm PSL particles using three diffusion dryers, a pressure of 15 psi in the atomizer, and heating the aerosol to 35 °C.

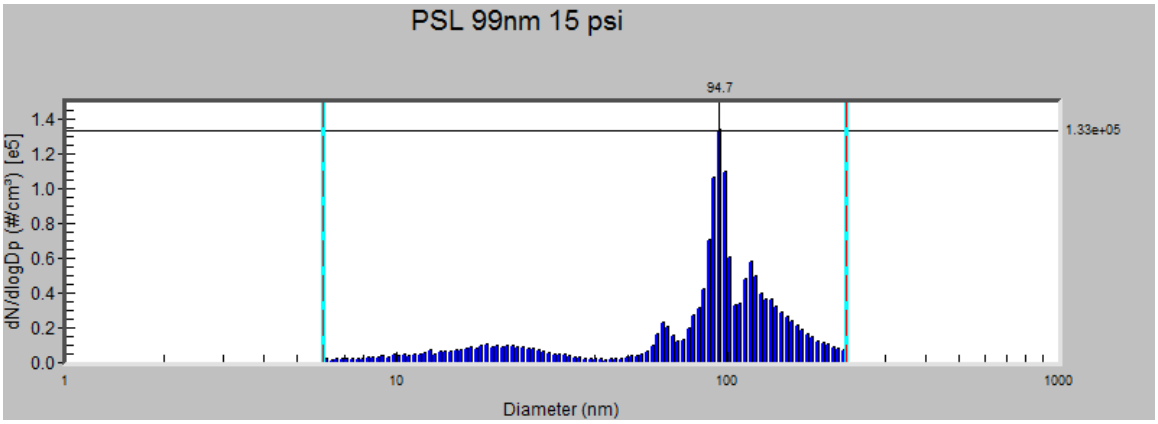

Figure 45. Size distribution of atomized 99-nm PSL particles using three diffusion dryers, a pressure of 15 psi in the atomizer, and heating the aerosol to 35 °C.

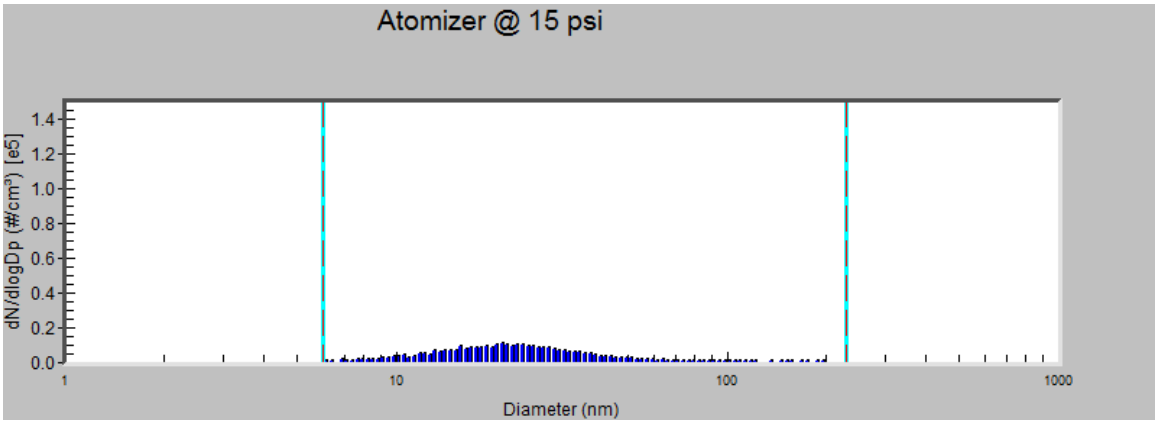

Figure 46. Size distribution of atomized de-ionized water (8 MΩ) with no solute, using three diffusion dryers, a pressure of 15 psi in the atomizer, and heating the aerosol to 35 °C.

4.3 Conclusions

Particle production by spark discharge has several advantages over atomization, producing "naked" nanoparticles made up of two materials. As long as they conduct electricity. The options of using electrodes of different materials and using alloyed electrodes are the most suitable for the kind of simulation we are performing, since nanoparticles are generated with a bimetal composition or as alloys, respectively. With these methods, nanoparticles can be produced even from a combination of metals that are immiscible in the macroscopic scale like silver-copper, gold-platinum, copper-tungsten (Tabrizi et al., 2010). It is even possible to produce nanoparticles from semi-conductors like silicon by doping the pure semiconductor material to decrease its electrical resistance (Vons et al., 2011). Given the higher uniformity in nanoparticles generated from alloyed electrodes, this method is preferable. Besides the generation of a two-component aerosol, particle characterization is needed to determine its composition and eventually explore how it affects the evolution of aerosol (specially in coagulation). As a continuation of the experiment by Simones and Loyalka (2015), we suggest some additions shown in Figure 47. The changes consist in installing alloyed electrodes to the spark generator (with

materials of interest to study the nuclear source term) and collect particles in a sampler for ICP-MS analysis to determine average particle composition at each of the sampling ports of the coagulation tube. These additions will allow us to have more detailed experimental information about aerosol evolution to compare with simulations, improve them, and determine coagulation rates.

For non-conductive soluble materials, the more convenient option is the use of an atomizer, even though special consideration must be given to assure proper drying of the particles and to investigate particle composition of the aerosol produced.

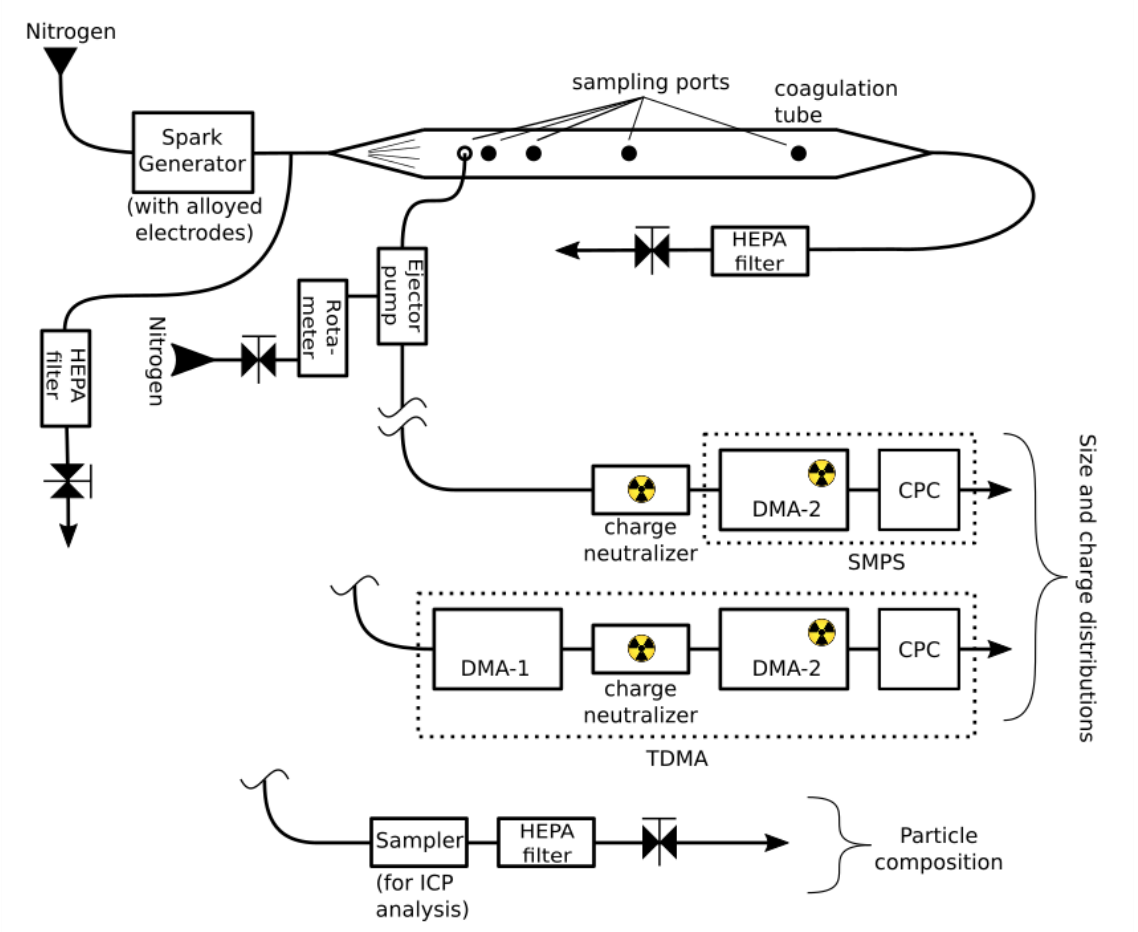

Figure 47. Suggested experimental setup for studying coagulation in two-component aerosols using alloyed electrodes to produce nanoparticles by spark discharge, a coagulation tube to sample the aerosols at different times, an SMPS and a TDMA to obtain size and charge distributions, and a sampler to collect particles and determine their composition by ICP-MS analysis.

5. EXPLORATION OF WEIGHTS USING THE DSMC TECHNIQUE

The DSMC technique has been used as an efficient way to simulate aerosol evolution with the versatility and capability to integrate more nonlinear, highly dynamic and synergistic aerosol processes in simulations, and to improve the fidelity of results to actual physics. However, the number of particles used in these simulations is in orders of magnitude smaller than the actual number of particles found in an aerosol. In an experiment, the number of particles is on the order of 10^{11} while DSMC simulations use around 10^{6}. As this number increases more computing time and memory is required, revealing a need for balance between good results and speed. Because we want to obtain good results with a limited number of particles in the simulation, the subset of particles representing the aerosol must be a good representation of the whole population at any time. In this chapter we explore the possibility and effects of assigning dynamic weights to the particles to get better results.

As previously mentioned, the number of particles used in a simulation is orders of magnitude smaller than the actual particles in the aerosol. However, this sample must fairly represent the aerosol population. For this purpose, the initial particle list used for simulations is obtained by sampling the mass or volume of a particle randomly from a known distribution function by a direct sampling method like the inverse method (when possible) or by a rejection-acceptance technique. The initial particle list can also be obtained from experimental measurements using devices such as SMPSs and TDMAs; then, the results are processed to get a list of particles as explained in Section 3.1. The

number of particles in the aerosol and the number of particles in the simulation will be related by factor *f*, as shown in equation (22).

$$f = \frac{N_{real}}{N_{sim}} \tag{22}$$

where N_{real} is the number of particles in the aerosol and N_{sim} is the number of particles used for simulation, expecting $N_{real} >> N_{sim}$.

This factor *f* can also be considered the weight of each particle, indicating how many real particles are represented by every simulated particle. To our knowledge, the works done on the DSMC technique have kept this particle weight constant by just scaling the values of the number of particles and volumes in the program particle lists, and then multiplying them by factor *f*. In the processes of deposition and coagulation, particles are constantly being deleted. In the first case, particles adhere to surfaces, and in the second case, two particles coalesce to form a new one resulting in the reduction of one particle per collision. The particles in the simulation are a subset of the real particles, and as the sample gets smaller, this subset become less representative. In size distributions with a limited number of sections (size bins), the sections with a smaller particle population get poorer results (Palaniswaamy and Loyalka, 2007b). If somehow the sample particles are not deleted but get their weight modified according to the running process; then, the sample can maintain its quality by not reducing the diversity of volumes in the initial particle list.

At first, due to the sampling process, all simulated particles have the same weight (*f*), given by equation (22). But with the intention of using different weights for each

particle, we define the total number of particles as the sum of all the particles' associated weights, as shown in equation (23).

$$N_{real} = \sum_{j=1}^{N_{sim}} \omega_j \tag{23}$$

where ω_j is the weight for particle *j*. In this manner, the values for ω_j may change in every step of the simulation. Combining equations (22) and (23), we obtain a relation (equation (24)) for the initial particle list where the values for ω_j are equal to factor *f* for all *j*s.

$$f\ N_{sim} = \sum_{j=1}^{N_{sim}} \omega_j \tag{24}$$

The different natures of the processes dictate how they affect the weights. In the following sections we will explore whether this approach can be used in the various aerosol processes and how the weights will change in time.

5.1 Deposition using weights

Deposition is a linear process; so, if *n* particles are selected for removal in a Δt of the simulation $n \times f$, particles are removed from the aerosol. This process can continue until there are no more particles to drop, assuming there is no source of new particles. With every particle dropped, the sample gets smaller, the variety of sizes is diminished, and the statistics become less reliable. The scaling approach in deposition is equivalent to having the binary weights of *f* and 0 for particles not dropped and dropped, respectively. With the intention of keeping the particles selected for removal, instead of deleting them we reduce their weights to half of the unselected particles. We will use the binary weights

of $\omega/2$ for dropped particles and a weight of ω for particles not yet dropped. The value for ω will change in every Δt in which particles are selected for deposition; ω varies according to the number of particles selected for deposition. Thus, ω is calculated by the following equation which distributes the total weight in each Δt (numerator) among the number of particles considering that a fraction has half the weight of the remaining particles (denominator):

$$\omega(t) = \frac{\sum_{j=1}^{N_{sim}} \omega_j (t - \Delta t) - f \cdot n_{pr}}{\frac{n_{\omega/2}}{2} + n_{\omega}} \tag{25}$$

where the summation accounts for the total weight or number of real particles resulting from the previous Δt. n_{pr} is the number of particles selected for removal in the current Δt. $n_{\omega/2}$ is the number of particles with a weight of $\omega/2$ (including particles removed in the current Δt), and n_{ω} is the number of particles with a weight of ω.

It is necessary to keep track of which particles have weights $\omega/2$ and ω so as to update their weights once the particles to be removed have been selected. Then, the new value for ω(t) is calculated. It is important to note that in this approach the total number of particles and their total volume is calculated in a method that is different from scaling. In scaling, the total number of particles is obtained by multiplying the number of particles in the simulation by *f* and the total volume is obtained by adding all the volumes of the particles and then multiplying by *f*. However, with weights the total number of particles at any time is given by equation (23), and the total volume results from multiplying each particle volume by its weight and then adding all these products, which is done using the following:

$$V_T = \sum_{j=1}^{N_{sim}} v_j \omega_j \tag{26}$$

where V_T is the total volume of the particles in the aerosol, N_{sim} is the number of particles in the simulation (which is kept constant), and v_j and ω_j are the volume and weight of the particle at position *j*, respectively. Table 18 summarizes the steps followed to simulate deposition using weights and compares it to regular scaling.

Table 18. Comparison of steps followed in regular scaling versus the use of weights.

Step	Regular Scaling	Using Weights
1. Select particle positions to remove	Every particle is tested for deposition.	Only particles which have not been deposited are tested, that is, particles with a weight = ω
2. Action to perform with selected particles	Remove particles from particle list.	1. Add their particle positions to a list tracking particles with weight = $\omega/2$ and remove them from the list tracking particles with weight = ω. 2. Calculate the new value for ω with equation (25). 3. Update the weight for all particles.

We compared the results from the DSMC simulations using scaling and weights with those of an exact solution. The problem considered is a single-component polydisperse aerosol undergoing constant deposition. The exact solution for this problem is shown in equation (27). The variables to compare are the total number of particles and the total volume of the aerosol at different times. The results in terms of percent error are shown in Figures 48 and 49.

$$n(v,t) = \frac{N_{real}}{v_0} \exp\left(-\frac{v}{v_0}\right) \exp\left(-r_0 t\right) \tag{27}$$

where *v* is the particle volume, v_0 is the mean particle volume of the initial distribution given by $n(v,0) = \frac{N_{real}}{v_0} \exp\left(-\frac{v}{v_0}\right)$. r_0 is the deposition rate (constant), and *t* is time.

The parameters used for this simulation were: $N_{real} = 10^8$ particles, $N_{sim} = 10^5$ particles, $r_0 = 10^{-1}$ 1/s, $v_0 = 3.817\times10^{-22}$ m^3 (equivalent to a spherical particle with a diameter of 90 nm), a Δt of 0.1 s, and 320 iterations (32 seconds). At 32 seconds the number of particles remaining were 4% of the initial particles. Each Δt removed approximately 1% of total number of particles resulting from the previous Δt. Both DSMC modules (scaling and weights) in the program started with the same initial particle list, generated by inverse sampling of the initial size distribution function $n(v,0)$.

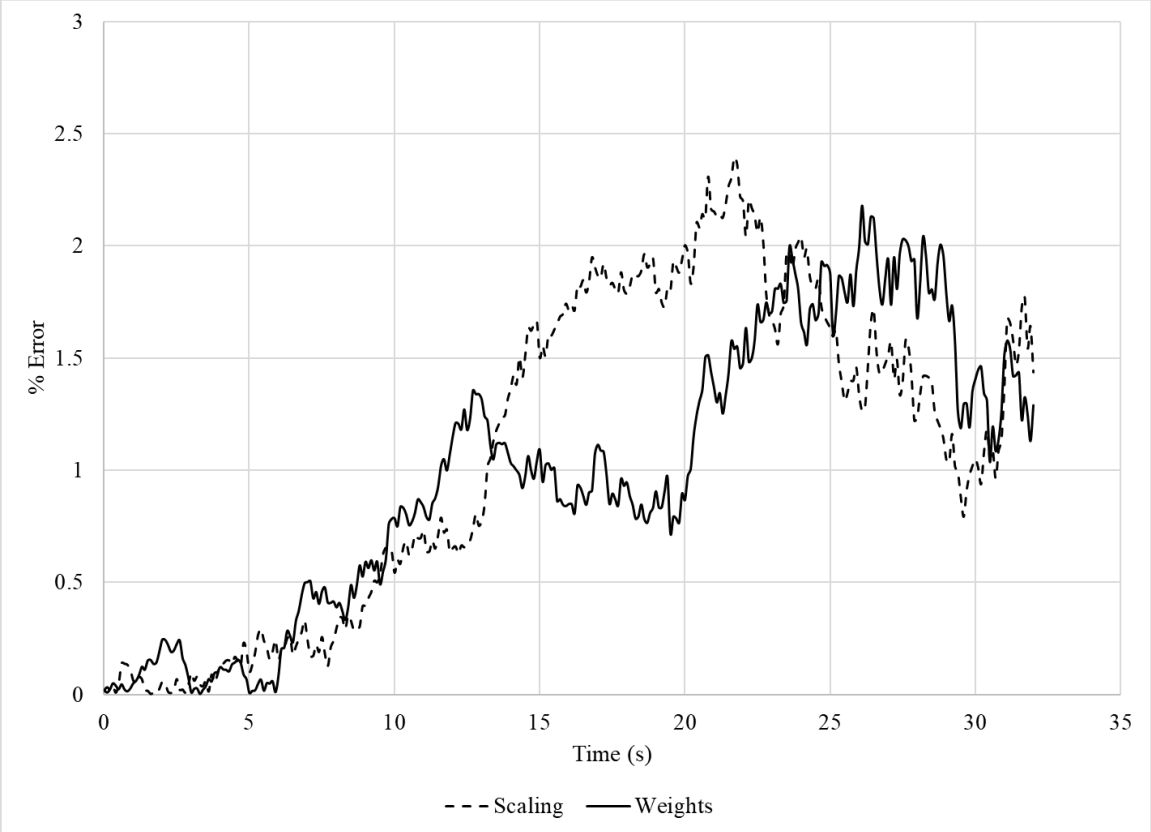

Figure 48. Comparison of calculated number of particles in a DSMC simulation of constant deposition using regular scaling and dynamic particle weights.

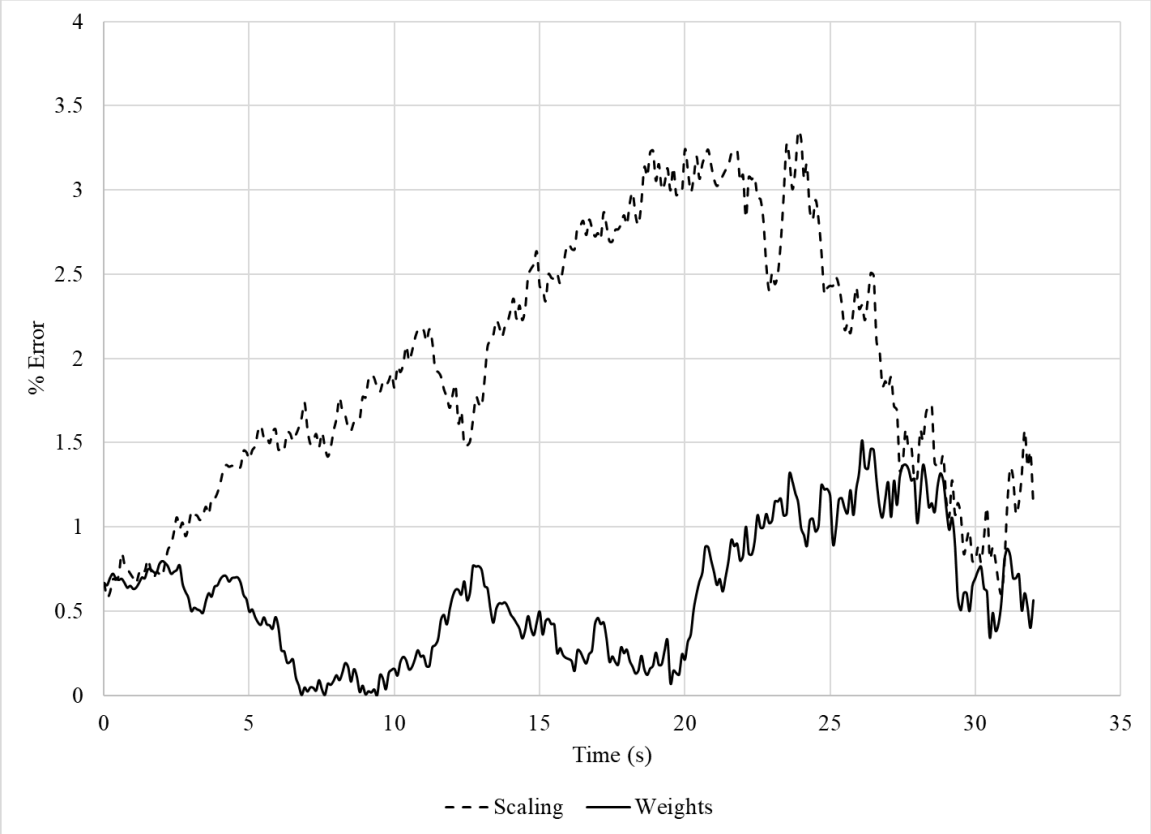

Figure 49. Comparison of the total volume of aerosol particles in a DSMC simulation of constant deposition using regular scaling and dynamic particle weights.

The error in the calculation of the number of particles is not very different between both approaches. The difference is due to the random processes involved in the selection of the number of particles to be dropped. However, in the calculation of total volume, the difference is more noticeable, as the simulation with weights had a reduced error over the time of simulation. We think this is result of keeping the particles, albeit with a lower weight so the simulated particles still had many volumes represented in the sample. Weight redistribution avoids the reduction of representative volumes, while deposition is estimated by reducing the weight (relevance) of each volume selected to be dropped. It is important to note that the total time of simulation using weights is still limited to the number of simulated particles, as it is in regular scaling. In other words, we

cannot drop more particles than the number of simulated particles at time zero. When the number of particles not dropped runs out, all weights become zero and the simulation ends.

5.2 Coagulation using weights

Coagulation is a more complex process to implement than deposition in DSMC simulations, and there is no straightforward way to apply the use of weights to it. To explore it, our description begins with how a problem with a constant coagulation rate is performed in a DSMC simulation with scaling. It involves four steps:

1) Calculate the number of random pairs of particles which will coagulate.
2) Randomly select those particles.
3) Create the new particles adding the volumes or masses of the particles which collided.
4) Delete the original particles which were randomly selected for coagulation.

The calculation of the number of pairs in Step 1 is done using the following equation, known as the no time counter method (NTC) (Bird, 1994):

$$n_{pairs} = \frac{1}{2} f \left(N_{sim} \right)^2 K_0 \Delta t \tag{28}$$

where *f* is the ratio of real particles to simulated particles, N_{sim} is the number of simulated particles, K_0 is the constant coagulation rate, and Δt is the time step considered for each run.

The random selection of the pairs of particles in Step 2 is done considering all particles have the same probability of being chosen. Creation of new particles in Step 3 adds the volumes or masses of the particles which collided, and these new particles maintain the same relevance or weight as the particles which originated them. Deletion of particles in Step 4 is necessary to maintain the conservation of mass in coagulation. Every collision (from randomly selected pair of particles) that results in coalescence represents *f* particles lost, but there is no loss in volume.

If we want to use weights and stick to our definitions in equations (23) and (24), for Step 1, the equivalent to equation (28) would be equation (29) where $f\left(N_{sim}\right)^2$ is substituted by $\frac{1}{f}\left(\sum_{j=1}^{N_{sim}}\omega_j\right)^2$.

$$n_{pairs}=\frac{1}{2f}\left(\sum_{j=1}^{N_{sim}}\omega_j\right)^2 K_0\Delta t \tag{29}$$

Following the logic of the use of weights in deposition, in Steps 2 and 3, the selection of random pairs of particles must consider particles which have not been selected previously for coagulation. As in scaling, the new particles resulting from coagulation must have the same relevance or weight as the rest of the particles which have not interacted yet, while the particles coalescing should have a lower weight. Then, in Step 4 we ideally would like to maintain or increase the number of simulated particles instead of deleting them by manipulating their weights. However, this is not possible in the way we did for deposition due to the conservation of mass. Once the volumes from two particles are added in a new particle, it is difficult to keep the volumes of the particles coalescing and at the same time maintain the conservation of mass. Let us consider a pair of particles with volumes v_1

and v_2, both with a weight of 1: ((v_1,1),(v_2,1)). After those particles coalesce, a new particle is added with a certain weight ω_h, i.e., ($v_1 + v_2, \omega_h$). If we want to conserve somehow the particle volumes, we would have the following particle list: ((v_1, ω_l),(v_2, ω_l), ($v_1 + v_2, \omega_h$)) with ω_l being a lower weight than ω_h. The sum of the weights for the new particle list must be one, and the total volume must be $v_1 + v_2$, so we can write the following equations:

$$\begin{aligned} &2\omega_l + \omega_h = 1, \\ &(v_1 + v_2)\omega_l + (v_1 + v_2)\omega_h = v_1 + v_2, \\ &\text{with} \quad 1 > \omega_l > \omega_h > 0 \end{aligned} \tag{30}$$

This is only satisfied when ω_l is zero and ω_h is one, which is what happens in regular scaling when the particles coalescing are deleted and the new particle gets the same weight and the sum of the volumes. Thus, new ways to approach this problem need to be found with the purpose of not deleting particles in the DSMC simulations of coagulation.

5.3 Other processes

Processes not mentioned yet in this section are electrostatic dispersion and condensation. Electrostatic dispersion can be treated in the same way as deposition in the manipulation of particle weight. This involves: assigning a weight of $\omega/2$ to the particles selected for removal, ω for the rest of the particles, and calculating the new value of ω depending on the number of particles dropped at Δt. Condensation does not require any manipulation of the particles' weight since particles are not added or removed in this process; they are simply gaining mass. The gained mass in the aerosol would be proportional to the mass gained in the particle list multiplied by the particle weight.

5.4 Conclusions

The way proposed to manipulate weights in deposition improves accuracy in the estimation of the aerosol's total volume by keeping the values of volumes in the particle list instead of deleting them. When particles are selected to be dropped, they instead obtain a lower weight. However, this approach does not extend the maximum time of simulation, which depends on the initial number of particles. The characteristics of the process of coagulation (implemented in the DSMC technique) do not allow application of a similar manipulation of the weights as in deposition. Yet it would be possible to combine deposition using weights and coagulation in a simulation if the value for the weights is updated every time a pair of particles undergoes coagulation. Particles would be deleted only in the coagulation process and mass would be conserved which may provide better results than relying on scaling for both processes.

6. DISCUSSION AND CONCLUSIONS

We have developed a DSMC program to simulate aerosol evolution, which successfully integrates the process of coagulation (with charge effects), deposition, condensation and electrostatic dispersion for multi-component polydisperse aerosols. It makes use of realistic physical models and can perform simulations which are very difficult to achieve using numerical techniques. With this type of program, it is relatively easy to compare simulations and experiments by converting measured number distributions (with size and charge information) into particle lists. These lists are both used as initial particle lists to start the simulation and subsequently as a means to compare measurements and simulations at any time step. The ability of handling several components opens the possibility of using different particle compositions, which is important since it affects the evolution of aerosols.

Besides simulating the evolution of aerosols, there is the possibility of performing a more detailed analysis of the characteristics of the particles interacting in each process and of measuring their influence on the activity of the other processes. The combination of validated physical models working together allow an exploration of their synergistic nature and the effects of their particle properties on them. An example of this is the observation that denser particles make coagulation stronger; that is, more particles coalesce, and the particles passing the test of coalescence have a larger size. Also, the particle composition in Problem 2 affected deposition but to a lower degree. Problem 2 observations showed how an increased activity in coagulation affects deposition and

electrostatic dispersion by changing the mean diameter of the particles and reducing the number of particles suspended.

Particle composition is strongly influenced by condensation, changing the mean particle density with time. DSMC programs can provide more realistic results for cases where mean particle density varies significantly. And to further improve these simulations, it is necessary to conduct experiments which involve particle characterization to compare with measurements. For this purpose, additions to previous experiments are proposed: producing nanoparticles from alloyed electrodes by spark discharge and the characterization of nanoparticles with techniques like ICP-MS. Alloyed electrodes seem to be the best alternative to producing two-component nanoparticles by spark discharge with a relatively uniform composition. With this type of particles and a system to determine their composition connected to the TDMA-coagulation-tube equipment, enough information can be obtained to compare with the simulation results of the DSMC program presented in this work.

Besides the proposed experiments, future work involves additions to DSMC such as: the incorporation of weights to simulated particles, the use of a distribution for particle composition in the initial particle list, a dynamic management of the order in which the different processes are applied, and the incorporation of other particle characteristics like radioactivity and shape. Particle weights could improve the accuracy in the estimation of total volume (and mass) by keeping the values of volumes instead of deleting them from the particle list. When particles are selected to be dropped or coalesce, they obtain a lower weight. We started exploring this idea obtaining good preliminary results for deposition, but also finding some difficulties in coagulation. More

work needs to be done here to possibly extend the time of the simulation by manipulation of the weights of particles and to find ways to make that manipulation work in coagulation. Particle composition has been found to have a distribution in nanoparticles generated by spark discharge. Because it influences aerosol evolution, it is necessary to explore its characteristics and apply them to the initial particle lists in simulations. Another alternative is determining if a fixed average value for the mass fractions is capable of performing realistic simulations. In long simulations, the activity of the processes will change over time as particles change in size, density and electrical charge. These activity changes may require a different order in the application of processes to get better results. Thus, implementing a way for the program to adapt to the different activities of the processes is desirable. Finally, the incorporation of radioactivity and shape effects would be a great step to make simulation even more realistic.

All the improvements mentioned up to this point must be accompanied by efforts to have an efficient code which saves time performing the required tasks and by the implementation of parallel processing. There is little advantage in having a very complete and thorough program if it becomes too slow to be useful. Another important aspect to consider is knowing in which areas it is viable to make approximations that do not have a significant effect on accuracy and that allow the reduction of simulation time.

REFERENCES

Adachi M., Okuyama K., Kousaka Y., (1981), Electrostatic Coagulation of Bipolarly Charged Aerosol Particles. Journal of Chemical Engineering of Japan 14, 467-473.

Bird G.A., (1994), Molecular gas dynamics and the direct simulation of gas flows. Clarendon Press, Oxford University Press, Oxford, New York.

Boraas M., Loyalka S.K., (2018), Mesh-Free Simulation of Spatially Inhomogeneous Aerosols in Arbitrary Geometries. Nuclear Science and Engineering, 1-22.

Brockmann J.E., (1987), Ex-vessel releases: Aerosol source terms in reactor accidents. Progress in Nuclear Energy 19, 7-68.

Byeon J.H., Park J.H., Hwang J., (2008), Spark generation of monometallic and bimetallic aerosol nanoparticles. Journal of Aerosol Science 39, 888-896.

Campbell S.A., Loyalka S.K., (2015), Computation of aerosol evolution under coagulation. Nuclear Science and Engineering 181, 137-159.

Campbell S.A., Palsmeier J., Loyalka S.K., (2016), Mesh-free simulation of aerosol evolution. Nuclear Science and Engineering 182, 287-296.

DiNunno J.J., Anderson F.D., Baker R.E., Waterfield R.L., (1962), Calculation of distance factors for power and test reactor sites. Division of Licensing and Regulation, AEC.

Friedlander S.K., (2000), Smoke, dust, and haze fundamentals of aerosol dynamics, Topics in chemical engineering, 2nd ed. Oxford University Press,, New York.

Fuchs N.A., (1964), The Mechanics of Aerosols. Pergamon Press, New York.

Gauntt R.O., Cole R.K., Erickson C.M., Gido R.G., Gasser R.D., Rodriguez S.B., Young M.F., (2000), MELCOR computer code manuals. Sandia National Laboratories, Alburquerque, NM.

Gelbard F., (1982), MAEROS User Manual. NUREG/CR-1391, SAND80-0822. Sandia National Laboratories.

Ghosh K., Tripathi S.N., Joshi M., Mayya Y.S., Khan A., Sapra B.K., (2017), Modeling studies on coagulation of charged particles and comparison with experiments. Journal of Aerosol Science 105, 35-47.

Hidy G.M., Brock J.R., (1972), Topics in Current Aerosol Research (Part 2). Pergamon Press.

Loyalka S.K., (2003), Direct simulation of multi-component aerosol dynamics, Transactions of the American Nuclear Society and Embedded Topical Meetings; Decommissioning and Spent-Fuel management and Risk Management, Jun 1 - 5 2003. American Nuclear Society, San Diego, CA, United states, pp. 334-334.

Loyalka S.K., Park J.W., (1988), Aerosol growth by condensation: A generalization of mason's formula. Journal of Colloid and Interface Science 125, 712-716.

Metropolis N., Rosenbluth A.W., Rosenbluth M.N., Teller A.H., Teller E., (1953), Equation of State Calculations by Fast Computing Machines. The Journal of Chemical Physics 21, 1087-1092.

Muntean A., Wagner M., Meyer J., Seipenbusch M., (2016), Generation of copper, nickel, and CuNi alloy nanoparticles by spark discharge. Journal of Nanoparticle Research 18, 229.

Murata K.K., Williams D.C., Griffith R.O., Gido R.G., Tadios E.L., Davis F.J., Martinez G.M., Washington K.E., Tills J., (1997), Code manual for CONTAIN 2.0: A computer code for nuclear reactor containment analysis. Nuclear Regulatory Commission, Washington, DC.

Palaniswaamy G., Loyalka S.K., (2006), Direct Simulation Monte Carlo Aerosol Dynamics: Coagulation and Collisional Sampling. Nuclear Technology 156, 29-38.

Palaniswaamy G., Loyalka S.K., (2007a), Direct simulation Monte Carlo aerosol dynamics: Collisional sampling algorithms. Annals of Nuclear Energy 34, 13-21.

Palaniswaamy G., Loyalka S.K., (2007b), Direct Simulation, Monte Carlo, Multicomponent, Aerosol Dynamics: Coagulation, Deposition, and Source Reinforcement. Nuclear Technology 160, 187-204.

Palaniswaamy G., Loyalka S.K., (2008), Direct simulation, Monte Carlo, aerosol dynamics: Coagulation and condensation. Annals of Nuclear Energy 35, 485-494.

Palsmeier J.F., Loyalka S.K., (2013), Evolution of Charged Aerosols: Role of Charge on Coagulation. Nuclear Technology 184, 78-95.

Park J.W., (1988), Numerical solutions of the aerosol general dynamic equation for nuclear reactor safety studies. University of Missouri - Columbia, Ann Arbor, p. 146.

Rangaraj D., Loyalka S.K., (2004), Direct Simulation Monte Carlo Aerosol Dynamics II-Role of Component Density Difference in Brownian Agglomeration. Transactions of the American Nuclear Society 90, 301-302.

Saldivar I., (2018), Direct Simulation Monte Carlo for Modelling Spatially Homogeneous Multi-Component Aerosols, Nuclear Science and Engineering Institute. University of Missouri, Columbia, MO, p. 128.

Saldivar I., De La Torre Aguilar F., Boraas M., Loyalka S.K., (2018), Benchmark problems in aerosol evolution: Comparison of some exact and DSMC results. Annals of Nuclear Energy 117, 213-222.

Sher R., Hobbins R.R., (2011), Transport and Removal of Aerosols in Nuclear Power Plants Following Severe Accidents. American Nuclear Society.

Simones M.P., Gutti V.R., Meyer R.M., Loyalka S.K., (2011), Measurements of Aerosol Charge and Size Distribution for Graphite, Gold, Palladium, and Silver Nanoparticles. Nuclear Technology 176, 211-226.

Simones M.P., Loyalka S.K., (2015), Measurements of Charged Aerosol Coagulation. Nuclear Technology 189, 45-62.

Tabrizi N.S., Ullmann M., Vons V.A., Lafont U., Schmidt-Ott A., (2008a), Generation of nanoparticles by spark discharge. Journal of Nanoparticle Research 11, 315.

Tabrizi N.S., Xu Q., van der Pers N.M., Lafont U., Schmidt-Ott A., (2008b), Synthesis of mixed metallic nanoparticles by spark discharge. Journal of Nanoparticle Research 11, 1209.

Tabrizi N.S., Xu Q., van der Pers N.M., Schmidt-Ott A., (2010), Generation of mixed metallic nanoparticles from immiscible metals by spark discharge. Journal of Nanoparticle Research 12, 247-259.

U.S. Atomic Energy Commission, (1950), Summary Report for the Reactor Safeguard Comittee, Oak Ridge, TN.

U.S. Atomic Energy Commission, (1957), Theoretical Possibilities and Consequences of Major Accidents in Large Nuclear Power Plants, The Brookhaven Report., Washington, DC.

U.S. Nuclear Regulatory Commission, (1975), Reactor Safety Study: An Assessment of Accident Risks in U.S. Commercial Nuclear Plants.

U.S. Nuclear Regulatory Commission, (1981), Technical bases for estimating fission product behavior during LWR accidents.

U.S. Nuclear Regulatory Commission, (2007), Next generation nuclear plant phenomena identification and ranking tables (PIRTs). NUREG/CR-6944.

Vemury S., Janzen C., Pratsinis S.E., (1997), Coagulation of symmetric and asymmetric bipolar aerosols. Journal of Aerosol Science 28, 599-611.

Vons V.A., de Smet L.C.P.M., Munao D., Evirgen A., Kelder E.M., Schmidt-Ott A., (2011), Silicon nanoparticles produced by spark discharge. Journal of Nanoparticle Research 13, 4867.

Williams M.M.R., Loyalka S.K., (1991), Aerosol science: Theory and Practice: With Special Applications to the Nuclear Industry, 1st ed. Pergamon Press, Oxford; New York.

Wolfram Research Inc., (2018), Mathematica, Version 11.3, Champaign, IL.

VITA

The author Fernando De La Torre Aguilar was born in Zacatecas, Zac., Mexico. He attended the *Universidad Autónoma de Zacatecas* in the same city from 1999 to 2004 and received a Bachelor of Electronics Engineering in 2004. He attended the *Universidad Autónoma de Zacatecas (Unidad Académica de Estudios Nucleares)* from 2008 to 2010 and received a Master of Science in Nuclear Sciences in 2010. He began working toward a Ph.D. in Nuclear Engineering at the University of Missouri Nuclear Science and Engineering Institute in 2012. He is co-author of the book Nuclear Batteries and Radioisotopes. Research interests include gamma spectrometry, radioisotopes, and aerosol dynamics.